

**The development and evaluation of a  
pseudo-histological staining and image processing system  
for use in point-of-care *ex-vivo* fluorescence histology**

AN ABSTRACT

SUBMITTED ON MARCH 29, 2018

TO THE DEPARTMENT OF BIOMEDICAL ENGINEERING  
IN PARTIAL FULFILLMENT OF THE REQUIREMENTS  
OF THE SCHOOL OF SCIENCE AND ENGINEERING

OF TULANE UNIVERSITY

FOR THE DEGREE

OF

DOCTOR OF PHILOSOPHY

BY



Katherine Nicole Elfer

APPROVED:



Quincy Brown, Ph.D.,  
(Committee Chair)



Andrew Sholl, M.D.



Kristin Miller, Ph.D.



Carolyn Bayer, Ph.D.

## ABSTRACT

Current microscopy-based tissue diagnostics, particularly hematoxylin and eosin (H&E) histology, requires multiple complex tissue processing steps: fixation, paraffin embedding, microtome sectioning, dyeing the tissue, and imaging individual slides through a bright field microscope. The time and labor-intensive result of this process makes it unsuitable for patient point-of-care evaluation. Therefore, many bedside procedures are completed without efficient real-time analysis of tissue adequacy and diagnostic results are unnecessarily delayed. Additionally, research experiments that require information regarding changes to tissue morphology or function before proceeding to the next experimental phase are severely interrupted by histology processing in their workflow. Fluorescence histology, which relies on rapid fluorescent staining of tissue, optical sectioning microscopy, and image processing for digital viewing, can provide an inexpensive, non-destructive, 3-dimensional, and fast alternative to traditional histology and point-of-care screening protocols. The objective of this work is to further advance the concept of “fluorescence histology,” in which traditional histopathology preparation methods are replaced by optical-sectioning (in lieu of physical sectioning), sensitive and flexible fluorescence-based contrast (in lieu of chromophore-based contrast), and computational strategies to replicate traditional color-schemes. In this work, we demonstrate the development and use of a fluorescent analogue to H&E on fixed and frozen tissue sections and fresh human biopsies. This fluorescent analogue, DRAQ5 & eosin, is compared against the current single-agent, monochrome fluorescence histology system, and their effects on diagnostic downstream molecular analyses, including quantitative-PCR and immunohistochemistry, is evaluated. We create a methodology to develop and characterize fluorescent analogues for any histological stain, with demonstration using Masson’s Trichrome and Periodic Acid-Schiff,

enabling the expansion of fluorescence histology for multiple applications. This work demonstrates the ability to improve point-of-care pathology and research by replacing destructive, incomplete, and time-consuming histology with fluorescence histology, which preserves the tissue for later analysis or experiments while providing accurate and rapid histology assessment.

**The development and evaluation of a  
pseudo-histological staining and image processing system  
for use in point-of-care *ex-vivo* fluorescence histology**

A DISSERTATION

SUBMITTED ON MARCH 29, 2018

TO THE DEPARTMENT OF BIOMEDICAL ENGINEERING

IN PARTIAL FULFILLMENT OF THE REQUIREMENTS

OF THE SCHOOL OF SCIENCE AND ENGINEERING

OF TULANE UNIVERSITY

FOR THE DEGREE

OF


DOCTOR OF PHILOSOPHY

BY



Katherine Nicole Elfer

APPROVED:

  
Quincy Brown, Ph.D.,  
(Committee Chair)

  
Andrew Sholl, M.D.

  
Kristin Miller, Ph.D.

  
Carolyn Bayer, Ph.D.



**THIS PAGE INTENTIONALLY LEFT BLANK**

## ACKNOWLEDGEMENTS

This work, and all the of the written and unwritten components, could never have been successful without the support of the wonderful mentors, colleagues, friends, and family who have directly and vicariously participated in its creation.

I would like to extend my everlasting gratitude to my advisor and mentor, Dr. Quincy Brown, for his guidance in laying the framework of my career in research, his support of my career goals and interests, and his patient mentorship in all aspects of my professional development. To Dr. Andrew Sholl, I offer my thanks for an introduction to the language of medicine and his constant willingness to try something new, and a little bit odd, for the sake of science. I also thank Dr. Kristin Miller and Dr. Carolyn Bayer, for their help in reviewing my work and continued guidance in research. Together, as my dissertation committee, you have set aside time outside of your schedules to aid in my success, and I sincerely thank you for your ideas and guidance.

I also would like to acknowledge the entirety of the current and former faculty and staff of the Department of Biomedical Engineering at Tulane University. In particular, John Sullivan, Cindy Stewart, Rebecca Derbes, and Lorrie McGinley all have had a direct hand in my health and success in my time here at Tulane. Beyond our department, Tulane University's administration and staff have served as mentors throughout my graduate career: Dr. Michelle Sanchez, Dr. Red Tremmel, Dr. Janet Ruscher, Dr. Michael Cunningham, Jennifer O'Brien, and Briana Mohan have each acted as a personal coach and mentor during my time here.

Research is a collaborative effort, and all my lab mates and collaborators, named and unnamed, have contributed to the success of this work. To name their individual contributions would make an unending list, but Dr. Mei Wang, David Tulman, Bihe Hu, Peter Lawson, Zhuge

Huimin, and Samuel Luethy have all brightened every work day with their intellect, humor, and dedication to our work.

Even graduate students must take time off from work and, for their constant reminders to focus on life outside of research, I would like to acknowledge my friends for their understanding and support. Jaicee Choate, Landon Meyer, Jason Ryans, Samantha Swanhart, and Ashwin Sivakumar have been with me the entirety of this journey. My friends, Nicholas Fears, Lydia Crawford, Dr. Cooper Battle, Dr. Jordan Adams, and Dr. Samantha Lantz were invaluable for their help in professional and personal development throughout my time at Tulane. Dr. Chastain Aalis Anderson, thank you.

Most of all, I would like to thank my parents. My robotics coach, the second part of my two-member science-fiction book club, and father, Norman Elfer, has freely given his support, acceptance, and encouragement throughout my life. He taught me that STEM accepts everyone and that failure is a welcome part of science. My mother, Mary Elfer, has given me her love and the understanding that life will become difficult but it is how I react to those circumstances that will allow me to succeed past every expectation.

## TABLE OF CONTENTS

<b>ABSTRACT</b>	<b>1</b>
<b>ACKNOWLEDGEMENTS</b>	<b>II</b>
<b>CHAPTER ONE: INTRODUCTION AND MOTIVATION</b>	<b>1</b>
<b>CHAPTER TWO: BACKGROUND</b>	<b>5</b>
2.1 HISTORY OF MICROSCOPY	5
2.2 INTRODUCTION TO BRIGHT FIELD MICROSCOPY	6
2.3 INTRODUCTION TO FLUORESCENCE MICROSCOPY	9
2.4 PATHOLOGICAL APPLICATIONS OF MICROSCOPY IN PATHOLOGY	14
2.4.1 <i>Tissue Processing: Fixation and Cutting</i>	14
2.4.2 <i>The Hematoxylin and Eosin Stain</i>	16
2.4.3 <i>Specialized Pathological Stains</i>	19
2.4.3 <i>Non-Microscopy Methods in Pathology</i>	21
2.5 INTRODUCTION TO FLUORESCENCE HISTOLOGY	23
2.5.1 <i>Relevance in point-of-care pathology</i>	25
2.5.2 <i>Need for improvement before adoption</i>	28
2.6 PATHOLOGICAL APPLICATIONS OF IMAGE PROCESSING	30
2.7 CLOSING REMARKS	31
<b>CHAPTER THREE: DEVELOPMENT OF D&amp;E FOR FLUORESCENCE HISTOLOGY</b>	<b>33</b>
3.1 INTRODUCTION	33
3.2 IDENTIFICATION AND DEVELOPMENT OF A H&E ANALOGUE	37
3.3 APPLICATION OF A PSEUDOCOLOR ALGORITHM	38
3.4 CHARACTERIZATION OF D&E ON TISSUE SECTIONS	45
3.5 CONCLUSION	49
<b>CHAPTER FOUR: MONOCHROME VERSUS DUAL COLOR FLUORESCENCE HISTOLOGY ON THICK TISSUE</b>	<b>51</b>
4.1 INTRODUCTION	51
4.2 OPTIMIZATION OF ACRIDINE ORANGE AND DRAQ5 AND EOSIN ON FRESH, INTACT TISSUE	53
4.3 APPLICATION OF D&E ON FRESH, INTACT, SURGICAL SPECIMENS	59
4.3.1 <i>Pathological review of intact, whole biopsy D&amp;E</i>	60
4.3.2 <i>First demonstration of fluorescence histology on an intact prostatectomy specimen</i>	65
4.4 COMPARISON OF ACRIDINE ORANGE AND D&E ON FRESH PROSTATE BIOPSIES	66
4.4.1 <i>Comparison of Acridine Orange and D&amp;E on Fresh Prostate Biopsies</i>	68
4.4.2 <i>Diagnostic analysis of monochrome and dual-color fluorescence imaging</i>	69
4.4 COMPARISON OF TIME, COST, AND INSTRUMENTATION	80
4.5 CONCLUSION	82
<b>CHAPTER FIVE: DOWNSTREAM ANALYSIS</b>	<b>84</b>
5.1 INTRODUCTION	84
5.2 FLUORESCENCE PERSISTENCE IN FORMALIN FIXED, PARAFFIN EMBEDDED PROCESSING	84
5.2.1 <i>Testing Fluorescence Persistence in FFPE Tissue</i>	85
5.2.2 <i>Results of FFPE Processing on SBR</i>	86
5.2.3 <i>Conclusion of FFPE effects on fluorescence histology</i>	92
5.3 IMPACT OF FLUORESCENCE HISTOLOGY ON PCR PREPARATION AND RESULTS	94
5.3.1 <i>Methods for PCR Evaluation of Fluorescence Histology</i>	95
5.3.2 <i>Results for PCR Evaluation of Fluorescence Histology</i>	98

5.3.3 Conclusions for PCR Evaluation of Fluorescence Histology	105
5.4 IMPACT OF FLUORESCENCE HISTOLOGY ON IMMUNOHISTOCHEMISTRY	105
5.4.1 Methods for IHC Evaluation of Fluorescence Histology	107
5.4.2 Results for IHC Evaluation of Fluorescence Histology	109
5.5 CONCLUSIONS FROM DOWNSTREAM ANALYSIS OF FLUORESCENCE HISTOLOGY	114
<b>CHAPTER SIX: EXPANSION OF HISTOLOGY</b>	<b>116</b>
6.1 INTRODUCTION	116
6.2 IDENTIFICATION OF FLUORESCENT COMPONENTS IN TRICHROME AND PAS SLIDES	117
6.3 CHOOSING A SPECTRALLY-COMPATIBLE NUCLEAR COUNTERSTAIN	122
6.4 APPLICATION OF A PSEUDOCOLOR ALGORITHM	124
6.5 CHARACTERIZING FLUORESCENCE HISTOLOGY IN FFPE SECTIONS	128
6.6 CONCLUSIONS	134
<b>CHAPTER SEVEN: DISCUSSION</b>	<b>136</b>
<b>APPENDIX</b>	<b>147</b>
APPENDIX A: ACRONYMS AND DEFINITIONS	147
Common Acronyms	147
Microscopy Acronyms	147
Pathology Acronyms	147
Molecular Analysis Acronyms	147
Chemical Acronyms	147
APPENDIX B: PCR PRIMERS	148
APPENDIX C: PSEUDOCOLOR PROGRAMS	148
D&E Pseudocolor	148
Masson's Trichrome Pseudocolor	149
PAS Pseudocolor	151
<b>REFERENCES</b>	<b>153</b>
<b>BIOGRAPHY</b>	<b>162</b>

## LIST OF TABLES

<b>Table 4.1:</b> Results of a blind review of prostate cancer as viewed with either monochrome contrast (AO staining) or dual-color contrast (D&E staining).....	<b>77</b>
<b>Table 5.1:</b> Results of pathologist evaluation of IHC FFPE sectioned tissue. ....	<b>111</b>

## LIST OF FIGURES

<b>Figure 2.1:</b> Beer's Law.....	<b>7</b>
<b>Figure 2.2:</b> Trans Illumination Microscopy. ....	<b>8</b>
<b>Figure 2.3:</b> Jablonski Diagram: Fluorescence.....	<b>10</b>
<b>Figure 2.4:</b> Beer's Law: Fluorescence.....	<b>12</b>
<b>Figure 2.5:</b> Fluorescence Microscopy.....	<b>13</b>
<b>Figure 2.6:</b> H&E Sections: FFPE vs FSA.....	<b>18</b>
<b>Figure 2.7:</b> Masson's Trichrome Stained Section. ....	<b>20</b>
<b>Figure 2.8:</b> Periodic Acid-Schiff Stained Section.....	<b>21</b>
<b>Figure 2.9:</b> Fluorescence Histology Workflow. ....	<b>25</b>

<b>Figure 2.10: Rapid On-Site Evaluation with Fluorescence Histology.....</b>	<b>27</b>
<b>Figure 3.1: Acridine Orange Binding. ....</b>	<b>34</b>
<b>Figure 3.2: Acridine Orange Stained Prostate Biopsy. ....</b>	<b>35</b>
<b>Figure 3.3: DRAQ5 Binding. ....</b>	<b>36</b>
<b>Figure 3.4: D&amp;E and H&amp;E Comparison of Prostate Section. ....</b>	<b>41</b>
<b>Figure 3.5: Nuclei Staining Comparison: D&amp;E vs H&amp;E. ....</b>	<b>42</b>
<b>Figure 3.6: D&amp;E and H&amp;E Nuclei Segmentation.....</b>	<b>43</b>
<b>Figure 3.7: D&amp;E and H&amp;E Nuclear Quantification.....</b>	<b>44</b>
<b>Figure 3.8: FFPE Sections: D&amp;E vs H&amp;E. ....</b>	<b>47</b>
<b>Figure 3.9: Frozen Sections: D&amp;E vs H&amp;E.....</b>	<b>48</b>
<b>Figure 4.1: Schematic of the VR-SIM System.....</b>	<b>55</b>
<b>Figure 4.2: Time and Concentration Effects with DRAQ5. ....</b>	<b>56</b>
<b>Figure 4.3: Time, Concentration and Solvent Effects with Eosin. ....</b>	<b>57</b>
<b>Figure 4.4: Visual Comparison of Solvents Effects with Eosin. ....</b>	<b>58</b>
<b>Figure 4.5: D&amp;E Fresh and H&amp;E Section of Kidney Biopsy. ....</b>	<b>61</b>
<b>Figure 4.6: D&amp;E Fresh and H&amp;E Section of CCRC Kidney Biopsy.....</b>	<b>63</b>
<b>Figure 4.5: D&amp;E Fresh and H&amp;E Section of Prostate Biopsy.....</b>	<b>64</b>
<b>Figure 4.8: D&amp;E of a Prostate Margin Posterior Surface.....</b>	<b>66</b>
<b>Figure 4.9: AO, D&amp;E, and H&amp;E of Prostate Biopsies.....</b>	<b>70</b>
<b>Figure 4.10: AO, D&amp;E, and H&amp;E of Benign Prostatic Glands.....</b>	<b>72</b>
<b>Figure 4.11: AO, D&amp;E, and H&amp;E of Chronic Inflammation in Prostate Biopsies. ....</b>	<b>74</b>
<b>Figure 4.12: AO, D&amp;E, and H&amp;E of Prostate Cancer in Prostate Biopsies.....</b>	<b>76</b>
<b>Figure 4.13: AO, D&amp;E, and H&amp;E Economic, Histological Comparison. ....</b>	<b>81</b>
<b>Figure 5.1: SBR Tracking of Control in Kidney Biopsies. ....</b>	<b>87</b>
<b>Figure 5.2: SBR Tracking of D&amp;E and AO in Kidney Biopsies. ....</b>	<b>88</b>
<b>Figure 5.3: SBR Tracking of 470nm Excitation Across FFPE Processing.....</b>	<b>89</b>
<b>Figure 5.4: SBR Tracking of 640nm Excitation Across FFPE Processing.....</b>	<b>90</b>
<b>Figure 5.5: DRAQ5 Nuclear Specificity Across FFPE Processing.....</b>	<b>92</b>
<b>Figure 5.6: Methodology for Measuring Impact of Fluorescence Histology on Fluorescence Measurements of Downstream DNA Analysis.....</b>	<b>98</b>
<b>Figure 5.7: Results of A260/A280 DNA Concentration Measurements.....</b>	<b>99</b>
<b>Figure 5.8: Results of RT-PCR Runs Post-Fluorescence Histology. ....</b>	<b>101</b>
<b>Figure 5.9: Results of Gel-Electrophoresis Post-Fluorescence Histology.....</b>	<b>104</b>
<b>Figure 5.10: Positive Control Sections of PAX8 and CK-7 IHC.....</b>	<b>107</b>
<b>Figure 5.11: Methodology for Analyzing Impact of Fluorescence Histology on IHC. ....</b>	<b>108</b>
<b>Figure 5.12: Images of the Results of the IHC Analysis Methodology.....</b>	<b>110</b>
<b>Figure 5.13: ROIs of IHC Stained Fluorescent and Control Specimens.....</b>	<b>111</b>
<b>Figure 6.1: Control Slide of Periodic Acid-Schiff Section with Fluorescence Imaging.....</b>	<b>119</b>
<b>Figure 6.2: Control Slide of Masson's Trichrome Section with Fluorescence Imaging.....</b>	<b>120</b>
<b>Figure 6.3: Fluorescence Imaging of the Components of the Masson's Trichrome Stain ...</b>	<b>121</b>
<b>Figure 6.4: Pseudocoloring of Masson's Trichrome Fluorescence Staining.....</b>	<b>126</b>
<b>Figure 6.5: Pseudocoloring of Periodic Acid-Schiff Fluorescence Staining.....</b>	<b>127</b>
<b>Figure 6.6: Masson's Trichrome Pseudocolor Comparison in Kidney.....</b>	<b>130</b>
<b>Figure 6.7: Masson's Trichrome Pseudocolor Compariosn in Liver.....</b>	<b>131</b>
<b>Figure 6.8: Periodic Acid-Schiff Pseudocolor Comparison in Kidney.....</b>	<b>132</b>
<b>Figure 6.8: Periodic Acid-Schiff Pseudocolor Comparison in Liver.....</b>	<b>133</b>
<b>Figure 7.1: Pipeline for Developing Fluorescence Histology Stain Systems.....</b>	<b>140</b>

## CHAPTER ONE: Introduction and Motivation

Real-time fluorescence imaging of *ex vivo* tissue provides an accelerated avenue to patient biopsy screening, definitive diagnosis, and surgical guidance. The current gold-standard histopathology preparation, formalin-fixation paraffin embedding (FFPE) and hematoxylin and eosin (H&E) staining, and other specialized histology stains needed for differential diagnosis or tissue composition analysis, require processing time on the order of hours or days, which is infeasible for use in point-of-care screening [1,2]. Point-of-care tissue diagnostics should be rapid, accurate, easy, cheap, and non-destructive. Tumor surgical margin analysis, bedside biopsy review, and quality assessment of biobanked tissues are all situations where rapid, on-site histology is required for adequate care. The less care is delayed, the better the patient outcomes. However, the current techniques used to address this problem are frozen section analysis and touch preparation which, respectively, are destructive and do not provide complete, accurate information on biopsy content. With the recent advances in *ex vivo* optical sectioning microscopy, fluorescence histology, a method to fluorescently stain and optically section tissue for non-destructive analysis, has been proposed to provide comprehensive *ex vivo* tissue review in the clinic [2]–[6].

A known difficulty in histopathology is that each pathologist is unique in their training and review of specimens, leading to inconsistencies in diagnostic decision-making and poor reproducibility in grading disease even with gold-standard H&E [3,4,7,8]. The introduction of fluorescence histology requires additional training and different modalities open the possibility for further interpretation error. We hypothesize that by combining a H&E-pseudocolor algorithm with topical fluorescent stains that have similar histochemical specificity as H&E we can create a diagnostically accurate fluorescent histology tool for rapid tissue screening. The combination of

DRAQ5, a DNA-exclusive far-red nuclear stain, and eosin Y, a histological dye and green-fluorescing anionic stain, is used to create a fluorescent analogue to H&E. This fluorescent analogue (“D&E”) can potentially provide greater accuracy than less specific stains reported in the literature, interfering with downstream molecular and genetic analysis of the tissue. Additionally, we hypothesize that by identifying fluorescent alternatives to other common histology stains, such as the connective tissue stain Masson’s Trichrome and the carbohydrate stain Periodic Acid Schiff, we will increase the versatility of fluorescence histology in both research and the clinic. The purpose of this work is to advance the concept of fluorescence histology toward routine applications in the clinic and laboratory while maintaining compatibility with standard downstream tissue analysis, as an adjunct or replacement for outdated traditional methods when fast, nondestructive, and three-dimensional results are desired. The goals of this work were achieved using the following framework:

**Aim 1 Develop a topical fluorescent H&E-analogue and image processing system for clinical use to aid researchers and pathologists in diagnosis by providing comparable information to FFPE H&E.**

- 1.1** Identify and develop DRAQ5 & Eosin (D&E) as a fluorescent stain system on fixed and frozen tissue sections
- 1.2** Apply pseudocolor image processing to fluorescently stained tissue to mimic the appearance of H&E
- 1.3** Characterize D&E diagnostic performance compared to H&E information on fixed and frozen tissue sections

We hypothesize that a histochemical and spectral fluorescent analogue for formalin fixed, paraffin embedded (FFPE) H&E, along with pseudo coloring, will make it possible to replicate the appearance of bright field H&E on fixed, frozen, or fresh tissues. The combination of DRAQ5, a nuclei specific fluorescent stain, and eosin Y, an original fluorescent component of H&E can provide a means to identify and diagnose tissue via fluorescence histology.

**Aim 2 Characterize and optimize DRAQ5, Eosin Y, and Acridine Orange as fluorescent stains for clinical examination of fresh biopsies and surgical margins.**



- 2.1** Optimize Acridine Orange and D&E for use on fresh, intact biopsies and other non-sectioned tissue
- 2.2** Compare the information provided by Acridine Orange and D&E to H&E by a blind pathological review
- 2.3** Compare the impacts of time, material cost, and system requirements of using Acridine Orange versus D&E

DRAQ5 and eosin Y, a spectrally compatible fluorescent analogue for H&E, mimics the histochemical behavior and appearance of H&E. By combining the fluorescent stain system on thick, uncut tissue with optical sectioning microscopy we will be able to create a rapid, accurate, and non-destructive alternative to both standard fluorescence imaging of tissue and traditional point-of-care histology evaluation methods.

**Aim 3** Determine the compatibility of D&E and Acridine Orange with downstream DNA quantification and molecular analyses.

- 3.1** Investigate the duration and intensity of fluorescence in fresh biopsies during H&E processing
- 3.2** Investigate the impact of topical fluorescent stains on the molecular techniques: DNA purity quantification, RT-PCR analysis, and gel electrophoresis
- 3.3** Investigate the impact of topical fluorescent stains on immunohistochemistry

The addition of fluorescent agents has the potential to interfere with later diagnostic processing of tissue. By examining some of the most common tests involved in diagnosis and tissue research, we will determine if there is any interference from the additives and, if so, what form the interference takes. With the aid of a pathologist, we identified the most common pathological tests tissue may undergo are formalin fixation, paraffin embedding; DNA purity quantification; quantitative real time polymerase chain reaction; gel electrophoresis; and immunohistochemistry staining. Quantifying the persistence of fluorescence histology signal in FFPE will determine whether there is the possibility of interference with further fluorescence quantification techniques downstream of preservation and indicate whether the stains can be used for retroactive analysis post-FFPE processing. PCR, which can be used on fresh or fixed tissue, relies on both DNA amplification and fluorescence quantification. Therefore, analyzing

the effects of DNA-intercalating fluorophores and the fluorophores that may interfere with fluorescence analysis is required to determine whether tissue used in fluorescence histology needs modification prior to PCR analysis. Finally, IHC, typically performed on FFPE tissue, is a very sensitive biochemical technique that can be altered by the addition of additional chemicals to the tissue. If there is an indication that stains remain in the tissue after FFPE processing, then IHC could potentially be altered in specimens exposed to fluorescence histology.

**Aim 4 Develop a fluorescence histology analogue in other primary diagnostic histology dyes: Masson's trichrome staining and Periodic Acid-Schiff staining.**

- 4.1** Identify the fluorescent components in Masson's Trichrome and PAS and fluorescent alternatives to their non-fluorescent components on fixed tissue.
- 4.2** Apply pseudocolor image processing to mimic the appearance of the original histology coloration.
- 4.3** Characterize the fluorescent diagnostic performance compared to bright field information on fixed tissue.

For fluorescence histology to be useful in both research and clinical settings, fluorescent analogues to the stains that are used when the pathologist requires more information than H&E can provide, such as the Masson's Trichrome stain and the Periodic-Acid-Schiff reaction, must be examined for potential additions to the fluorescence histology toolset. As with Aim 1, diagnostic utility will be improved by the application of custom pseudocolor processing and the results are characterized against the standard staining of human liver and human kidney tissue.

Together, these aims develop, characterize, and analyze novel methods to achieve fluorescent analogues to standard (i.e. bright field) pathological stains, to further advance the concept of "fluorescence histology" toward widespread application.

## CHAPTER TWO: Background

### 2.1 History of Microscopy

Much of natural history is interested in seeing beyond the constraints of the human eye, whether in terms of distance or size; however, the focus has not been merely on observation but also interpretation of these formerly invisible objects [9]. Microscopy, the study of objects too small to be seen with the human eye, started as a simple series of tubes and lenses to increase magnification of very small objects. The contributions of Antonie van Leeuwenhoek, Joseph Jackson Lister, Robert Hooke, and countless others mean that over the centuries we have increased magnification, reduced lens aberrations and irregularities, and can see what is normally hidden from human perception [9,10]. Since its infancy in 1590, microscopy has become a routine medical, research, and industrial tool [11]. Yet, being able to see microscopic details is only useful when we can also interpret the meaning behind what we see. Leeuwenhoek, colloquially known as the “Father of Microbiology” [9], emphasized the importance of training and repetition in microscopy for accurate interpretations:

No Body must Publish or bring to light, new Discoveries, and judge by one sight, but he must see the same over and over several times, for it doth happen often to me, that People looking through a Magnifying-glass, do say now I see this, and then that, and when I give them better Instructions, they saw themselves mistaken in their opinion, and what is more, even he that is very well used to looking through Magnifying-glasses may be misled by giving too sudden a Judgment, of what he doth see [12].

There are few places where such rote training is as critical as in the medical field, where microscopes are used daily for the interpretation and diagnosis of disease [10,11]. Beyond medicine, microscopy is a critical foundation in many industrial advancements and basic

research innovations. The microscopes of today share little resemblance to the simplistic tubes and lenses of past centuries, but the fundamental principle of using lenses to focus and magnify visible light remains the same [13,14]. It is also possible to combine microscopes with other technology to gather multi-faceted data; data that would be unobtainable with basic microscopy alone. A sample can be imaged with beams of visible light (optical microscopes), electrons, sound, X-rays, radio waves, radiation, and combinations of all the above. Yet, the single most used imaging method remains light microscopy [10,14]. Within the field of light microscopy there are multiple methods to sub-classify instruments, one of which is whether the visualization method depends on the transmission or reflection of light in a sample. In the next section, we focus on the fundamentals of transmission, otherwise known as bright field, microscopy and why it remains the favored tool scientists and clinicians.

## **2.2 Introduction to Bright Field Microscopy**

Bright field, or transmission or standard, microscopy is the oldest microscopy method dating back to the turn of the seventeenth century [9]–[11]. Specimens that are either extremely small or extremely thin (on the order of microns) are illuminated from one side by a white light. Light passes through the specimen, usually placed on a microscope slide, from one side through to the other. The specimen blocks portions of the light, creating contrast, and what light is permitted through is then funneled through a series of magnifying tubes and lenses, to reach a final eyepiece or camera. A specimen needs both transparency and optical contrast for trans-illumination. Most samples, particularly biological specimens, need to be extremely thin for the successful transmission of light through a sample. When a specimen is cut this thin, it loses much of its innate contrast. To enhance contrast, chromatic dyes (chromophores) can be added to the specimen to block the full transmission of light, highlighting specific structures within the

specimen that are of research or diagnostic relevance [15]. As specific wavelengths of the white light are absorbed, the structures bonded to different dyes can take on one or more colors allowing multiple colors in a single specimen to be visualized.

As light passes through a non-opaque medium, such as a microscope slide, a dyed piece of tissue on the slide, and the cover glass protecting the tissue from air, the energy of light is lost in this system. Some of the light is scattered; bounced off molecules in the medium and even reflected towards source of light. Some of the light is absorbed in the system, unable to move further as a photon and transformed into other forms of energy. Therefore, the intensity of light that enters a medium is some relation less than the intensity of light that exits [11, 16]. This relationship is described the Beer-Lambert Law, illustrated in Figure 2.1 below.

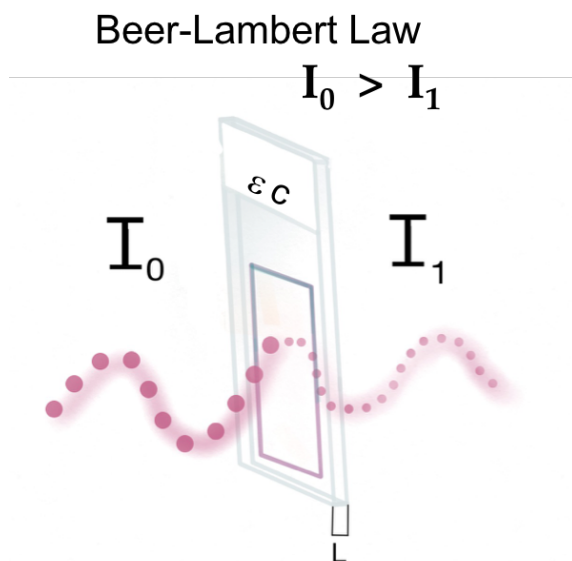


**Figure 2.1:** An illustration of the attenuation of light passing through a microscope slide as modeled by the Beer-Lambert law. The relationship of the intensity on either side of the absorbing medium is determined, in simplification, by the cross-sectional area of the absorbing medium, path length, the absorptivity coefficient ( $\epsilon$ ) of the optical absorbers, and the concentration of the absorbers in the material.

An example of a common dye-system applied to microscopy specimens is the hematoxylin and eosin Y (H&E). Hematoxylin stains nuclei blue-purple and eosin Y is an anionic counterstain

that appears bright pink-red. The dyes are applied to a thin section of tissue, then the tissue is rinsed, covered with a very thin glass (a microscopy coverslip) and imaged with a bright white light. When combined, the dyes in the tissue give morphological context to cellular structures and tissue histology. A simplistic explanation of bright field microscopy is depicted in Figure 2.2. The light is focused through the microscope's condenser lens into the specimen, which is then diffracted by the details within the specimen. The objective collects the diffracted light into a single image plane, creating a resultant image, viewed by either an eyepiece or camera.

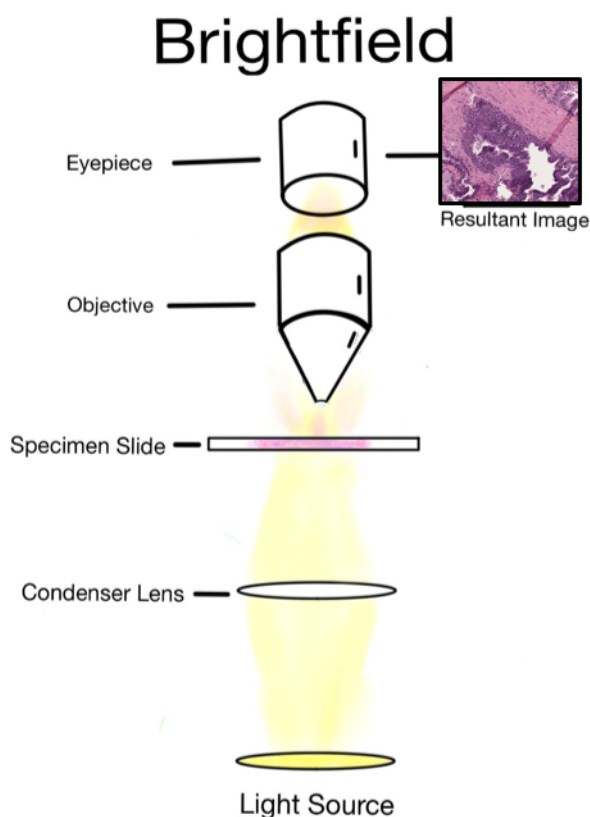


**Figure 2.2:** An example optical train for a standard transmission light microscope. The resultant image is created from the subtraction of light where chromophores are added to the specimen creating areas of dark colors against a bright background.

Bright field microscopy is the most common form of microscopy as its components are cheap, require little training, and has been utilized in a variety of applications for well over a century [15]. In spite of its ubiquitous use and low cost, transmission microscopy has limitations that make it impractical for many of the applications that modern research and medicine now require. The foremost problem, and the most physically difficult to overcome, is the need for transparency that can only be achieved by cutting the tissue into very thin sections [2–4]. Both the requirement for transmitted light and its resolution limit necessitated the development of other microscopy techniques.

### **2.3 Introduction to Fluorescence Microscopy**

A fluorescent microscope can share many similarities with standard bright field microscope in both construction and use, except for the light traveling through the system. In this form of imaging, a fluorophore, which can be endogenous or exogenous to the sample, is excited by high intensity, highly specific wavelengths of visible light. Upon irradiation of light, a fluorophore will absorb a photon of a given quantum energy (given wavelength), causing a transition in the molecule from a quiescent ground state to an excited state. Each fluorophore molecule has an energy gap between these two states of differing amounts, therefore different wavelengths will excite different fluorophores. Although a fluorophore can be excited by less ideal wavelengths, higher densities of input photons are needed to achieve the same effect that can be achieved with targeted wavelengths centered at the excitation maximum wavelength of the fluorophore [17].

In its excited state, an electron in the fluorophore molecule will move to a higher atomic orbital, but the extra energy cannot sustain itself. As the electron relaxes back into the ground state, energy is shed from the system. The resultant energy can dissipate in many ways, including thermal energy or the release of another photon. In the case of fluorescence, a small amount of

energy is lost to non-radiative processes, followed by release of a photon, in which the photon will consist of less energy and a longer wavelength than the original exciting photon. The difference in energy between the two photons is referred to as Stoke's Shift, or red shift for its movement towards the red end of the visible light spectrum [13,18,19]. In Figure 2.3 a Jablonski diagram illustrates the energy path through a fluorescent system.

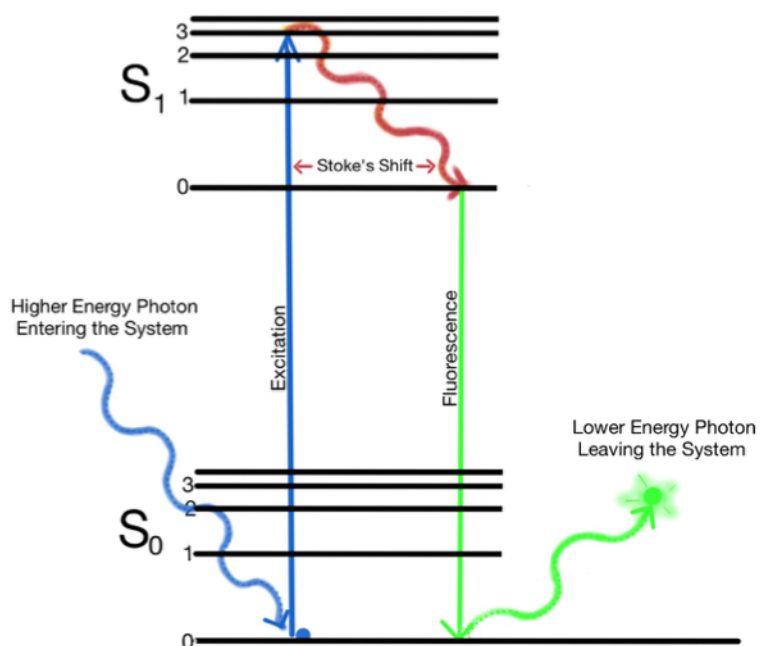


**Figure 2.3:** A Jablonski Diagram depicting a high energy (short wavelength) photon inducing fluorescence by exciting an electron within a system to a higher energy state. As the electron relaxes back to the ground state, some energy is lost to the system and the rest is released by emitting a photon of a lower energy (longer wavelength) than the original, exciting photon.

Fluorescence microscopy uses fluorophores as its contrast mechanism. When the fluorophores in a tissue release a photon upon relaxation, the areas of tissue containing that fluorophore are visualized by imaging the emitted photons. Therefore, in a general fluorescent system there are two types of light that need to be controlled: the excitation wavelength and the



emission wavelength [17,18]. Being able to isolate these photons of different energies is a necessary component of fluorescence microscopy. The fluorescent microscope will contain many of the parts of a bright field microscope but also include a series of special filters for wavelength separation. An excitation filter allows the desired wavelengths of light to pass through the system to the sample, but the secondary barrier filter (typically in the form of a dichroic beam splitter and emission filter in series) prevents all but the emitted photons from passing through to the eyepiece or microscope camera.

The core visualization difference between these two optical microscopy methods is that bright field microscopy is the subtraction of light from the system (via absorption) and fluorescence microscopy is addition of light (signal at alternate wavelengths) to the system. Bright field microscopy's transmission method means that the image is comprised of the combination of light that passes through and blocked by the dyes in the sample (dark against a bright background); whereas, a fluorescent image is the result of the light generated by the fluorophores in the sample. Typically, fluorescent images are rendered as bright areas of signal against a dark background. Remembering the previous modeling of light passing through a microscope with Beer's Law, a comparison of fluorescence microscopy is that light changes, but intensity changes are comparatively much lower. This change is depicted in Figure 2.4 for the Beer-Lambert Law modeling fluorescence.

## Beer-Lambert Law Fluorescence

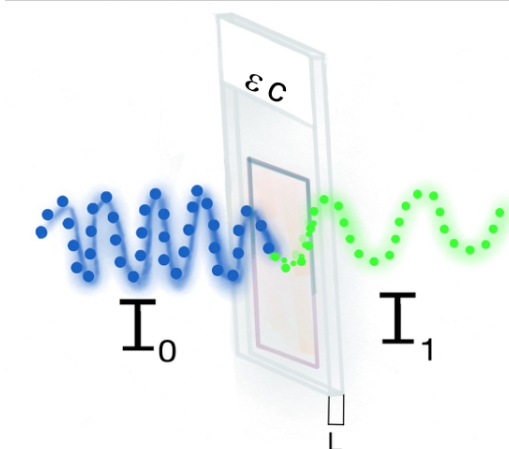


**Figure 2.4:** An illustration of the fluorescence phenomena as modeled by the Beer-Lambert law. The excited fluorophores emit photons, thereby adding signal to the system rather than losing overall intensity.

High quality images are those with a high signal intensity compared to the background intensity, called signal-to-background ratio [14,17]. Therefore, fluorophores with a high quantum yield, as well as those with specific known binding like standard chromophores, are preferred and contribute to higher sensitivity to dye concentration than absorption based methods [15,17]. As fluorescence microscopy increases in prominence, there has been a corresponding increase in the synthesis of fluorophores to meet the needs of researchers: spectral, chemical, and biological capabilities are all balanced to suit the desired outcome.

Arguably the greatest advantage of fluorescence microscopy is the potential for epifluorescence. Epi-illumination is the ability to view samples from the same side as that being illuminated, allowing thicker and/or more opaque samples to be imaged than could normally be accomplished. With epifluorescence, the excitation light penetrates the tissue to excite the

fluorophores within, but instead of the emitted light needing to transmit through the rest of the sample, the light that is 'reflected' into the system is collected for the image (Figure 2.5) [17,19].

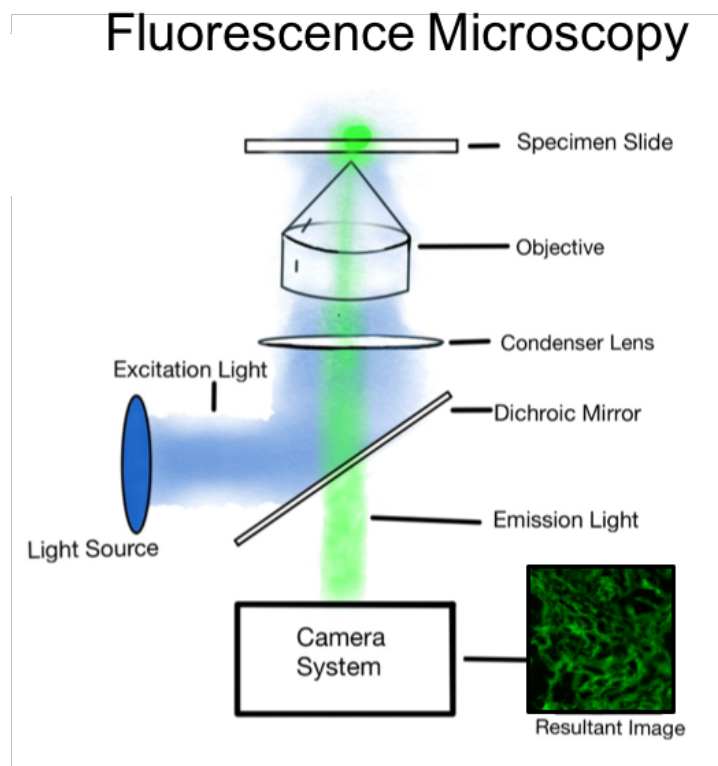


**Figure 2.5:** Optical train for an epi-fluorescence microscope. Light of a specific wavelength is funneled through the system, through the emission filter, and into the sample. The fluorophores in the sample are excited and emit photons of a longer wavelength than the excitation light. This light is channeled back through the system into viewing port. The resultant image is created from the addition of light where fluorophores are excited in the specimen.

This imaging method means that if a photon can reach the fluorophore, and the photon from the fluorophore can make it back into the system (considering scattering, absorption, and reflection phenomena), the thickness of the sample does not impede imaging. Furthermore, by controlling the detection of in-focus and out-of-focus illumination, it is possible to image a single point or plane within a specimen and obtaining a thin optical section of the intact tissue. With the use of epi-fluorescence microscopy, highly specific stains can be used in combination with thicker samples, thereby surmounting the current limitations of bright field microscopy [2, 14].

## **2.4 Pathological Applications of Microscopy in Pathology**

Pathology is the evaluation and diagnosis of disease and pathologists are the medical doctors charged to interpret various analyses needed to make the diagnosis [10, 20]. Once, pathologists may have reasonably expected to spend the large majority of their work looking through a bright field microscope at multiple slides along with overseeing the occasional batch of medical students. With the advancement of technology for molecular analyses, laboratory medicine, medical imaging, and disease screening, there has been a corresponding increase in the amount of data a single piece of tissue can provide. However, one of the oldest tools of diagnosis, histology – the microscopic study of tissues, is still a significant portion of a disease identification and staging [10,11,21].

Histology is the study of both the structural and functional aspects of biological materials, and the primary tool in the field is the bright field microscope [11,22]. Medical specimens are evaluated with microscopy for most preliminary evaluations, and the result of these evaluations usually guide further advanced analyses. Histological evaluation of tissue typically consists of the same steps: fixation, cutting, application to a microscope slide, and staining with one or more contrast agents [15].

### **2.4.1 Tissue Processing: Fixation and Cutting**

Histological analysis requires that the specimen be preserved with minimal alteration from its original composition and thin enough to allow the passage of light through a sample. Fixation is the term applied to the multiple methods used to preserve the tissue and consists of two broad categories: physical fixation methods and chemical fixation methods [15, 23]. Physical methods comprise of the application or removal of heat from a specimen. Small specimens can be

rapidly and highly accurately fixed by using a microwave oven in combination with chemical fixatives to promote diffusion of chemicals in the tissue, but larger samples can create temperature differentials that damage the specimen [15]. Freezing the sample is another alternative and the one most commonly used for rapid on-site evaluation (ROSE) of biopsies [24–26]. Freezing tissue can result in the formation of ice crystals that tear the specimen making later analysis difficult [27–29]. This frozen artifact is minimized by reducing the size of the specimen and the application of cryoprotective agents. The ideal cryopreservation is a mixture of immersion in a solution and a freeze on the order of a few hours. However, even a few hours are too short for ROSE. Snap-freezing for frozen section analysis is the standard ROSE fixation method, but the variation within tissue and short time frame mean that frozen artifact is frequently a concern [29–31] and studies have shown that it is best paired with another method, touch preparation cytology, for the most accurate results [25,32,33].

For every chemical fixative method, there is also a drawback to its use - whether in penetration time, physical shrinkage or swelling of the tissue, hardening of the tissue, or interaction with molecular components of the tissue and additive dyes [15,23]. The gold-standard chemical fixative used in pathology labs is 10% formalin, a formaldehyde solution. It has a reasonably fast penetration time (on the order of hours with samples a couple of centimeters thick), but the permanent effects of formalin can take over a week to develop. Formalin preserves tissue volume, lipids, and enzyme reactions, but it causes excessive hardening and result in molecular changes with prolonged storage. It also minimally interacts with both cationic and anionic dyes, making it useful for histological analysis. Other common chemical fixatives include ethanol and picric acid. While ethanol is non-toxic compared to most fixatives and very fast acting, it causes extreme shrinkage and destroys cell organelles, thus making it suitable only for very small samples like smears and sections. Picric acid is a slow fixative agent that is easily

removed from tissue with water and useful because of its strong chemical interactions with tissue and ability to also act as a stain. However, its slow penetration and tissue distortion when used alone means that picric acid is typically used in conjunction with other fixative agents. The most common picric acid combination is Bouin's fixative solution, which also includes the fixatives formalin and acetic acid [15]. In combination, the hazards of these fixatives are outweighed by their usefulness with multiple dyes and for specialized stains.

Once the tissue has been fixed, it needs to be cut into sections thin enough for viewing with a trans-illumination microscope. Frozen sections, such as those used for ROSE analysis, are embedded in an optimal cutting temperature (OCT) compound then cut to the several micron thick sections using a cryostat. Although OCT provides some protection from both temperature and physical damage, it is still easy to tear the tissue even under ideal conditions [11,29]. When the time needed for complete preservation is possible, the tissue is fixed in formalin, dehydrated, cleared in xylene or a derivative as preparation for molten paraffin wax infiltration, and embedded in a solidified paraffin wax block. This process is referred to as formalin fixed, paraffin embedded (FFPE) tissue and is the gold standard for pathological tissue analysis. The entire process takes multiple hours as fixation, dehydration and clearing, infiltration, and embedding takes several hours to complete for each step. Tissue larger than 3mm can take more than a day simply for dehydration and wax infiltration. From the paraffin block, the tissue can be cut into very thin sections with little distortion. However, unlike frozen sections which can be stained immediately after cutting, the FFPE sections must have the paraffin wax removed with a xylene and then dehydrated through ethanol to remove the xylene before any staining can be completed [15].

#### **2.4.2 The Hematoxylin and Eosin Stain**

Simply cutting the tissue will not provide enough optical contrast for diagnostic analysis. Exogenous dyes, called chromophores, are added to the tissue to create this contrast. A chromophore both binds to the components in a sample and contains a chromogen to block out light while lending color to the tissue. There are multiple methods that chromophores can bind with a substrate: electrostatic interactions; hydrogen bonding; hydrophobic interaction; and with the aid of intermediary substances, such as mordant binding. Multiple chromophores can be used in a single specimen, isolating different features or providing context for viewing. Of all stains in use for pathology, the hematoxylin and eosin Y pairing, and its variants, is the most versatile and widely used stain system in pathology [11].

As briefly mentioned previously, hematoxylin and eosin Y (H&E) is considered the gold-standard of histological stains [34–36] as it provides useful preliminary information on tissue architecture prior to more advanced analysis [11,15]. H&E stains nuclei a dark color (shades of blue, purple, and black are all common based on the specific method) and counterstains the cytoplasm and extracellular matrix a lighter contrasting color (pink to dark red based on tissue and methods). Figure 2.6 shows both the appearance of H&E in tissue and how different fixation and sectioning methods can alter the appearance of the tissue.

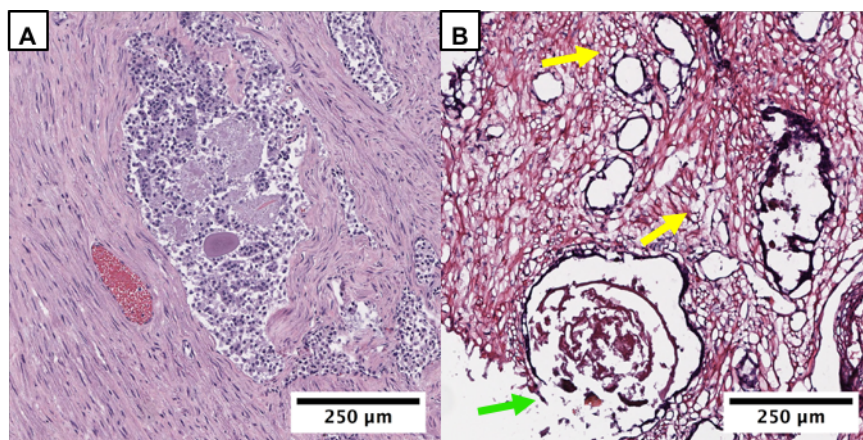


**Figure 2.6:** Prostate biopsies stained with H&E from a FFPE section (A) and a frozen section (B) with areas of frozen artifact from the formation of ice crystals in the tissue (yellow arrow) and tearing of the tissue (green arrow).

As shown in Figure 2.6 B, frozen section analysis can easily result in torn and distorted tissue, which impairs pathological evaluation. Even though the same stain is used, it is much more difficult to identify nuclei in the tissue and the frozen artifact gives the same appearances as lipid droplets in the tissue. For this reason, when describing H&E as the gold-standard of histology, it is the entire FFPE H&E process that is being referenced.

H&E was first reported as a two-dye sequential method in the 1874 and remains the most fundamental stain of histology [22]. Both hematoxylin and eosin are very cheap and easy to use, lending themselves well to teaching, diagnostic, and commercial use [15]. Eosin, a fluorescein derivative, is well-understood as an anionic dye which binds to the cationic groups of proteins and other positively charged molecules. The hematoxylin stain is obtained by extracting hematoxylin (the original component in the stain) from a tree found in South America, but must be oxidized into haematin, which then forms a metal complex with aluminum to create the stain haemalum. Haemalum is much less commonly used, however, therefore this text will refer to the haemalum stain by its colloquial name, hematoxylin [15,36]. As a metal-mordant stain, hematoxylin mixes with a metal salt usually aluminum or iron ions, or in specialized cases



chromium or copper ions, to stain nuclei and other metal-complexing components. Hematoxylin reliably and strongly stains nuclei regardless of DNA content and one mechanism suggested for its staining ability is an extremely high affinity for chromatin [15]. By using H&E, the overall structure of a tissue and its components can be determined and therefore inform the researcher or pathologist what further specialized stains might be needed for more specific information.

### **2.4.3 Specialized Pathological Stains**

Although H&E is extremely useful to triage samples, it is unsuitable for purposes beyond general tissue architecture, such as gaining molecular information; visualizing anionic components such as the extracellular matrix of connective tissue; glycogens; granules of mast cells; and very fine components that need greater contrast than a single counterstain can provide [11,15]. Therefore, specialized stains are used to provide more information than can be determined with only a H&E stain [34,37–39]. Two of the more common specialized stains used in pathology are the Masson's Trichrome stain and the periodic acid-Schiff stain.

Masson's Trichrome is one of a subset of specialized techniques called trichromes which are particularly useful for investigating connective tissues. Trichromes specifically refer to the combination of two anionic dyes and a heteropolyacid, sometimes called a colorless anionic dye [7,15,40]. They selectively stain collagenous and reticular fibers and basement membranes and, depending on the trichrome, may also stain for other specialized components or use a tertiary stain for nuclei or other features. Although the components of trichrome stains are well known, the exact interactions of the anionic stains with each other and the tissue is still under hypothesis. What is known is that while the heteropolyacid (which can be phosphomolybdic or phosphotungstic acid or both) does not lend color to the specimen, the trichrome stain requires its use for specific and bright staining. The heteropolyacid binds strongly to collagen, and has

long been shown to increase staining specificity of connective tissue stains [41]. Specimens that are to be stained with a trichrome need a specialized fixative, such as Bouin's Solution, to target dye interactions within a specimen and improve the end results [40]. The Masson's' Trichrome uses Bouin's solution, Weigert's iron-hematoxylin, biebrich scarlet-acid fuchsin, phosphomolybdic acid-phosphotungstic acid, and either aniline blue or fast green. Weigert's iron-hematoxylin stains nuclei a dark blue-black and not a core component of the trichrome [15]. Biebrich scarlet-acid fuchsin stains cytoplasm shades of pink while blood cells, keratin and myelin are deep red (Figure 2.7). Collagen is stained blue in this stain, allowing for easy identification of connective tissue disorders.

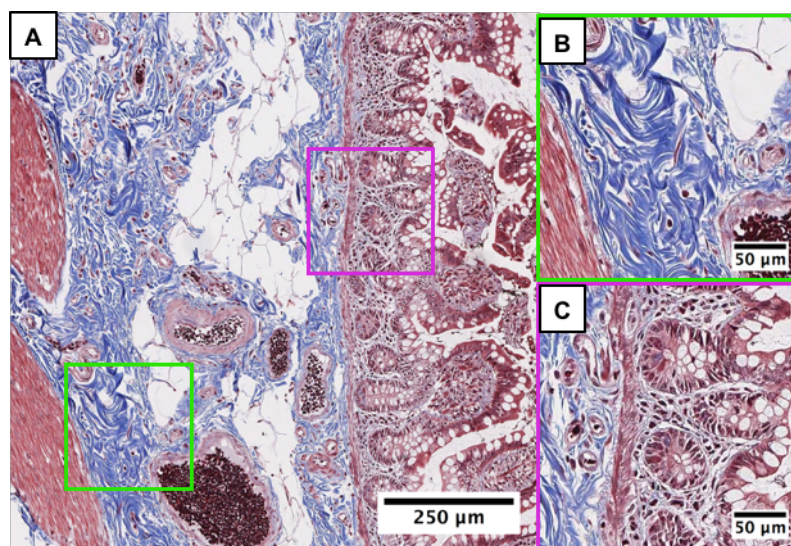


**Figure 2.7:** FFPE sectioned intestinal tissue stained with Masson's Trichrome (A). Areas of higher magnification show detailed histological features, such as blue-stained collagenous fibers and red-stained muscle tissue (green box) and black nuclei with goblet cells (purple box).

Carbohydrate histochemistry is also best observed with methods other than the H&E stain. The Periodic Acid-Schiff (PAS) method is the most common technique used for carbohydrates. It is a positive or negative (PAS+/PAS-) test where positive structures, those

containing neutral hexose sugars and sialic acids, are stained a vivid magenta against negative structures which consist of a paler purple-pink background, as shown in Figure 2.8 [42].

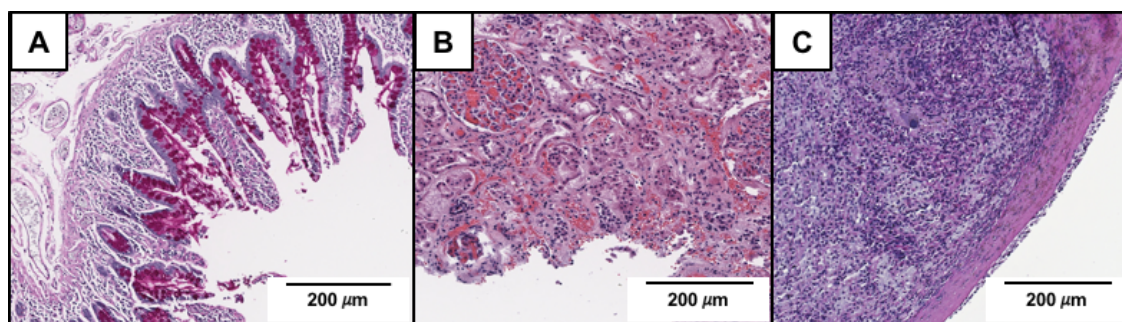


**Figure 2.8:** FFPE sectioned tissue stained with Periodic Acid-Schiff as represented by a positive control slide (A), human kidney tissue (B), and human liver tissue (C).

Here, neutral sugars primarily consist of glucose, galactose, fructose and sucrose and other similar glycols, therefore basement membranes and mucous glands are PAS+ structures [37]. There are two steps to the method, an oxidation via periodic acid and then colorization of the oxidized groups with Schiff's reagent. This stain can be used by itself or is commonly partnered with secondary stains, such as hematoxylin for nuclei, fast green for collagen, and diastase [15]. PAS is routinely used in pathology for kidney, liver, and muscle biopsy evaluation; fungal analysis; and specific pathologies including adenocarcinoma, breast cancer cytology, and Whipple's disease in the small intestine [11].

### **2.4.3 Non-Microscopy Methods in Pathology**

While microscopy is a standard tool for diagnostics, there are many other tools that are useful for providing information on the molecular composition of specimens. Two of the most common techniques for this purpose are the polymerase chain reaction (PCR) and immunohistochemistry (IHC). Both techniques are commonly used in conjunction with standard histology. A pathologist will provide a preliminary report on tissue after viewing it with H&E

and other histological dyes. Based on that report, further testing may be ordered to better differentiate tissue and disease.

The polymerase chain reaction (PCR) has two sub-types: standard, or traditional, PCR and quantitative real time PCR (RT-PCR). Standard PCR uses gel electrophoresis as a positive/negative test for determining whether a specific gene sequence is present in a sample. Multiple types of samples can be used for this purpose, including cultured cells, fresh tissue, FFPE tissue, blood, and non-mammalian cells. The first step after sample acquisition is DNA extraction and purification. Then, the DNA is combined with a polymerase and DNA primers selected for the gene of interest in a thermocycler. The thermocycler alternates between the ideal temperatures for the DNA-primer length to denature the dsDNA, anneal the primers to the relevant DNA segments, and extend the gene sequence of interest through polymerization. The DNA-primer-polymerase mixture cycles for several times (typical is about 40 cycles depending on the desired product, primer, and polymerase). The PCR products are then added to an agarose gel with a dye or fluorescent stain for gel electrophoresis. Small and large products differentiate themselves through movement in the gel, which can be viewed with a UV-illuminator [43].

The preliminary steps to achieve RT-PCR are like that of standard PCR, except the amplification process of the DNA is monitored using UV fluorescence and a fluorophore additive that fluoresce only when bound to the DNA. The RT-PCR (RT-PCR) reaction takes place in a specialized thermocycler which uses fluorescence signal (primarily UV and Blue excitation) to directly measure DNA concentration through the addition of a DNA-binding fluorophore during the length of the reaction. As the amount of product increases, the fluorescent signal also increases [43]. This method is most often used to monitor the amplification products in PCR and to determine the amount of template at the start of the reaction. With RT-PCR, no secondary step after amplification is needed and multiple analyses can be performed based on the type of assay

desired: rate of amplification, melt curve analysis through the dissociation of the fluorophore from the DNA, and gene expression for RNA analysis.

In contrast to the DNA focus of PCR, immunohistochemistry (IHC) uses the antibody binding sites to reveal molecular information separate from typical histological analysis. The principle theory of IHC is that it is possible to covalently bind a dye to antibodies, which then, when bound to their molecular match, will accumulate in specific sites within tissue, thereby lending color to the tissue and creating contrast [44]. Since its start in 1930, immunohistochemistry, and its sister science, immunofluorescence, have been used as a molecular analysis technique to help differentiate their labeling targets in both pathology and basic research [45]. In pathology, IHC is extremely useful as it can provide molecular information within the context of the histological architecture, which is not possible with PCR [38,44]. Along with the primary colorization imparted by the dye-antibody-antigen complex, IHC stains often include a counterstain to aid in both differentiation of the target and provide visualization of the entire microenvironment. With the IHC-counterstain combination, IHC is evaluated in percentages of the areas positively-stained structures compared to the area of the entire specimen [44].

## **2.5 Introduction to Fluorescence Histology**

Accurate analysis of histology requires the expertise of highly-trained pathologists who are accustomed to traditional H&E colorization (dark purple nuclei and pink stroma) [14,20,35]. The gold-standard of histology FFPE's lengthy process is important because it carefully preserves the histologic features relevant to diagnosis while allowing for bright field imaging. In FFPE, the formalin-fixation hardens the tissue so it can be thinly sliced without damaging the chemistry or morphology. However, it can take days for the tissue to then be interpreted by a pathologist who

makes an official diagnosis of disease in the tissue [10,15]. Currently, the only real-time screening techniques are frozen section analysis (FSA), which completely exhausts the specimen [14,28, 31], and touch-preparation cytology, which provides only an impression of the specimen while depleting the biopsy of tissue [33,46].

An alternative to trans-illumination to view tissue histology is the use fluorescence microscopy. By combining standard fluorescence microscopy with optical sectioning capabilities, a virtual 'slice' of tissue is created with equivalent thickness and appearance to sections cut from the biopsy using standard histology processing. Thus, it is possible to create a virtual fluorescent image with the same features shown in a microscope slide without hardening or physically cutting the tissue [14,17]. Research on the use of fluorescent *ex vivo* imaging methods for bedside biopsy screening and/or pathological analysis has been completed using confocal microscopy [2], [47–50], multiphoton microscopy [51,52], light sheet microscopy [6], and structured illumination microscopy [53–55]. These methods can preserve the tissue, be time efficient, and resemble gold-standard histology, but they all rely on the use of endogenous or exogenous agents to generate the image. Current techniques are either unsuitable for clinical use due to time or damage to the tissue, non-specific for the features that pathologists rely on for diagnosis. Thus, the information they provide pathologists may be extremely different from standard histology, requiring advanced training for accurate diagnosis if fluorescence microscopy is to be adopted for clinical use. Surgeons and pathologists, the clinical diagnostic experts, require a diagnostically accurate stain system that can easily adopt with little training and interruption to their workflow.

*Fluorescence histology* is the application of fluorescent stains that mimic the pathological features of traditional histology, followed by rapid non-destructive *ex vivo* microscopy, which conserves the tissue for future pathological and molecular analysis. Fluorescence histology integrates easily into the clinical workflow as it uses non-destructive fluorescent stains and

optical sections to create histology-like images of tissue with no fixation or physical sectioning. As shown below, in fluorescence histology the fresh specimen will be stained with a fluorescent solution that ideally replicates the histochemical specificity of traditional histology stains and imaged with optical sectioning microscopy. Then the specimen will either continue in experiments or proceed to standard histology processing. Once the histology slides are processed they still need to be viewed by a pathologist through a bright field microscope, as shown in Figure 2.9.

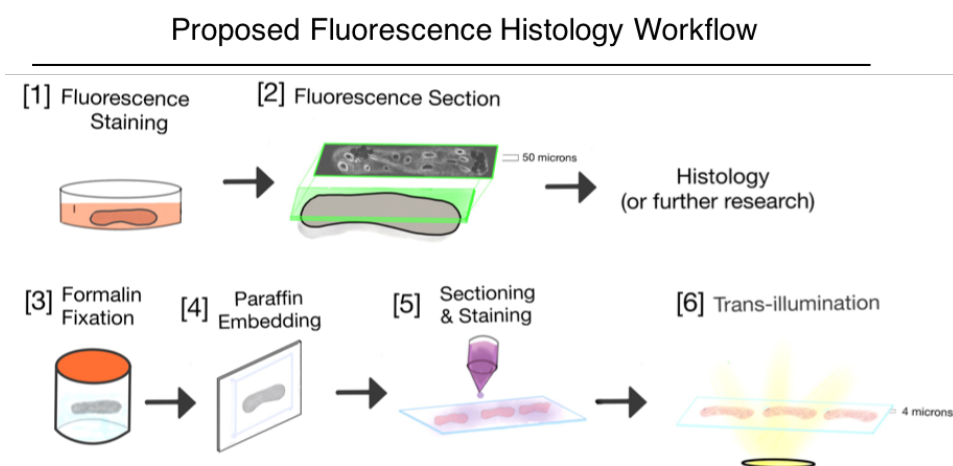


**Figure 2.9:** Fluorescence histology workflow with proposed procedures. After the fluorescent staining and imaging [1-2], the specimen is ready for either further experiments or histology processing [3-6].

### 2.5.1 *Relevance in point-of-care pathology*

After a patient presents with signs of disease, for example elevated prostate specific antigen (PSA) or an abnormal digital rectal examination (DRE) for prostate cancer, a diagnosis is obtained through core needle biopsy. In diagnostic biopsy and biobanking, biopsy procedures are guided through a mixture of previous medical imaging, on-site imaging guidance like ultrasound, and informed “saturation biopsy” techniques [56,57]. However, it is difficult to

reliably identify soft tissue tumors via ultrasound guidance, and systemic saturation techniques rely on biopsies obtained from equal areas throughout the organ [58]. For example, in prostate cancer 8-14 cores are obtained in a single biopsy session, but the lack of suitable tools to locate the cancer within the prostate means initial biopsies may fail to reveal cancers in up to 30% of men even with the most thorough saturation protocols [1]. As approximately one million prostate biopsy procedures are performed each year, this leaves about 300,000 patients incorrectly diagnosed via biopsy analysis and approximately 70,000 of patients require repeat biopsy procedures [59]. In musculoskeletal tumors, a study by Wu *et. al.* found that biopsy diagnostic yield was independent of both imaging guidance and size of needle used for the biopsy [60]. Their recommendation was that patients undergo a minimum of 3-4 biopsies to ensure high diagnostic yield. Another study with both bone and soft tissue lesions found that only 60% of biopsies obtained were useful for guiding clinical decision making [58]. Therefore, there is a critical need for rapid on-site and non-destructive evaluation of diagnostic biopsies to maximize the diagnostic utility and minimize repeat procedures.

The current approach of frozen section analysis (FSA) for in-procedure histopathology damages the tissue sections used to the point of being unable to re-analyze them using traditional pathological staining methods [27,28]. Once the tissue has been frozen, any structures sensitive to temperature changes are irrevocably damaged [29]. Multiple studies on using FSA in intraoperative analysis have also reported low sensitivity and emphasized the importance of evaluators being highly experienced with FSA to achieve consistent results [30–32]. Ideal frozen section analysis takes time, time that is infeasible for diagnostic biopsies. Intraoperative touch preparation cytology (TPC) is also used for rapid biopsy and margin analysis, but provides a partial understanding of the entirety of the tissue with accuracy subjective to an experienced cytopathologist's interpretation [1,25,33]. Given these difficulties, several studies have reported



that the ideal intraoperative assessment would include both FSA and TPC for the best outcomes, yet this doubles both the processing and interpretation time [32,33].

Screening methods that rely on random sampling with limited feedback result in missed opportunities and destroyed tissue. These numbers could be reduced through the ability to accurately screen biopsies for tumor content during a procedure. An alternative to these methods in diagnostic biopsy is fluorescence histology, which both provides rapid, point-of-care analysis and preserves the tissue for future evaluation or biobanking. make on-site corrections to ensure that enough tumor is collected for analysis by taking additional specimens as needed (Figure 2.10).

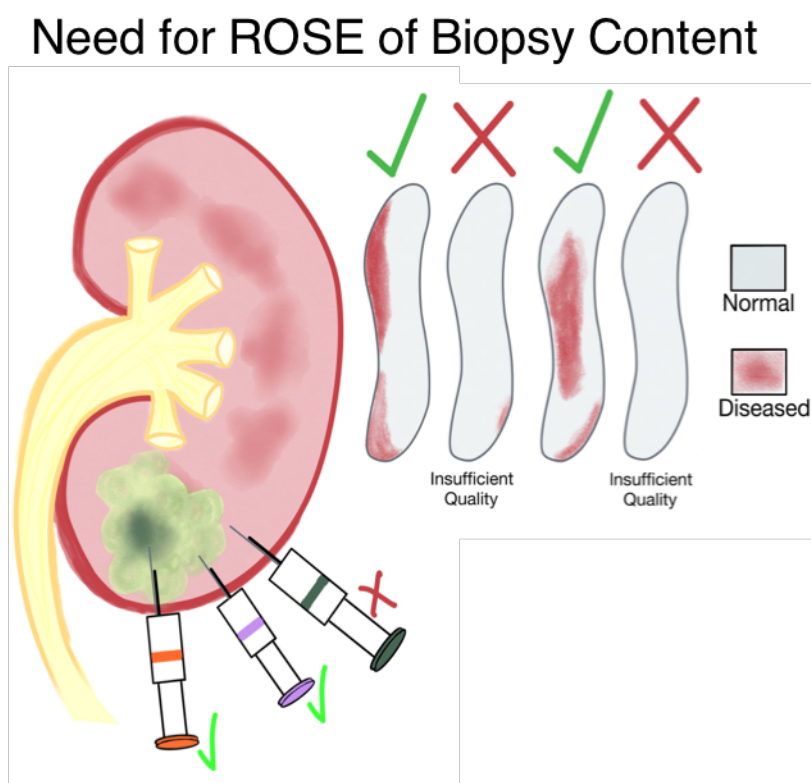


**Figure 2.10:** Using saturation biopsy protocol combined with fluorescence histology, a biopsy specimen can quickly be analyzed for tumor content, corrections can be immediately made to acquire more tissue as necessary, and all samples are preserved for either further analysis or biobanking.

For this method, the pathologist will interpret the fluorescent images of intact tissue with the same accuracy of traditional histology but minimal additional training. While optical sectioning microscopy provides the means for creating extremely thin virtual slices of tissue, it still relies on fluorophores for contrast agents. These fluorophores cannot be relied on to interact with tissue and each other the same way histological dyes do. Therefore, to reproduce the diagnostic efficacy of traditional histology, a topical fluorescent system that highlights the same nuclear, cellular, and extracellular features as histology stains is necessary for clinical use [2, 5, 52].

### ***2.5.2 Need for improvement before adoption***

A known difficulty in histopathology is that each pathologist is unique in their training and review of specimens, leading to inconsistencies in diagnostic decision-making and poor reproducibility in grading disease [61]. This training is dependent on the use of standard histological dyes, such as H&E, Masson's Trichrome, and Periodic-Acid Schiff. Due to the nature of bright field microscopy, interpretation of these dyes is dependent on their coloration as well as their histochemical specificity [2,3,11,16,62]. For example, traditional H&E consists of variations of eosin's anionic staining (pink-to-red) and hematoxylin stained nuclei (dark purple). Masson's Trichrome stains collagen green or blue, hematoxylin stained nuclei are dark purple, and muscle and cytoplasm are red and pink, respectively [24-26]. Periodic Acid-Schiff, useful for glycogen and carbohydrate staining, stains nuclei blue; collagen pink; and glycogen, mucin, mucoproteins and glycoproteins magenta [27-28]. A pathologist's training depends on interpreting where there is a mismatch between expected coloration and expected morphology. Therefore, ideal fluorescent analogues to traditional histology dyes will replicate both the histochemical appearance of the dyes as well as their coloration.

Prior work in fluorescence histology emphasizes the importance of replicating the appearance of traditional histology but was ineffective in creating exact replicas of histological stains. Previous research on the use of reflectance[2], AO [63], propidium iodide[64], and auto-fluorescence [21] combined with image processing to achieve fluoresce histology [2,52]. We have also previously demonstrated the utility of AO for ROSE with biopsies, radical prostatectomy tumor margins, and partial nephrectomy kidney margins. However, this work has not met the conditions for an ideal histology analogue because they either do not show the same histology as traditional dyes or cannot work on both fresh and fixed tissue [5]. Introduction of fluorescent stains for traditional dyes in standard protocols, such as the PAS-acridine orange stain, were shown to lend an increase in both sensitivity and specificity, but required the same extended processing time and methods as the traditional bright field dye [37,65]. Therefore, a true innovation in the field of fluorescence histology is the development of quick staining methods that can be applied to fresh tissue while still replicating the histochemical specificity of bright field dyes and extended processing methods.

Importantly, for adoption in both research settings and the clinic, these fluorescent stains will need to be quickly applied and not interfere in other traditional processing methods, such as PCR, immunohistochemistry or standard histology. They also cannot require extensive processing to bind with the tissue – with the benefit of being able to use on fresh or fixed specimens. Additionally, if more than one fluorescent stain is being used they must be spectrally and chemically compatible with each other. Spectral compatibility refers to the excitation and emission wavelength of a fluorophore where overlapping fluorescent spectra can make it difficult to isolate individually stained components without extensive image processing. Chemically compatible refers to the ability of stains to work together in a tissue without altering each other's binding interactions [18].

## 2.6 Pathological Applications of Image Processing

The final component in the development of a successful fluorescent histology analogue is the ability to mimic the appearance of bright field microscopy. As fluorescent images represent positive contrast, the images are traditionally viewed as areas of bright signal against a dark background. For a single fluorophore's signal, referred to in this work as a fluorescent channel, this is represented as grayscale pixel intensity against a black background. Multiple fluorescent channels in a system are recolored so each channel is a different color (ex: blue, green, red, or magenta.) Remapping colors in a traditional grayscale image is called pseudocoloring. For fluorescence histology to replicate the appearance of traditional histology, which uses negative contrast, the images must be transformed from the linear additive signal of fluorescence microscopy to the exponentially subtractive appearance of transmission microscopy then be pseudocolored to match the color of the traditional histology dyes being mimicked [3].

Pseudocoloring the fluorescent image to resemble traditional histology allows pathologists to use the same skills they developed during training, which focuses on color differentiation tied to expected morphology, to be applied to fluorescent images [66]. Ideally, pathologists can direct their attention to the same color-morphology pairings they would in traditional histology, such as clusters of large purple nuclei that could indicate chronic inflammation in diseased tissue. To convert a fluorescent image to one resembling bright field microscopy, the image must be inverted and the intensities of each fluorescent channels mapped to the *rgb*-color spectrum. Each fluorescent channel is assigned a unique vector value related to the ratios of red, green, and blue desired for its corresponding component in the pseudocolor image. Then, the resultant individual images are combined into a single image matrix [2,8,16,62].

In 2009, Dr. Daniel Gareau published a pseudocolor program using linear color remapping to replicate the coloration of H&E on tissue stained with acridine orange and reflectance imaging [2]. While the program was successful, the imaging modality resulted in a mismatch between the virtual image and the corresponding H&E section due primarily to the differences in the staining specificity of acridine orange and reflectance compared to H&E. Giacomelli *et al* later improved this program to recolor breast tissue imaged with multiphoton microscopy to the appearance of a H&E slide viewed with trans-illumination microscopy. By applying the principles of Beer-Lambert's Law (i.e. color remapping via exponential attenuation) to the pseudocolor algorithm, he could more closely replicate the colors of an image that has light transmitted through a slide than prior efforts [3]. The pseudocolor process provides direct comparison between freshly extracted tissue and later analysis of the same area with H&E. This process must also account for variations in H&E coloration between histology laboratories, histologists, and individual slides [16,35]. Each pathologist has their own preferences for color variations and brightness, and a balance must be found to both characterize and replicate the ideal coloring of H&E slides and to provide a measure of individual control to each pathologist for their comfort, speed, and accuracy.

## **2.7 Closing Remarks**

The current workflow in the clinic is hampered using current ROSE techniques as clinicians must choose between the potential damage of FSA, the incomplete analysis of TPC, or the time constraints of using both methods. Laboratory research also suffers from current histology techniques due to the interruption in their workflow and often requires sacrificing one sample for intermediary analysis before proceeding with the experiment with a secondary, theoretically identical, specimen. Instead of current methods which result in wasted specimens and patients

suffering repeat procedures, we propose the use of fluorescence histology as an intermediary step, like TPC, with the histological information possible with, like FSA, however without the inherent damage to the tissue that is the current ROSE standard. We propose a method for fluorescence histology where the tissue will be excised, stained and imaged with fluorescence microscopy to achieve high fidelity virtual images of tissue histology. The tissue can then proceed through standard FFPE processing and later analysis. These digital fluorescent images are pseudocolored, which can be modified for evaluator preferences, and reviewed from any location.

## CHAPTER THREE: DEVELOPMENT OF D&E FOR FLUORESCENCE HISTOLOGY

*Parts of this chapter are reproduced from the following publications and presentations:*

- Wang M, Kimbrell HZ, Sholl AB, Tulman DB, Elfer KN, Schlichenmeyer TC, Lee BR, Lacey M, Brown JQ. "High-resolution rapid diagnostic imaging of whole prostate biopsies using video-rate fluorescence structured illumination microscopy." *Cancer Research*, 75(19): 4032-4041. 2015.
- Elfer KN, Sholl AB, Wang M, Tulman DB, Mandava Sree, Lee, BR, Brown JQ. "DRAQ5 and eosin ('D&E') as an analog to hematoxylin and eosin for rapid 'zero-cut' fluorescence histology of fresh tissues," *PLOS One*.]
- Elfer KN, Wang M, Sholl A, Kimbrell H, Miller C, Brown JQ\*, "A Topical Fluorescent Analogue for Virtual Hematoxylin and Eosin Histology in Point-of-Care Ex Vivo Microscopy." 2015 European Conferences on Biomedical Optics, June 2015.
- Elfer KN, Sholl AB, Wang M, Tulman DB, Brown JQ. "DRAQ5 and Eosin as a Topical Fluorescent Analogue for H&E in Digital Pathology." 2016 32<sup>nd</sup> Southern Biomedical Engineering Conference, March 2016, pp. 53-54.

### 3.1 Introduction

Previously discussed was the use of topical exogenous fluorescent components for their staining specificity, utility with specialized imaging systems, and ease of application. Among the more common of these stains is acridine orange (AO). AO is favored in fluorescence histology for its capabilities as a general anionic stain while being differential for RNA and DNA [64]. However, its lack of specificity makes it unsuitable as an H&E analogue [65]. It is a dual-spectra cationic stain that both intercalates with dsDNA and forms electrostatic bonds with RNA and other cationic structures. As shown in Figure 3.1, when bound through loose intercalation of the A-T bases in the major groove of dsDNA, AO is strongly green-fluorescent. When acting as a cationic stain, AO demonstrates electrostatic binding interactions, such as to RNA and collagen, and is orange-red fluorescence depending upon its concentration. Due to its electrostatic interaction, pH changes in AO solution can increase or decrease the specificity of binding. Additionally, AO demonstrates extremely rapid stain mechanics as it primarily is electrostatic in nature [15,63,67].

## Acridine Orange Binding

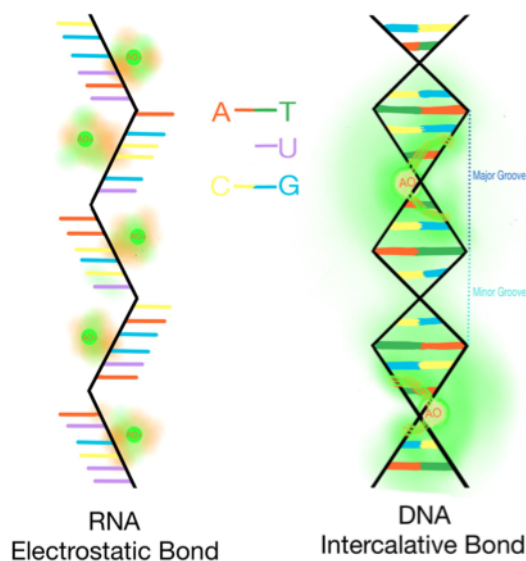


**Figure 3.1:** Acridine orange has two modes of binding in tissue: electrostatic, such as in RNA, and intercalating in dsDNA.

We have previously demonstrated that acridine orange's semi-specific binding is useful in biopsy and positive surgical margin analysis [54,55]. An example of the appearance of a fresh prostate core biopsy stained with acridine orange, from our 2015 publication in *Cancer Research* is shown below in Figure 3.2. Other research groups have demonstrated its use in both *in vivo* and *ex vivo* studies but the its use still requires advanced training for accurate interpretation or extensive post-processing of the images [2,52, 63].



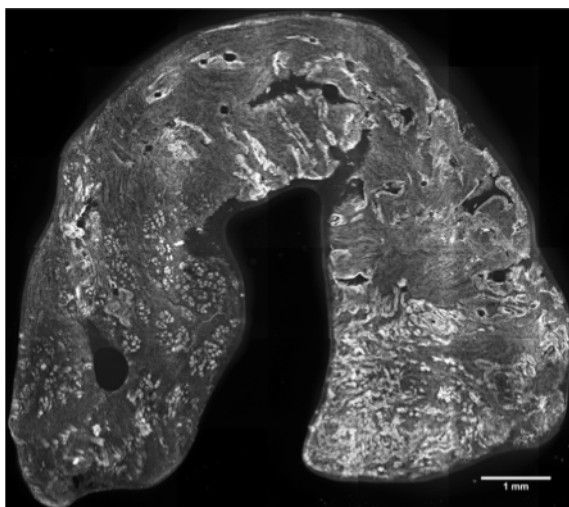


**Figure 3.2:** A prostate biopsy stained with acridine orange. Fluorescent signal is emitted from multiple tissue components, resulting in a complex grayscale image where evaluation requires knowledge of both morphology and context [54].

Acridine orange's generalized staining can create difficulty for pathologists whose training has been dependent on the relationship between morphology and color-specificity. Therefore, utilization of acridine orange in diagnosis requires specialized training for pathologists to interpret the images or risk confusion and misdiagnosis [3–5,52].

An ideal H&E analogue is one that separately stains nuclei, replicating hematoxylin, and an anionic stain that replicates eosin Y's staining specificity. The eosin in H&E is a derivative of fluorescein and therefore is yellow-fluorescent under blue-green excitation ( $\lambda_{\text{ex}} = 490\text{nm}$ ,  $\lambda_{\text{em}} = 530\text{--}620\text{nm}$ ) [68]. It is an anionic dye shown to bind strongly to elastin and other connective fibers in both fluorescent and bright field imaging, indicating a retention of specificity in both modalities [69]. Therefore, eosin Y is a direct fluorescent analogue for bright field eosin in H&E. An ideal nuclear pairing with eosin Y is both spectrally compatible with the wide UV-blue excitation range of eosin Y and specifically stains nuclei. Therefore, DAPI and the Hoechst stains, common nuclear stains with ultraviolet excitation are unsuitable for this purpose. Other stains, such as propidium iodide, cannot permeate live cells and therefore are unsuitable for freshly

excised tissue which will be a combination of living and dead cells [64]. A relatively new fluorophore, DRAQ5 (deep red-fluorescing bisalkylaminoanthraquinone number 5) is a far-red nuclear stain that has been demonstrated as a successful stain at concentrations between 200uM-20uM in live and fixed cells [70]. DRAQ5 intercalates between the A-T bases in the minor groove of dsDNA, shown in Figure 3.3. The highly specific binding results in a 1:1 stoichiometric correspondence between DNA content and intensity and is not susceptible to overstaining, while also allowing for a very simple wash step to remove extraneous stain solution [70–73].

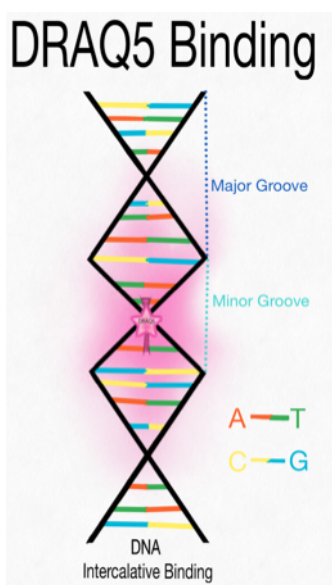


**Figure 3.3:** The binding mechanics of DRAQ5, a highly specific far-red nuclear stain that exhibits a 1:1 stoichiometric relationship between intensity and DNA quantity.

DRAQ5 has excitation and emission properties in the far red to near infrared spectrum ( $\lambda_{\text{ex}} = 647 \text{ nm}$ ,  $\lambda_{\text{em}} = 665\text{-}780 \text{ nm}$ ) and is commonly used as a marker for DNA content in flow cytometry [70,71]. The nuclear specificity of DRAQ5 suggests its potential use as a hematoxylin replacement in a fluorescent H&E analog. Given eosin Y's blue excitation and green fluorescence spectra, it is therefore a spectrally compatible fluorescent counterstain to DRAQ5.

### 3.2 Identification and Development of a H&E Analogue

*Tissue procurement.* A 10  $\mu\text{m}$  frozen prostate biopsy section was obtained using IRB approved protocols from the Louisiana Cancer Research Center (LCRC) Biospecimen Core. The section was stained first with DRAQ5 and eosin Y, as described below, and then delivered to the Tulane Histology Laboratory for standard H&E processing.

*Tissue staining and imaging.* DRAQ5 (5 mM, Biostatus, Ltd.) was diluted from 5 mM to 50  $\mu\text{M}$  in PBS, which was the recommended concentration by the company for flow cytometry applications, the closes correlation to fluorescence histology purposes in DRAQ5 literature. Eosin Y (E4009, Sigma-Aldrich) was dissolved to [2% w/v] in 80% ethanol – the standard histological concentration used by the Tulane Pathology Lab. Stains were applied directly to tissue sections without further modification. The section was incubated with 50  $\mu\text{M}$  DRAQ5 for 20 minutes (the recommended time for flow cytometry, rinsed once with PBS, then stained with eosin Y 2% v/v for two minutes (the histological standard time). The slide was rinsed three times with PBS before imaging on a Nikon A1 Confocal Microscope. The 488 nm - FITC: 480 nm<sub>ex</sub>-510 nm<sub>em</sub>, and 638 nm - Cy5: 620 nm<sub>ex</sub>-660 nm<sub>em</sub> combinations were used to image eosin Y and DRAQ5, respectively.

*Pseudocolor application and comparison to H&E.* After imaging, the individual channels were processed with the pseudocolor algorithm, described below, to recapitulate the appearance of H&E using two-channel fluorescent images.

*DRAQ5 specificity validation and comparison to H&E color deconvolution segmentation.* To validate nuclear specificity correspondence with hematoxylin, a section of tissue stained with both D&E and H&E was analyzed with *ImageJ* to identify nuclear size and correspondence with H&E. Nuclei quantification is often necessary for quantitative diagnostic methods. Typically, H&E sections are digitally imaged and then processed using custom color deconvolution algorithms [74]. Because D&E uses two completely spectrally separate fluorescent channels, it is

possible to have a completely nuclear segmented image without the tedious deconvolution process. The H&E image was digitally separated using an ImageJ plugin, *ColorDeconvolution* [75]. Both the individual DRAQ5 fluorescent channel and the digitally segmented H&E nuclear image were then processed for nuclear morphology and quantification using *Cell Profiler*[76, 77].

### 3.3 Application of a Pseudocolor Algorithm

Pathologists are trained to diagnose tissue using traditional histology methods, dyes in tissue sections viewed through bright field microscopy. Even fluorescent stains that have the same histochemical interactions as standard histology dyes will not visually match what the pathologist is expecting for diagnosis. While the pathologist can be trained to accurately interpret fluorescent coloring, it is much easier for clinical adoption if the images are re-colored to match bright field appearances. The first article on re-mapping fluorescence images to the H&E *rgb* color-metrics was published by Gareau in 2009. The pseudocolor program he developed (eq. 1-3) uses two fluorescent channels, one taking the place of hematoxylin and one of the eosin [2].

$$R: 1 - \text{Hematoxylin}(1 - 0.24) - \text{Eosin}(1 - 0.88) \quad \text{eq. 3.1}$$

$$G: 1 - \text{Hematoxylin}(1 - 0.21) - \text{Eosin}(1 - 0.27) \quad \text{eq. 3.2}$$

$$B: 1 - \text{Hematoxylin}(1 - 0.62) - \text{Eosin}(1 - 0.66) \quad \text{eq. 3.3.}$$

To replicate the appearance of bright field microscopy the image matrix must be inverted because fluorescence microscopy creates high intensity signal against a dark background. Each fluorescent channel is then multiplied by a color ratio to represent contribution of *r*, *g*, or *b* in the color spectrum. The three new *rgb* image matrices are then merged into a single-color image.

While Dr. Gareau's work was the first to implement a pseudocolor replication of H&E, it did not quite replicate the appearance of dyes blocking out light shining through a microscope slide. Giacomelli, *et. al.* improved upon Gareau's original algorithm by implementing the

principles of Beer-Lambert's Law to simulate the appearance of trans-illumination microscopy (eq. 3.4-6) [3].

$$R: \exp(-\beta_{\text{HematoxylinRed}} * \mathbf{Hemeatoxylin} * k) \exp(-\beta_{\text{EosinRed}} * \mathbf{Eosin} * k) \quad \text{eq. 3.4}$$

$$G: \exp(-\beta_{\text{HematoxylinGreen}} * \mathbf{Hemeatoxylin} * k) \exp(-\beta_{\text{EosinGreen}} * \mathbf{Eosin} * k) \quad \text{eq. 3.5}$$

$$B: \exp(-\beta_{\text{HematoxylinBlue}} * \mathbf{Hemeatoxylin} * k) \exp(-\beta_{\text{EosinBlue}} * \mathbf{Eosin} * k) \quad \text{eq. 3.6}$$

Where *Hematoxylin* and *Eosin* represent the nuclei and cytoplasm fluorescent channels respectively;  $k$  is a scaling constant that accounts for instrument variation such as gain, detector sensitivity and other factors; and the  $\beta$  values are the color coordinates of H&E for each dye:

$$\begin{array}{lll} \text{HematoxylinRed}=0.860, & \text{HematoxylinGreen},=1000, & \text{HematoxylinBlue}=0.300, \\ \text{EosinRed}=0.050, & \text{EosinGreen}=1.000 & \text{EosinBlue}=0.544 \text{ [4].} \end{array}$$

By incorporating the above pseudocolor algorithms with our own image processing we can transform our standard fluorescent images into ones more familiar to pathologists for easier diagnosis.

Raw 16-bit TIFF images from each channel, DRAQ5 and eosin, were processed in MATLAB. They were converted to double precision arrays and a flat-field correction procedure was performed by dividing the raw image frame by a calibration image for each respective channel. In the case of multiple frames in an image, the correction process was followed by stitching the frames into a larger mosaic. An empirically determined coefficient was then applied to the mosaicked image for each channel to match their intensities. The pre-processing steps described above are shown in equation 3.7 and equation 3.8, below:

$$D5 = A \left[ \frac{I_{D5}}{\max(I_{D5})} \right]^{1/\gamma_1} \quad \text{eq. 3.7}$$

$$E = B \left[ \frac{I_E}{\max(I_E)} \right]^{1/\gamma_2} \quad \text{eq. 3.8}$$

where  $I_{D5}$  and  $I_E$  are the flat-field corrected mosaics for each channel and  $A$  and  $B$  are the linear coefficients used to match the mean intensities of the two channels. This coefficient

typically ranged from 0.8 to 4, where the  $B$  ranged from 1.5-4 and  $A$  ranged from 0.8-2. Gamma correction is a non-linear method to correct for the different response curves between cameras and the human eyes [78]. Here, we implement gamma correction for both channels to better match the histological sections. The DRAQ5 gamma ( $\gamma_1$ ) typically ranges from 0.95-1 and the eosin Y gamma ( $\gamma_2$ ) typically ranges from 0.7-1. Following these preprocessing steps, we re-mapped the DRAQ5 and eosin channels into a composite RGB image using the pseudocolor algorithm described by Bini, *et al* [48].

A side-by-side comparison of a frozen prostate section imaged with D&E and then stained with H&E is shown in Figure 3.4 This figure shows eosin staining all non-nuclear cellular material (Figure 3.4 A,B), DRAQ5 bound to the nuclei (Figure 3.4 C,D), and the combined image of the two channels in green/magenta pseudo-coloring (Figure 3.4 E,F,K). The prostate section was later stained with H&E and then scanned with a digital slide scanner (Figure 3.4 I,J,M). After re-coloring the D&E image to simulate the appearance of H&E (Figure 3.4 G, H, L), the two images are shown to be highly similar.

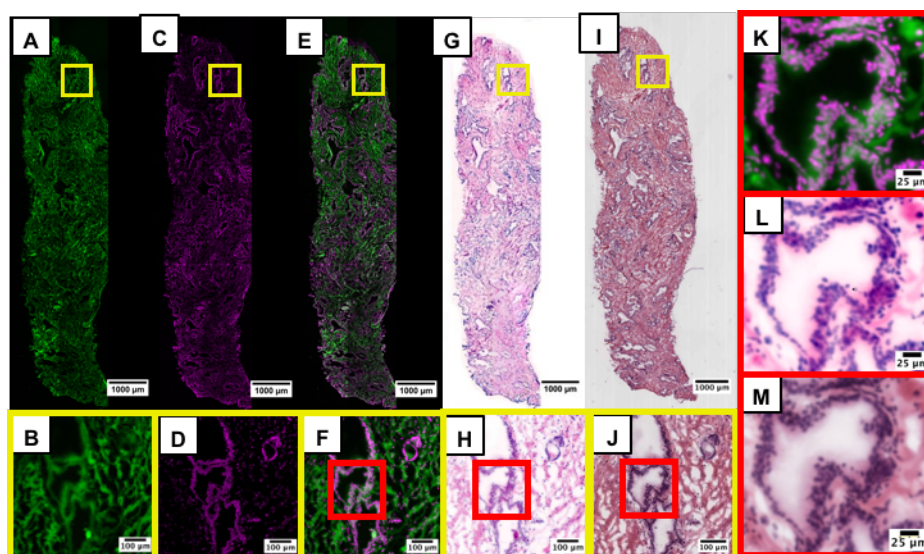


**Figure 3.4:** A 10 µm prostate biopsy section stained first with D&E then with H&E. The fluorescent eosin channel (A,B), fluorescent DRAQ5 channel (C,D), fluorescent composite overlay (E,F,K) and the pseudo-H&E fluorescent image (G,H,I) are compared against the gold-standard H&E image (I,J,M) of corresponding histology.

Specifically, in the eosin channel (Figure 3.4 A, B), cytoplasmic and stromal material is clearly visualized as well as the absence of fluorescence signal where nuclei are located. The DRAQ5 channel (Figure 3.4 C, D) demonstrates specific nuclear staining; the morphology of individual nuclei forming glands and fibroblast nuclei throughout the stroma are clearly visualized and spatially consistent with hematoxylin staining in H&E. Merging the two separate channels creates a single fluorescent image that shows nuclei, cytoplasmic and extracellular material together (Figure 3.4 E, F, K). The fluorescent composite image of the DRAQ5 and eosin channels shows that the nuclear (magenta) and cytoplasmic/extracellular (green) compartments are each uniquely stained and spatially consistent with H&E. The individual fluorescent channels of A and C were then combined the Gareau pseudocolor method to create Figure 3.4 G, H, L, recapitulating standard H&E histology (Figure 3.4 I, J, M).

A closer examination of Figure 3.4 [L,M] shows correspondence between the DRAQ5 and hematoxylin glandular morphology (Figure 3.5 A, B). An even more magnified image shows a

near direct match between nuclear size and shape (Figure 3.5 C,D) even with the differences in resolution from the Nikon A1 (10x objective) and the Aperio Slide Scanner (20x objective).

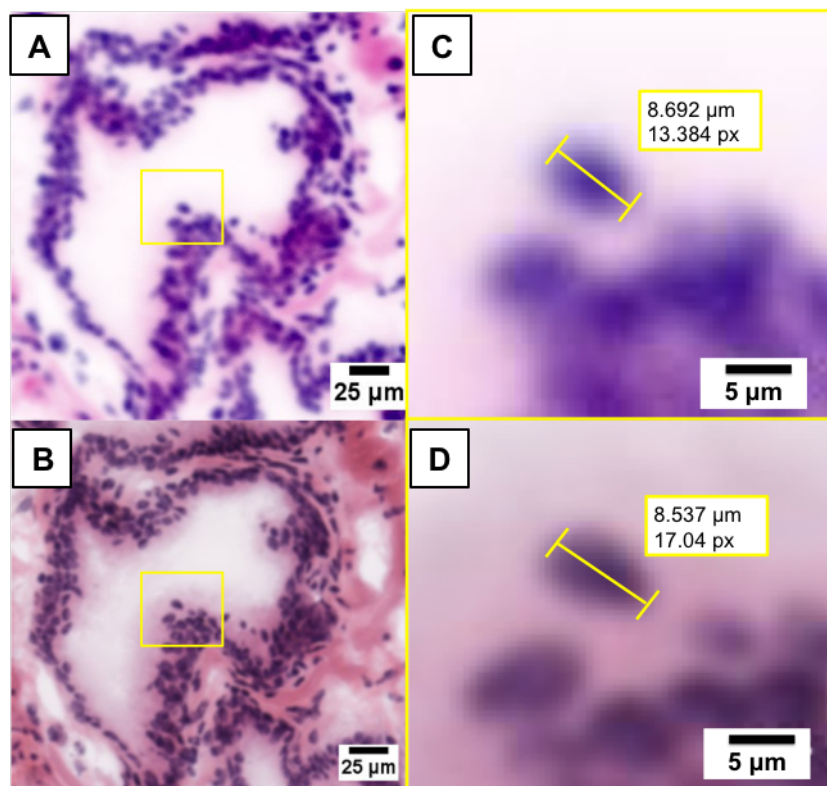


**Figure 3.5:** Modified version of Figure 3.4 L-M, showing even deeper zooms of a single nucleus for D&E (top right, A, C) and H&E (lower right B, D). Even though the H&E image is inherently higher resolution because of differences in the imaging hardware, the sizes of the nucleus measured in each image are within 200 nm of each other.

Automated nuclear segmentation via examination of the DRAQ5 channel was compared to digital image segmentation via color deconvolution of an H&E section. Each step of the nuclear segmentation process was recorded in Figure 3.6, below. As shown in Figure 3.6 [A], the DRAQ5 channel requires no further processing for nuclear segmentation. The H&E section, however, required three intermediate steps before the image could be analyzed with automated nuclear quantification processing.



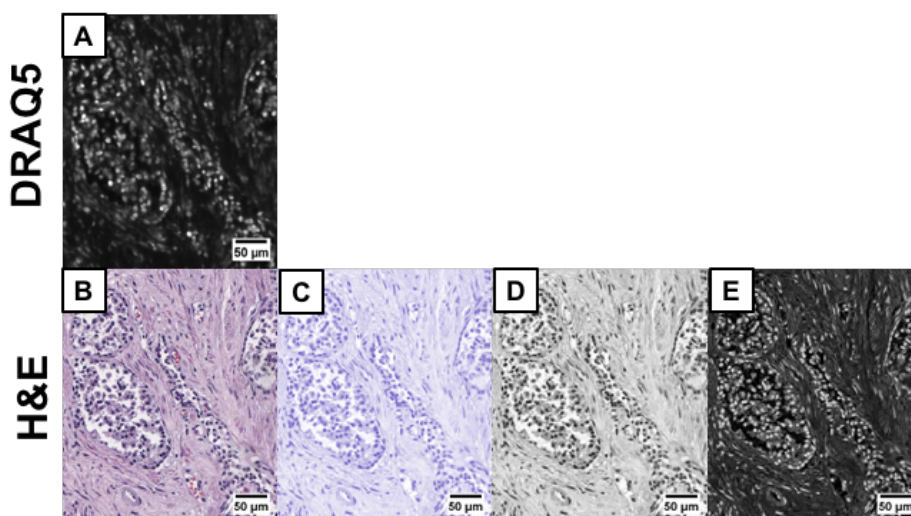


**Figure 3.6:** Nuclear segmentation of a D&E stained section and a H&E stained section. The DRAQ5 nuclear channel (A). The digital H&E section (B), the hematoxylin color deconvolution channel (C), the grayscale LUT conversion (D), and the inversion of the grayscale image for automated processing (E).

After segmentation, images can be processed using image analysis programs, such as *Cell Profiler*. The focus of this analysis was nuclear size and quantification. Each segmented image was analyzed and the total number of nuclei, a histogram of sizes increasing in half micron steps, and the average size of the nuclei were determined. In Figure 3.7, the visual result of this analysis is shown where each color represents an individual bin of the histogram.

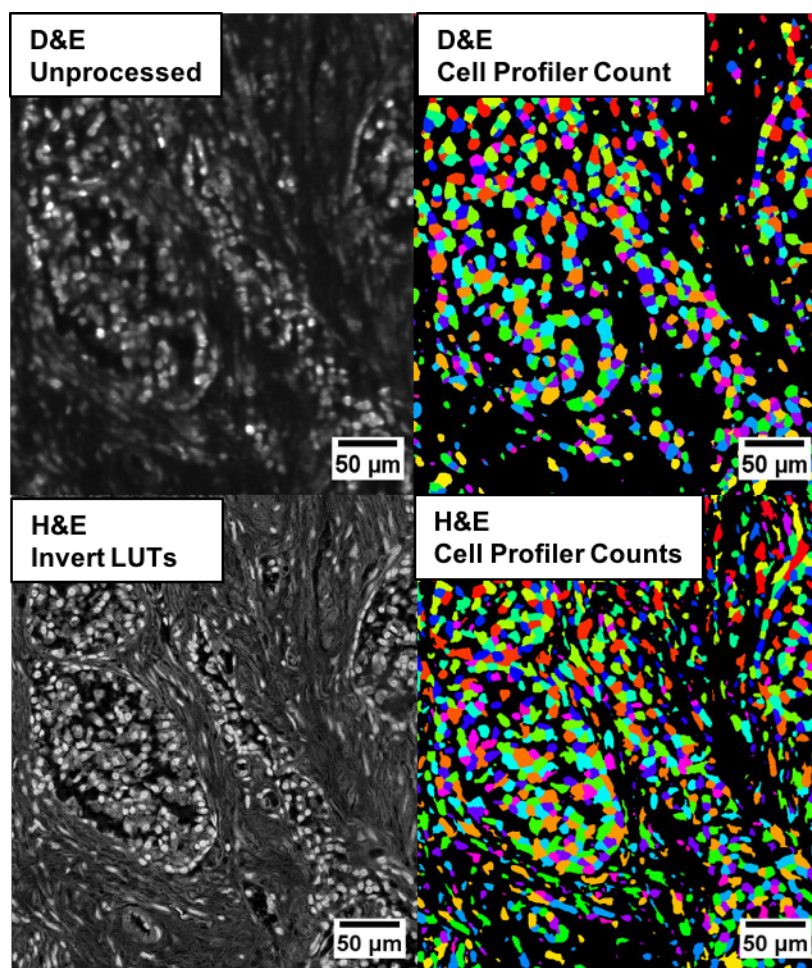


**Figure 3.7:** Nuclear quantification through *Cell Profiler* analysis of the D&E and H&E nuclear segmented images. Color-mapping corresponds to the histogram bins generated during analysis where similarly colored nuclei are in the same size-classification.

The average size and quantity of the nuclei were on a similar scale, although the H&E segmented image produced average nuclei sizes that were approximately four microns smaller than the DRAQ5 image and about 10% more than the D&E image. Additionally, the average nuclear size is approximately 2x smaller in H&E, and 1.75x smaller in D&E than would be expected for benign prostatic tissue. This difference was attributed to the lack of specificity of the H&E segmentation process and the *Cell Profiler* script, which was not developed for robust clinical analysis and can be written to increase specificity depending on application.

Although some variations in appearance between D&E and H&E is evident, the primary source of these differences appear to be the effects of linear fluorescence signal versus the exponential absorption of bright field, which is corrected with the application of Giacomelli's version of the pseudocolor algorithm. Additional factors are color saturation and intensity, which is easily correct by changing the *A* and *B* coefficients in the pseudocolor program. Furthermore, there are multiple histology protocols, automated devices, and individual preferences for color saturation and variation. Further characterization of D&E on tissue sections was conducted to better determine if D&E would be a suitable fluorescent analogue for H&E.

### **3.4 Characterization of D&E on Tissue Sections**

For D&E and the pseudocolor process to be a viable alternative to rapid-histology methods and to be adopted in the research and clinical workflow, its performance against FFPE H&E and frozen sections must be analyzed. For a direct evaluation of the performance of fluorescent stains, tissue must first be examined with as close to standard H&E processing as possible: tissue sections. However, FFPE sections, as previously described, undergo extensive processing that changes both its chemistry and structure. Therefore, comparison to frozen sections, which is as close as we can come to fresh tissue sections, is also needed. For this study, both frozen and fixed tissue sections were stained with D&E, H&E processed, and then a pathologist compared the resultant virtual image and microscope slides.

*Tissue collection and processing.* De-identified FFPE tissue sections (n = 12) were obtained from the Tulane Medical School Histology core under a Tulane Institutional Review Board (IRB)-approved protocol. Samples were chosen from tissue that most frequently benefits from rapid histological review: lung (n=3), prostate (n=2), thyroid (n=2), liver (n=2), kidney (n=1), adrenal

gland (n=1), and colon (n=1). They were stored at room temperature until immediately prior to staining, at which point the sections were de-paraffinized, stained per the protocol below and imaged. After fluorescence imaging, they were processed for H&E through the Tulane Medical School Histology Department and scanned at 200X with an Aperio whole slide scanner (Leica Biosystems). De-identified, flash-frozen tissues (n=25) were obtained from the Louisiana Cancer Research Center (LCRC) Biospecimen Core under an IRB-approved protocol. Six tissues were represented among the 25 individual specimens: lung (n=6), prostate (n=6), colon (n=4), kidney (n=3), breast (n=3), and bladder (n=3). They were then processed into 10  $\mu$ m thick sections on microscope slides and stored frozen at -18°C until immediately prior to staining and imaging the tissue. The slides were removed from the freezer, gently rinsed with room-temperature PBS to thaw the tissue, stained using the protocol described below, and imaged. After imaging, the sections were sent to Tulane Medical School Histology Department for standard H&E processing, then scanned with the whole slide scanner.

*D&E section staining.* Both de-paraffinized FFPE and thawed frozen sections were stained with the same D&E protocol. A section of tissue was exposed to 2% eosin in ethanol for 20 seconds and then rinsed in PBS. Next, 50  $\mu$ M of DRAQ5 was applied for three minutes before a single rinse with PBS. The specimens were imaged with a custom epi-fluorescence microscope with optical sectioning structured illumination microscopy (SIM) capability. For tissue section imaging, this microscope was operated in standard wide-field illumination (non-SIM) epifluorescence mode. Both channels used an integration time of 110 ms and each LED was adjusted to maximize signal while not saturating the camera.

The pathologist accurately identified tissue type and specific morphological features in both the FFPE sections and the frozen sections of D&E. Review of the FFPE sections demonstrates a complete morphological match between modalities, with select regions of interest shown in

Figure 3.8. The pathologist could easily identify the three layers of an artery in a lung section (Figure 3.8 A,B) and distinguish it from a bronchus (Figure 3.8 C,D). The ductular reactions in cirrhotic liver (Figure 3.8 G,H) and the nuclei of thyroid nodules along with eosin-only staining of the inner feature (Figure 3.8 E,F) are equally distinguishable.

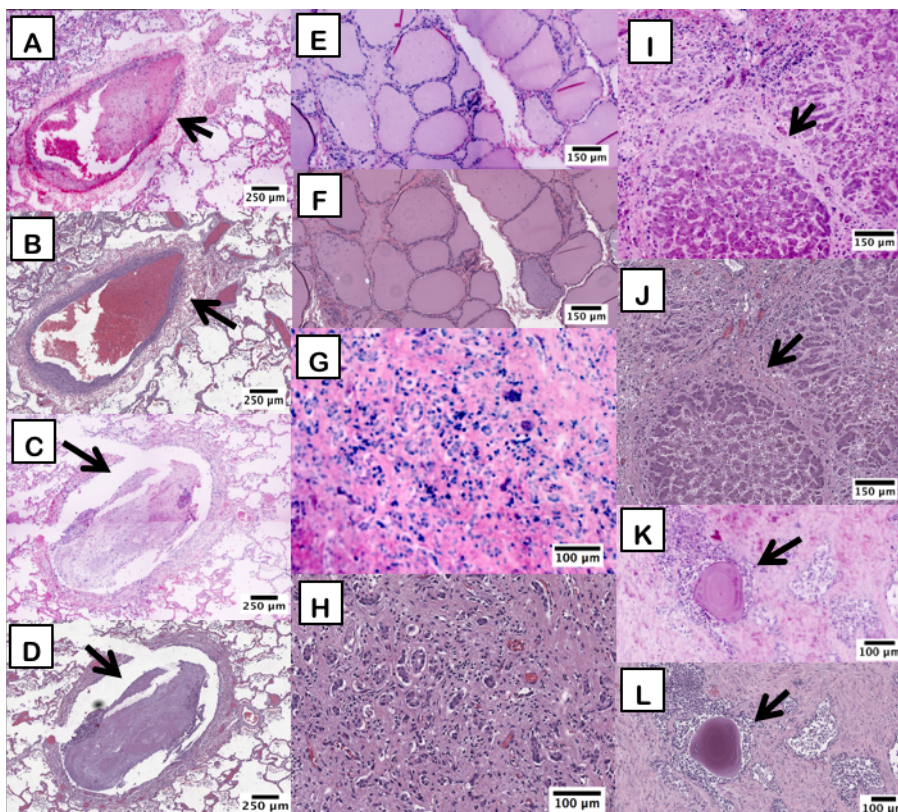


**Figure 3.8:** FFPE sections of human tissue. D&E (A) and H&E (B) of lung parenchyma and small pulmonary artery branch with blood clot (arrow). D&E (C) and H&E (D) of thyroid follicles. D&E (G) and H&E (H) of cirrhotic liver showing ductular reaction (in box). D&E (I) and H&E (J) of prostate glands with corpora amylacea (arrow).

Although the pseudo-colored D&E replicates H&E with high fidelity spatially, potentially useful color variations between D&E-processed images and standard H&E are evident. Areas of liver cirrhosis were identified in both the D&E and H&E images (Figure 3.9 G, H,I,J) and robust collagen fibrosis in the liver sections appears more strongly on the D&E sections. The fluorescent D&E image creation also allows for increased contrast, as in the ductular



reaction in liver tissue (Figure 3.9 G,H) and the lamellations of the corpora amylacea (Figure 3.9 K).

In Figure 3.9, the frozen sections demonstrate similar correspondence of feature morphology and coloration as shown in the fixed sections. Renal medullary tubules, (Figure 3.9 A,B) as well as normal colonic crypts (Figure 3.9 C,D). In a single area of lung tissue, identification of important morphological features including a pulmonary artery branch, terminal bronchiole and alveolar macrophages were all clearly identified on D&E and confirmed in H&E (Figure 3.9 I,J).

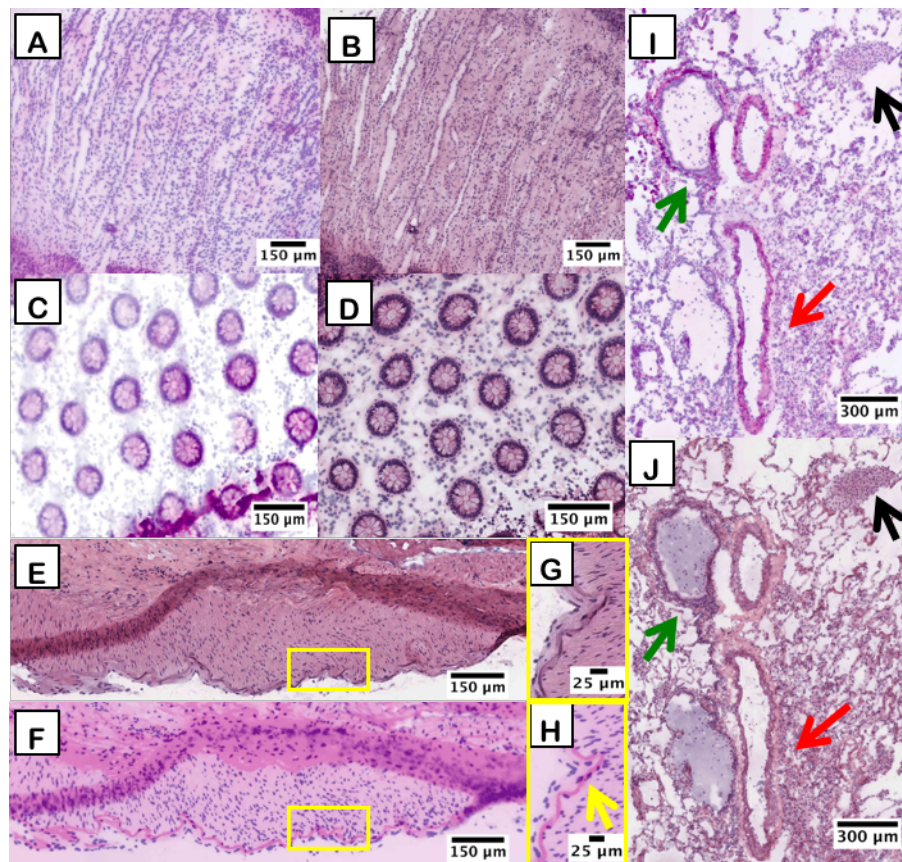


**Figure 3.9:** Frozen sections of human tissue. D&E (A) and H&E (B) of renal medullary tubules. D&E (C) and H&E (D) of prostate tissue with corpora amylacea and vessel (arrows). D&E (E) and H&E (F) of lung showing pulmonary artery branch (red arrow) with terminal bronchiole (green arrow) and alveolar macrophages (black arrow).

As evident before, there are some useful differences between the two staining methods exist, most notable of which is the emphasized elastic lamina seen in bright pink in the D&E version (Figure 3.9 E,G) compared to the H&E version (Figure 3.9 F,H) of the outer pleural surface of the lung. The elastic lamina is typically best visualized with a special elastin stain and is used to stage pleural invasion in lung carcinomas.

### 3.5 Conclusion

In this work, we evaluated the use of DRAQ5 and eosin (“D&E”) as a direct fluorescent analog to traditional H&E staining. By combining the nuclear fluorescent stain, DRAQ5, and the cytoplasmic stain, eosin Y, we have demonstrated the ability to create a rapid, non-destructive fluorescent histological analogue to H&E that is also compatible with later traditional H&E staining of the same tissue. D&E was demonstrated on both FFPE tissue sections and frozen sections with high histological correlation with H&E staining. By combining this staining technique with pseudocolor image processing, we created virtual H&E images with the same coloration and specificity as the bright field technique. The pseudocolor program also allows convenient alteration of color and intensity levels of the two stains, making it easy to change the final appearance of the image to suit the preferences of the evaluator. The fidelity of D&E staining compared to traditional H&E was validated in frozen and fixed sections from a variety of human tissues.

The topical staining method introduced here, combined with fluorescent *ex vivo* microscopy, could enable routine non-destructive histological assessment of fresh human tissues at the point-of-care for a variety of applications. Although we demonstrate extremely high fidelity with staining specificity, the intensity and coloration of the fluorescent images does show some variations from the H&E counterpart. One reason for these changes may be the imaging

method; as areas of higher dye uptake provide a corresponding higher fluorescent signal, they can appear brighter against the background. This effect is conserved during the pseudocolor process. On the other hand, the higher stain uptake in bright field microscopy results in a subtly darker shading in the resultant image – which can be more difficult to differentiate in an already saturated background. Further work characterizing the performance of D&E on intact and in regards to current fluorescence histology methods is needed to understand the full potential of this stain-pseudocolor system.



## CHAPTER FOUR: Monochrome versus Dual Color Fluorescence Histology on Thick Tissue

Parts of this chapter are reproduced from the following publication and presentations:

Elfer KN, Sholl AB, Wang M, Tulman DB, Mandava Sree, Lee, BR, Brown JQ. "DRAQ5 and eosin ('D&E') as an analog to hematoxylin and eosin for rapid 'zero-cut' fluorescence histology of fresh tissues," *PLOS One*.]

Elfer KN\*, Sholl AB, Wang M, Tulman D, Brown JQ, "Comparison of Monochrome versus Dual-Color Images in Fluorescence Histology on Prostate and Kidney Specimens," Optical Society of America: 2017 Optics in the Life Sciences. April 2017.

Elfer KN\*, Sholl AB, Brown JQ, "Topical Fluorescent Stain System for Point-of-Care Lung and Prostate Cancer," Optical Society of America: 2016 Congress on Biomedical Optics, Cancer Therapeutics. April 2016.

### 4.1 Introduction

Fluorescent images can be evaluated using two contrast methods: monochrome (grayscale) or pseudocolor. Both contrast methods are used for research studies; however, the successful adoption of fluorescence histology in point-of-care imaging will rely on determining which contrast modality is fastest, most accurate in diagnosis, and easiest for pathologists to use. Rapid, non-destructive, on-site review of freshly excised tissue is useful in clinical practice and research for diagnostic biopsy, correction of positive tumor surgical margins, quality review for bio-banking, and preservation of samples for genetic and molecular analysis [47,49,54,55,79,80]. The diagnostic gold-standard of formalin-fixed, paraffin embedded hematoxylin and eosin (H&E) requires both processing and analysis time of one day or longer, which is unfeasible in point-of-care pathology. The ideal solution will be rapid, accurate, and non-destructive so the tissue is preserved for later genetic and molecular analyses. Methods that both provide complete histological information as well as preserve the tissue for these purposes are preferred. This goal can be achieved via advances in epifluorescence optical sectioning microscopy, such as confocal, structured illumination, and multiphoton microscopy. These *ex vivo* techniques require minimal interference with the tissue and the clinical workflow[2,4,5,53]. Therefore, they provide promising avenues to accurately and non-destructively view the histology of fresh, intact tissue

while preserving the sample for later use. However, the adoptability of fluorescence histology is dependent on its accuracy and ease of use, which requires a thorough understanding of how the contrast modality of its images effect these factors.

Either monochrome or H&E pseudocolor is preferable for different uses in research and clinic, but at this time there has been no evaluation of which method is ideal for use in point-of-care fluorescence pathology where accuracy and time are both critical factors in a patient's outcome. These factors include complexity of the staining system, the specificity the stains, the amount of additional training for pathologists to diagnose the images, and the cost of the stain systems [20,26,81]. While the importance of these factors may vary depending on the end goal, such as clinical point-of-care diagnostics versus research that spans across several fields, they must be kept at the forefront of consideration when choosing a histology method.

In this work, we optimized the fluorescent stains DRAQ5 and eosin Y for use on fresh, thick (>0.5 mm) samples. In Chapter 3, we demonstrated the fidelity of D&E on sections of tissue and the use of an image processing program to replicate the appearance of H&E. The purpose of fluorescence histology, however, is the ability to image thick (>0.5 mm) masses of tissue without the need to physically section them. Staining and imaging thick tissue is made more difficult than on sections by the need to control the stain penetration and background signal of the thick tissue [10,13]. Thick tissue imaging additionally requires the use of an optical sectioning microscopy capable of imaging an entire area of fresh tissue. Therefore, we demonstrate the use of D&E with video rate structured illumination microscopy (VR-SIM) on kidney and prostate biopsies from discarded surgical tissue and on the surface of an intact prostate margin from a radical prostatectomy procedure. We then compare the dual-color D&E stain against the single-contrast fluorescence histology stain, acridine orange (AO), on fresh, intact prostate biopsies. A pathologist evaluated the diagnostic capabilities of the two contrast modalities in a blind review

against their H&E bright field counterparts. Finally, single-contrast, dual-contrast, and standard FFPE were evaluated on the basis of cost, time, and histological utility.

#### **4.2 Optimization of Acridine Orange and DRAQ5 and Eosin on Fresh, Intact Tissue**

When determining the feasibility of D&E on sections, histological and prior literature concentrations were chosen but thick tissue presents a more complex problem as uneven application of stains can affect diffusion through the tissue, resulting in poor signal and staining specificity. The recommended concentration for DRAQ5 varies between 200  $\mu$ M to 10  $\mu$ M based on its use, such as flow cytometry or evaluation of individual cells [71–73]. According to current literature, the concentration of eosin Y varies based on its solvent and lab preference [15,68]. Histology labs differ on whether they use a progressive or regressive eosin staining technique. Progressive techniques use water-based eosin to gradually increase the appearance of the stain. On the other hand, regressive techniques use ethanol to retroactively remove excess stain from the specimen. Therefore, both PBS and 80% ethanol were evaluated to determine the best solvent for fluorescence histology. Additionally, the ideal fluorescent concentrations and staining times are likely to be different than the histological ideal to optimize fluorescence for use in clinical applications. Extremely rapid staining of eosin was previously observed when applied to sections, although the histological standard is on the order of minutes. Furthermore, ethanol based eosin runs a risk of drying out, shrinking, and preemptively fixing the tissue if applied for extended time periods.

*Stain optimization on bovine muscle.* A seven-step serial dilution of DRAQ5 (5 mM, Biostatus, Ltd.) in PBS was performed from 200  $\mu$ M to 1  $\mu$ M. Eosin Y (E4009, Sigma-Aldrich) in 80% Ethanol was evaluated from 7.5 mM to 15  $\mu$ M in a ten step dilution series, diluting from standard histological dye concentration downwards. Eosin Y dissolved in PBS was also evaluated

ranging from 3.8 mM to 30  $\mu$ M. Each stain dilution was individually applied to a piece of commercially available bovine muscle and imaged on a custom video-rate structured illumination microscope. Images were acquired at four different power levels of a 640 nm laser and a 470 nm laser for DRAQ5 and eosin, respectively. Images were evaluated through both visual examination and comparison of mean normalization factors.

The optimal time needed for thicker samples to be exposed to tissue was evaluated by immersing the bovine muscle in a stain for different time intervals. DRAQ5 was applied via immersion for 1 minute, 3 minutes, and 5 minutes. Eosin Y was applied for 10 seconds and 45 seconds. Stain order was determined by choosing the concentration and time with the highest intensity for each stain and then applied cuts of bovine muscle. DRAQ5 and eosin Y were alternated as the first stain applied to the tissue. The intensity before and after application of the secondary was determined via imaging and mean normalization.

*Thick tissue imaging with VR-SIM.* Specimens were imaged with a custom epi-fluorescence microscope with optical sectioning structured illumination microscopy (SIM) capability based on an automated modular platform (RAMM, Applied Scientific Instrumentation) described in our previous publications. Figure 4.1 contains a schematic of the VR-SIM system with a six line (405/445/470/520/528/640 nm) multimode-fiber-coupled laser engine designed for widefield imaging (LDI, 89 North) laser channels are combined with a dichroic beam combiner (DBS1) (Prizmatix) and imaged onto a ferroelectric spatial light modulator (SLM, 3DM, Forth Dimension Displays). The SLM projected patterns for structured illumination microscopy through a 10X, 0.45NA Plan APO objective lens (OL) onto the sample. A Semrock multiband filter cube (DBS2) was used to allow excitation and emission of both stains. All dual-component images were taken sequentially at each frame position.

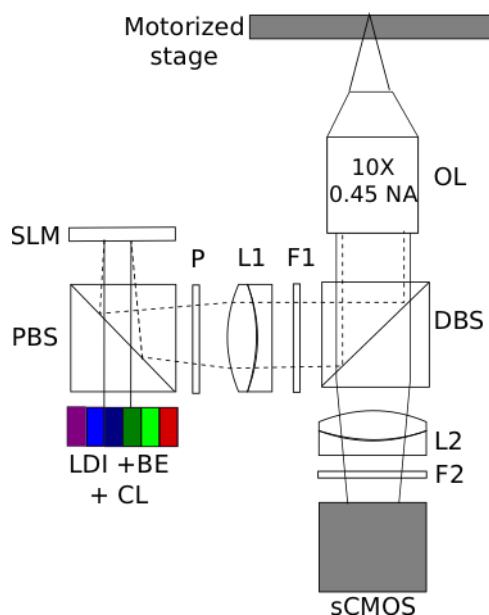


**Figure 4.1:** Schematic of the video rate structured illumination microscopy system used for imaging thick samples. LDI – laser engine; BE – beam expander; CL – collimator; SLM – spatial light modulator; PBS – polarizing beam splitter; P – polarizer; L – achromat lens; F – multiband filter; DBS – multiband dichroic beamsplitter; OL – objective lens; sCMOS – camera.

Raw images from each fluorescent channel were computationally combined into a single optically sectioned image using either three phase SIM within Labview [82] or the HiLo ImageJ plugin [83]. These raw images were then processed and using the correction and pseudocoloring algorithm described in Chapter 3.

While in most literature DRAQ5 is applied for a minimum of 20 minutes up to several hours, this time frame is not useful for clinical timelines. Figure 4.2 below demonstrates the increase and plateau of DRAQ5's fluorescence intensity versus concentration. In the comparison of concentrations, we can see that although the highest concentration of 200  $\mu\text{M}$  has the highest signal, at three minutes' incubation on the highest power the concentration is only slightly higher than that of 50  $\mu\text{M}$  while also being an efficient use of resources.

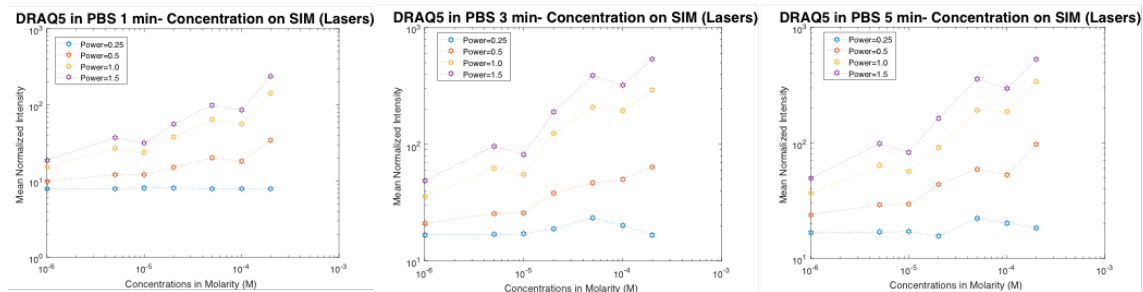


**Figure 4.2:** Comparison of bovine muscle exposed to DRAQ5 for one minute, three minute, and five minutes across a seven-step dilution series.

Eosin was previously shown to exhibit high fluorescence with only a brief staining time (< 1 minute), and this time frame is particularly necessary when ethanol is the primary solvent as tissue drying or premature fixation are a concern for both clinical and research applications. Figure 4.3 shows fluorescence intensity increases with even a few additional seconds of staining, corresponding to the color of the tissue turning a bright pink with within thirty seconds of exposure to the staining solution.

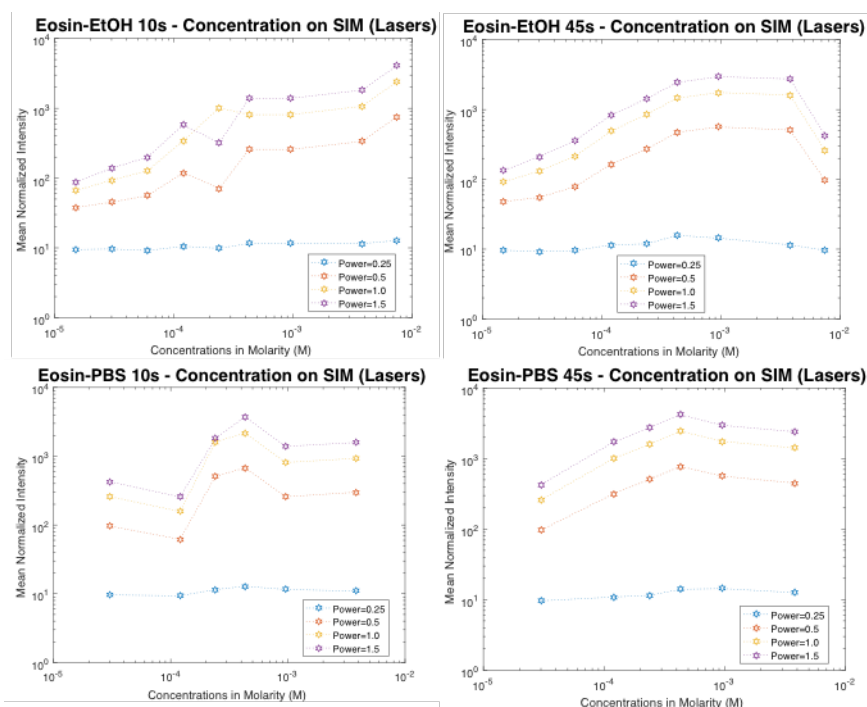


**Figure 4.3:** Comparison of bovine muscle stained with eosin Y dissolved in either 80% Ethanol or PBS. Specimens were stained for either 10 seconds or 45 seconds in a nine-step dilution series.

Eosin's fluorescent signal is relatively steady between 3 mM and 430  $\mu$ M, although there is a significant peak at 430  $\mu$ M with PBS as a solvent. Additionally, it appears that the use of PBS as a solvent provides a higher intensity than ethanol. However, when we visually examine different regions of interest of the two stained meats with 3.3 mM concentration at 45 seconds there is less differentiation of features in PBS than in ethanol (Figure 4.4).

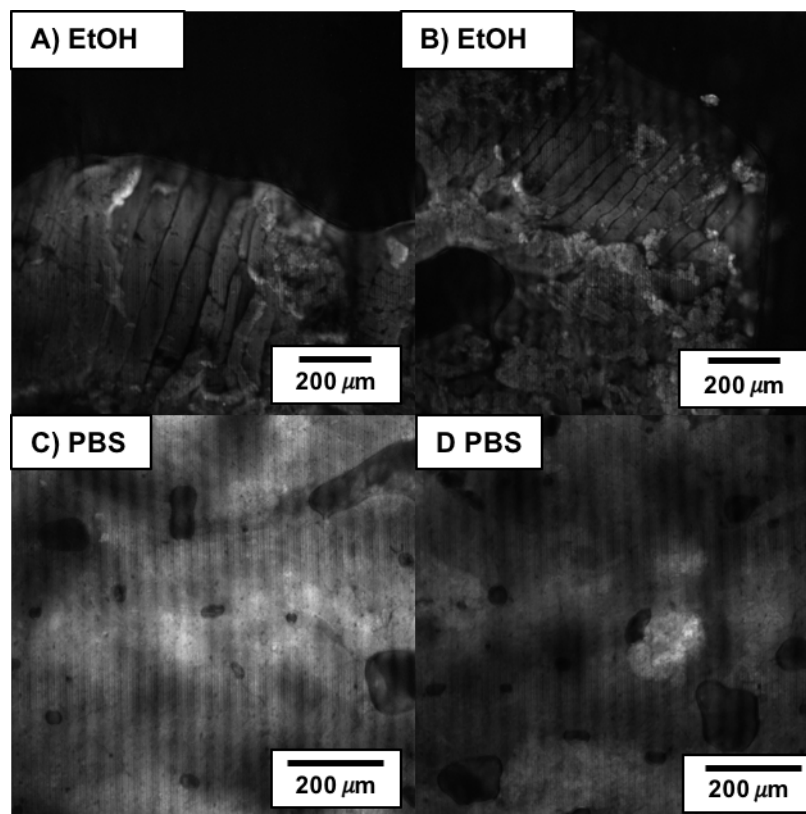


**Figure 4.4:** Visual comparison of bovine muscle exposed to eosin Y dissolved in both 80% Ethanol and PBS. Two areas from the same tissue are shown with both the ethanol solvent (A,B) and PBS solvent (C,D).

Given the need to balance signal intensity, specificity, staining time, and conservation of materials, DRAQ5's fluorescent peak at 50  $\mu\text{M}$  at three minutes of staining, which is near equal to its intensity peak at the same concentration at 5 minutes, is used for all further analysis. Similarly, eosin Y's concentration of 3 mM was only improved by increasing the stain time from 10 seconds to 45 seconds. Factoring in the knowledge that the ethanol-solvent improves specificity at the cost of potentially drying out the tissue, shorter time frames (under 45 seconds) decrease the risk of permanent alteration to the tissue. Thus, eosin Y's optimized protocol uses a 3 mM concentration, dissolved in 80% ethanol, for a minimum of ten seconds with the knowledge that if the situation allows, longer staining will improve intensity.



The concentrations and staining times with the highest normalized intensity and feature specificity were then used to determine that DRAQ5's intensity was minimally decreased after application of eosin, compared to the reverse case in which eosin Y's signal was greatly reduced with a subsequent DRAQ5 staining step. This experiment led to the finding that DRAQ5 being applied first as the best practice to maximize signal for both dyes. Once these parameters were determined, they were applied to fresh human biopsies from partial nephrectomy and radical prostatectomy patients.

#### **4.3 Application of D&E on fresh, intact, surgical specimens**

*Simulated biopsy acquisition, staining, and imaging.* Two fresh renal biopsies from nephrectomy procedures and one fresh prostate punch biopsies from radical prostatectomy procedures were obtained under a Tulane IRB approved protocol. Biopsies were collected from excised tissue specimens for research purposes and not necessary to the clinical diagnostic workflow. Renal biopsies were obtained using an 18-gauge core-needle biopsy device (Bard Monopty) from freshly excised partial and total nephrectomy specimens from benign renal parenchyma. The prostate biopsy was taken as from specimens containing prostatic adenocarcinoma. The biopsies were delivered to the imaging suite in saline directly from the operating room. They were stained using the optimized procedure determined from the work described in Chapter 4.2. The biopsies were submerged in 50  $\mu$ M DRAQ5 for 3 minutes. After incubation in DRAQ5, the biopsy was briefly rinsed by immersion in PBS and dried by patting with lab tissue (Kimtech). It was then submerged in 3 mM eosin in 80% ethanol for 20 seconds and rinsed by immersion in phosphate buffered saline (PBS) to remove excess stain. The biopsy was thoroughly washed via immersion in PBS for several seconds and then blotted dry with lab

tissue. The stained tissue was placed on a glass slide, ensuring maximum contact with the surface of the slide. The entire staining process took approximately 5 minutes and could be parallelized for multiple biopsies using cassettes.

*Acquisition, staining, and imaging of an excised human prostate.* An excised prostate from a radical prostatectomy procedure was also obtained from patients providing informed consent using IRB standard protocol. The intact prostate was delivered to the imaging suite immediately after removal. Once in the imaging suite, specimens were stained using the optimized D&E staining procedure, imaged, then sent to the Tulane Medical School Histology Department for H&E processing. Resulting H&E sections were scanned with the previously described Aperio whole slide scanner. The biopsies were imaged with the previously described VR-SIM system and processed using three phase SIM and the previously described pseudocolor algorithm, Gareau method.

*Surface imaging of a prostate.* After staining, the prostate was placed on a large glass slide, posterior surface down. The posterior side is typically the flattest surface of the prostate, and combined with the natural deformity of fresh tissue, the majority of the surface makes direct contact with the slide. The prostate was imaged using VR-SIM and processed using HiLo and the Giacomelli pseudocolor method (for maximum optical section thinness and bright field-like coloring).

#### **4.3.1 Pathological review of intact, whole biopsy D&E**

Three intact, 18-gauge core-needle renal biopsies and one prostate punch biopsy were fluorescently stained and imaged with VR-SIM. Pathologist review of the D&E images identified a healthy glomerulus in one biopsy and a sclerotic glomeruli pair, shown in Figure 4.5, which was confirmed in the H&E-stained FFPE section taken after imaging.

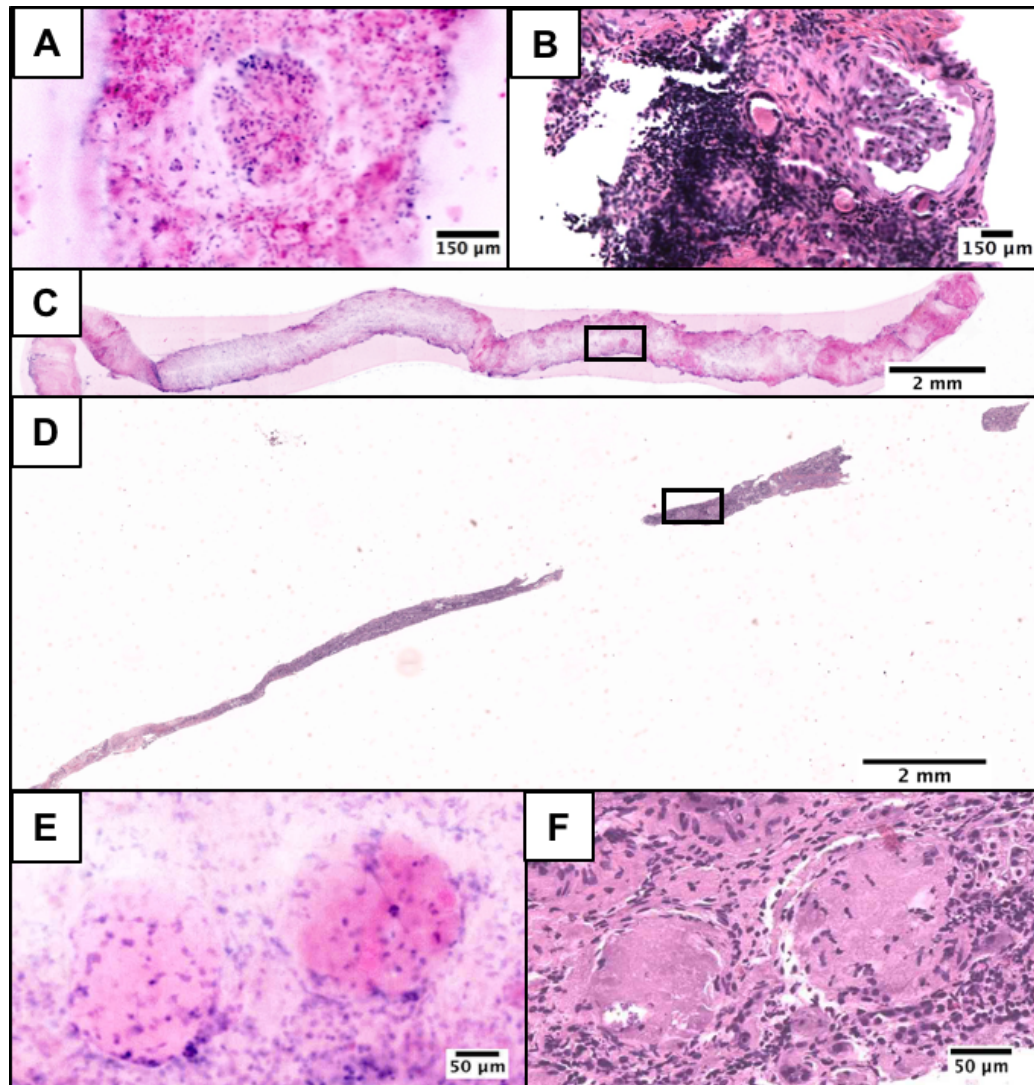


**Figure 4.5:** D&E (A) and H&E (B) of a healthy glomerulus from an intact kidney needle biopsy core. D&E (C) of an entire intact kidney needle biopsy core, and (D) subsequent H&E section. D&E (E) and H&E (F) of sclerotic glomeruli from the kidney biopsy.

The D&E (Figure 4.5 A) staining and imaging provides information on the entirety of the biopsy compared to the fragmented appearance of the FFPE sectioned biopsy (Figure 4.5 B). The area of the optical section in the biopsy D&E image is 20.5 mm<sup>2</sup>, whereas after physical sectioning and H&E processing, the remaining tissue section comprises an area of only 6.7 mm<sup>2</sup>. Increased differences between the D&E and H&E images are apparent in the biopsy, but these can be

attributed to the thickness of the tissue being imaged in D&E and the loss of tissue during standard histopathology processing. Normal glomeruli were identified in the first biopsy, as well as a sclerotic glomeruli pair in the second biopsy. The glomerulosclerosis in the second biopsy is characterized by a loss of nuclei and the replacement of the round glomerulus with eosinophilic fibrosis, seen in both the D&E and H&E images.

Clear cell renal cell carcinoma (CCRCC) was diagnosed in an intact 18G renal core biopsy, shown in Figure 4.6. In both the D&E (Figure 4.6 A) and H&E (Figure 4.6 B) images there is a clear loss of normal renal architecture with replacement by a homogenous proliferation of neoplastic tumor cells, encompassing the entire biopsy specimen. The homogenous nature, lack of tubules and glomeruli, and light coloration of the eosin signal compared to the DRAQ5 signal (Figure 4.6 C) are all features indicative of the presence of a neoplasm, confirmed as clear cell renal cell carcinoma on histology (Figure 4.6 D).

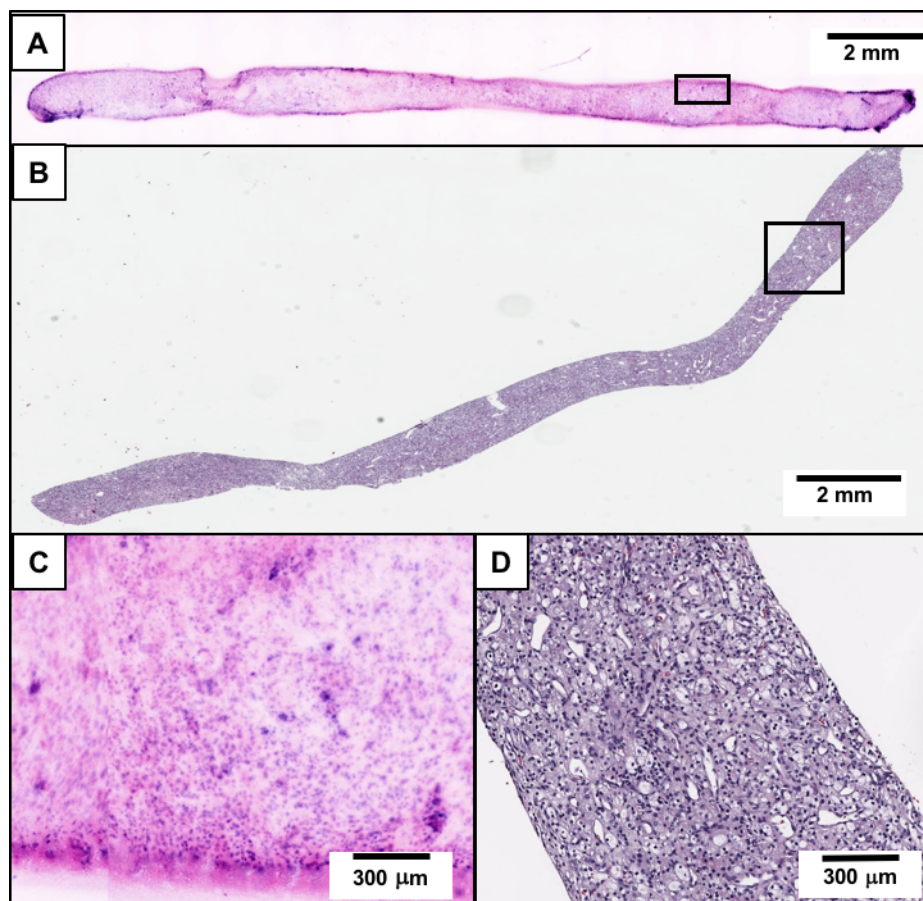


**Figure 4.6:** D&E (A) of clear cell renal cell carcinoma in an intact 18G core needle kidney biopsy and (C) an area of higher magnification showing loss of normal renal architecture. H&E (B) of a 4  $\mu$ m section from the same kidney biopsy showing clear cell renal cell carcinoma and (D) an area of an area of higher magnification showing loss of normal renal architecture.

A prostate biopsy containing adenocarcinoma is shown in Figure 4.7. As an example of the use of D&E for assessment of cancer biospecimen quality, we evaluated the tumor content of each modality; 10% tumor content was observed in the D&E image (Figure 4.7 A), matching the 10% tumor content observed in the H&E section (Figure 4.7 B). Within the biopsy, areas of healthy glandular structures (black arrows) are shown adjacent to areas of malignant adenocarcinoma gland infiltration (yellow box) in both D&E (Figure 4.7 C) and H&E (Figure 4.7 D) images. The comparable tumor content in both methods supports the ability of D&E to be

used as a non-destructive tissue triage method for personalized medicine and downstream molecular analysis.

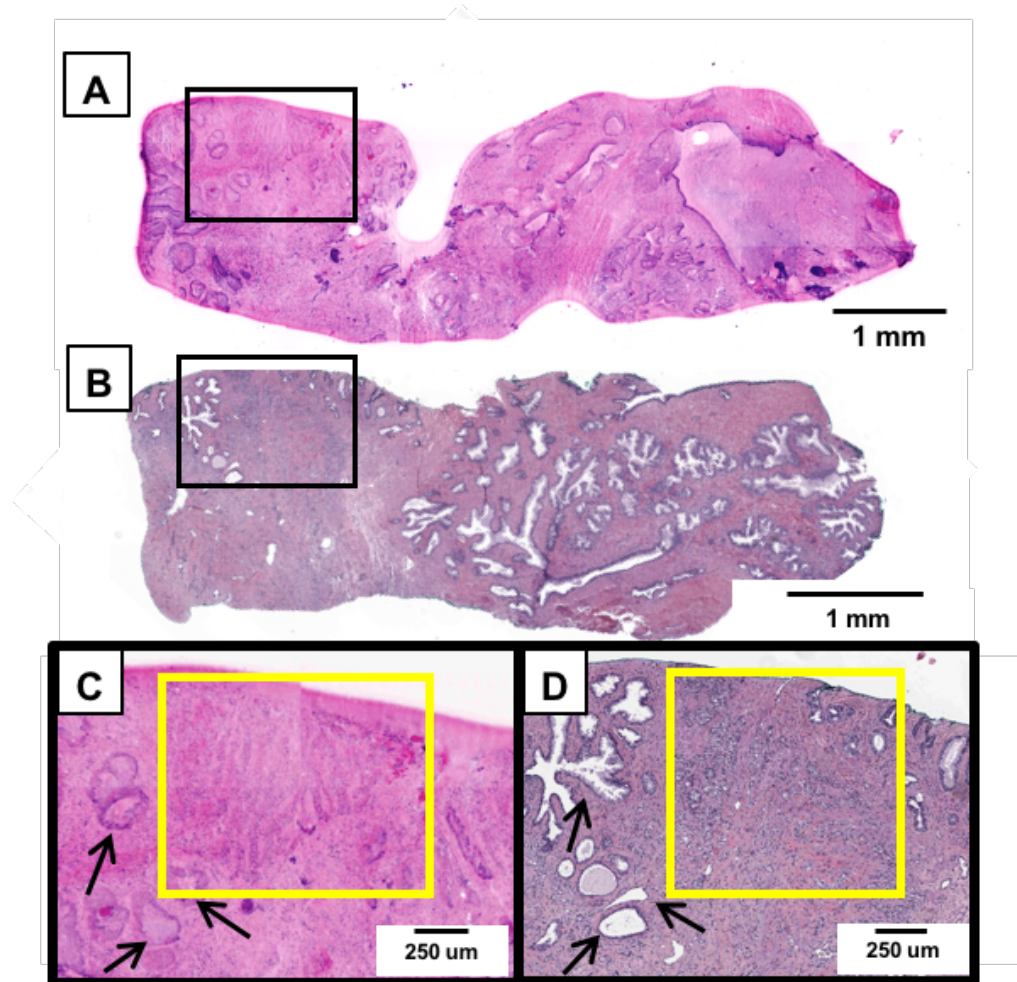


**Figure. 4.7:** D&E (A) of an intact prostate large core needle biopsy with adenocarcinoma and a 4  $\mu\text{m}$  H&E (B) section from the same tissue. D&E (C) and H&E (D) of infiltrating prostatic adenocarcinoma (yellow box) adjacent to normal prostatic glands (black arrows).

By confirming the diagnostic utility of D&E on intact, biopsies, we can expand it to other tissue types and sizes. Our group has previously published on the ability to use acridine orange to microscopically visualize the margins of radical prostatectomy specimens, but the ability to use dual-color fluorescence histology on these specimens has not yet been shown. We therefore

investigated the ability to uniformly stain and image the surface of an excised prostate specimens with the dual-color D&E stain and image processing system.

#### ***4.3.2 First demonstration of fluorescence histology on an intact prostatectomy specimen***

The surface of a prostate margin, removed during a standard radical prostatectomy procedure, stained with D&E and imaged using the VR-SIM system is shown in Figure 4.8. Within the surface, areas of fat content (Figure 4.8 B) and a neurovascular bundle (Figure 4.8 C) are clearly visualized.



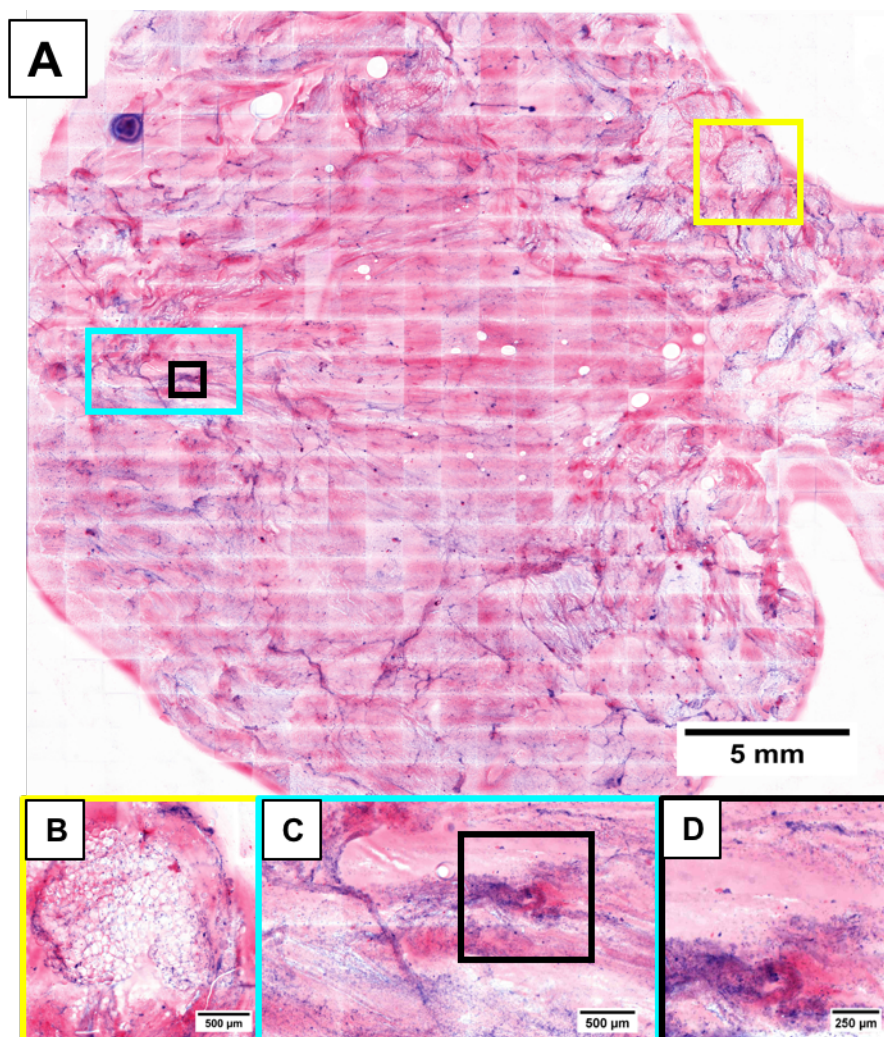


**Figure 4.8:** D&E of the posterior surface of an intact prostate margin from a radical nephrectomy with an area of fat content (B) and a neurovascular bundle (C,D).

To date, six prostate specimens have been imaged using dual-color D&E. Further work to image the entirety of a prostate margin is currently in progress.

#### 4.4 Comparison of Acridine Orange and D&E on Fresh Prostate Biopsies

Currently, both single-agent and dual- (or more) agent stains are used for fluorescence microscopy. The reasoning behind choices of stains varies and is usually purpose-dependent; however, our work in fluorescence histology requires the interpretation of experts in tissue



histology, pathologists. Pathologists are trained to interpret a wide variety of specialty stains that vary in both appearance and imaging method. AO as a general histological stain and the combination of DRAQ5 and eosin (D&E) as a dual-color method in histology as previously been discussed [5,54,55]. While both stains show diagnostically accurate information, clinical adoption requires a method that is both specific and easily utilized by trained pathologists. Single-agent stains have the benefit of low levels of complexity involved in both the staining procedure and creation of the image. Acridine orange stains DNA, cytoplasmic RNA, collagenous stroma, muscle fibers and other extracellular material [15,63,67]. It is commonly used to create a grey-scale histological representation of tissue within a few minutes of staining.

We demonstrated acridine orange as a reliable diagnostic stain in prostate and kidney biopsies and prostate margin analysis [54, 55]. Our results show that AO as a single-contrast agent can be used to detect cancer in fluorescence histology and correspond with others who use AO as a single-contrast diagnostic tool [63,64]. However, the non-selective nature of AO and the limitation of greyscale contrast can result in the need for advanced training for use in fluorescence histology. Pseudocolor, the creation of a RGB image from a monochrome image, is often preferred in visual analysis because the human eye can discern more variations in color from an image than shades of gray [8,11]. In the previous chapter we showed that D&E, when pseudocolored to resemble bright field imaging, can create a near-identical fluorescent analogue to H&E [84]. We have also demonstrated in the first part of this chapter the use of D&E on fresh, intact biopsies and organ specimens from surgical procedures, similar to our previous work with AO in prostate biopsies and prostate margin analysis. While the traditional dark background created from fluorescence histology is suitable for grayscale imaging to aid in differentiation of shades, pseudocoloring fluorescence histology to mimic the appearance of bright field illumination has been suggested to facilitate pathologist's interpretation of fluorescent images [2–

5,52]. Yet, to the best of our knowledge, no previous work directly comparing the two modalities for diagnostic analysis has been published.

In this study, we conducted a blind review with a pathologist to determine if the different contrast modalities performed equally in diagnostic evaluation of prostate biopsies. Both quantitative (accuracy of diagnosis compared to FFPE H&E sections of the biopsies) and qualitative (ease of review, mental fatigue, expertise of the reviewer) factors were considered.

#### **4.4.1 Comparison of Acridine Orange and D&E on Fresh Prostate Biopsies**

*Stains.* From the optimized protocol, DRAQ5 (5 mM, Biostatus, Ltd.) was diluted from 5 mM to 50  $\mu$ M in PBS. Eosin Y (E4009, Sigma-Aldrich) was dissolved to [1% w/v] in 80% ethanol. Using our lab standard methods, acridine orange was diluted from 2% solution to 3.3mM in PBS. Stains were applied directly to intact tissue via immersion without further modification.

*Tissue Acquisition.* Fresh prostate biopsies (n=49) for this study were obtained in accordance with an Institutional Review Board-approved protocol. These biopsies were collected for research purposes from radical prostatectomy specimens containing prostatic adenocarcinoma.

*Specimen Staining.* Whole biopsies were submerged in saline immediately after collection until time of staining. The biopsies were then either stained with 3.3 mM AO (n=21) for 45 seconds by submersion or stained with D&E (n=28) by submersion in 3 mM in ethanol eosin for 15 seconds, blotting dry with a lab tissue (Kimtech), then submersion in 50  $\mu$ M DRAQ5 for 3 minutes. After staining with either method, the biopsy was rinsed thoroughly in PBS and dried by patting with lab tissue and placed on glass slide for imaging.

*Specimen Imaging.* Biopsies were imaged with the previously described custom VR-SIM system. Once imaging is complete, the biopsy is removed from the slide and the side that was

imaged is stained with histological ink before fixation in 10% formalin. The inked biopsy is then sent to the Tulane Medical School Histology Department for fixation, sectioning, and standard H&E processing. Resulting H&E sections were scanned with an Aperio 20x whole-slide scanner. Optical sectioning was computed with the three phase SIM algorithm. AO images were processed with a standard flat-field correction procedure to account for illumination uniformity. D&E images were flat field corrected and then pseudocolored using the algorithm previously described in Chapter 3 [84].

*Blinded Diagnostic Review.* A pathologist reviewed the VR-SIM images and the H&E slides from the inked side of the biopsies as two separate cohorts. The pathologist first analyzed the 49 H&E slides as a single cohort using 10x-20x magnification to determine what histological features were contained within each biopsy. After identifying features related to the biopsies' histology and diagnostic factors, the pathologist then identified which of these features could be found in the VR-SIM images by analyzing them as a single cohort. The pathologist also applied a Gleason grade independently to the H&E slides and VR-SIM images where prostatic adenocarcinoma was identified. A secondary unblinded review was conducted to resolve discrepancies between the VR-SIM images and the H&E sections.

#### **4.4.2 Diagnostic analysis of monochrome and dual-color fluorescence imaging**

In this study, the presence of histological features identifiable in the monochrome and dual-color VR-SIM were compared against their presence in the corresponding H&E sections. With all viewing techniques, the pathologist first surveys the tissue at a low magnification before using higher magnification to examine regions of interest. Figure 4.8 shows examples of biopsies in all modalities and points out the features identified in H&E where corresponding features were also identified in the VR-SIM images. Prostatic stroma and corpora amylacea are found in

the biopsy stained with acridine orange (Figure 4.9 A) and its H&E section (Figure 4.9 B). Both benign glands and a seminal vessel is located the D&E biopsy (Figure 4.9 C) and its H&E section (Figure 4.9 D).

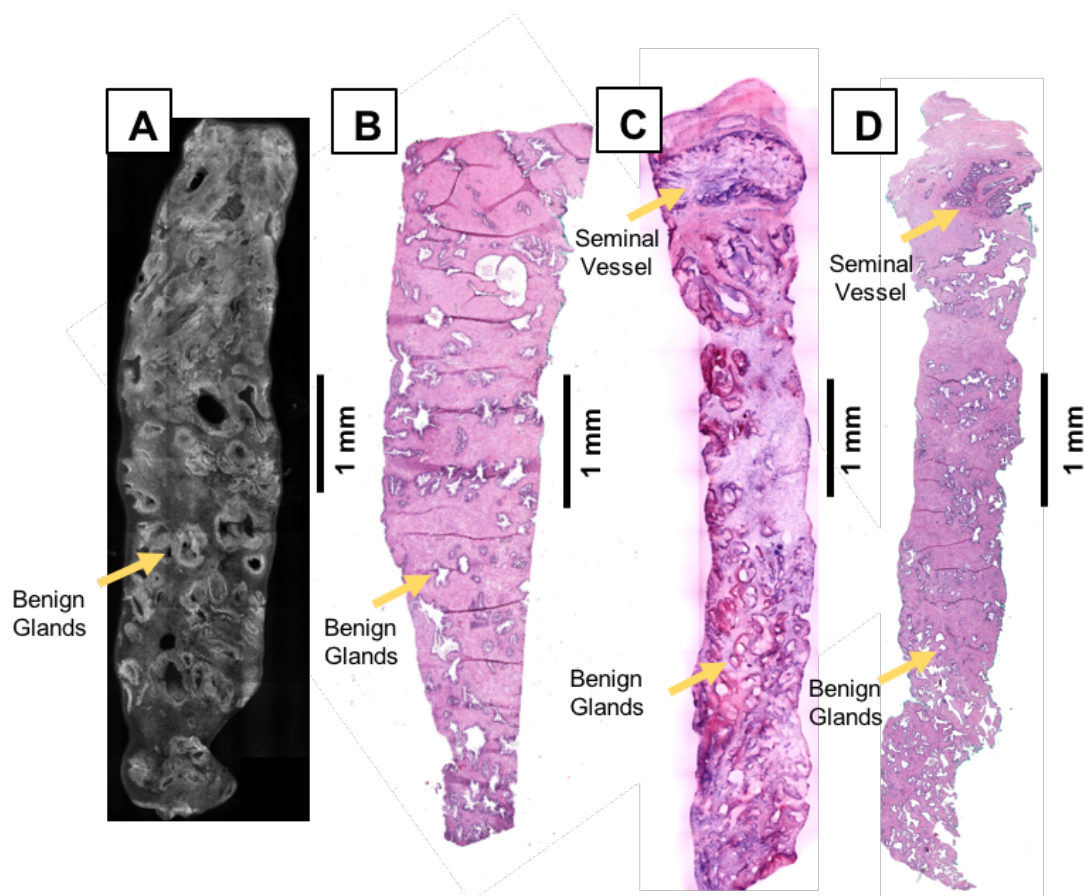


**Figure 4.9:** Intact, fresh punch-core prostate biopsies fluorescently stained with acridine orange (A) and D&E (C) and their respective 4  $\mu$ m H&E section counterparts cut from the imaged surface (B, D).

In the monochrome image, all stained components appear as white against a dark background, with size and form the major identifiers for features. Dual-color images differentiate color as well as size and shape. In the D&E stain, all nuclei are purple, with eosin staining cytoplasm and extracellular components, against a white background.

The pathologist noted twelve features in the H&E slides which the monochrome and dual-color VR-SIM images were validated against: prostatic adenocarcinoma, chronic inflammation, benign glands, smooth muscle, prostatic stroma, vessels, corpora amylacea, nerves, basal cells, stromal hyperplasia, and seminal vesicles. As shown in the figure above, the presence of features varied depending on individual biopsies and were not consistent across all samples. Of those twelve, seven features were present in both monochrome and dual-color images and three are directly related to diagnostic utility: benign glands (Figure 4.10), chronic inflammation (Figure 4.11), and prostatic adenocarcinoma (Figure 4.12). In Figure 4.10, representative images of benign prostate glands are depicted with both monochrome (Figure 4.10 A) and dual-color contrast (Figure 4.10 C) along with their H&E counterparts (Figure 4.10 B,D).

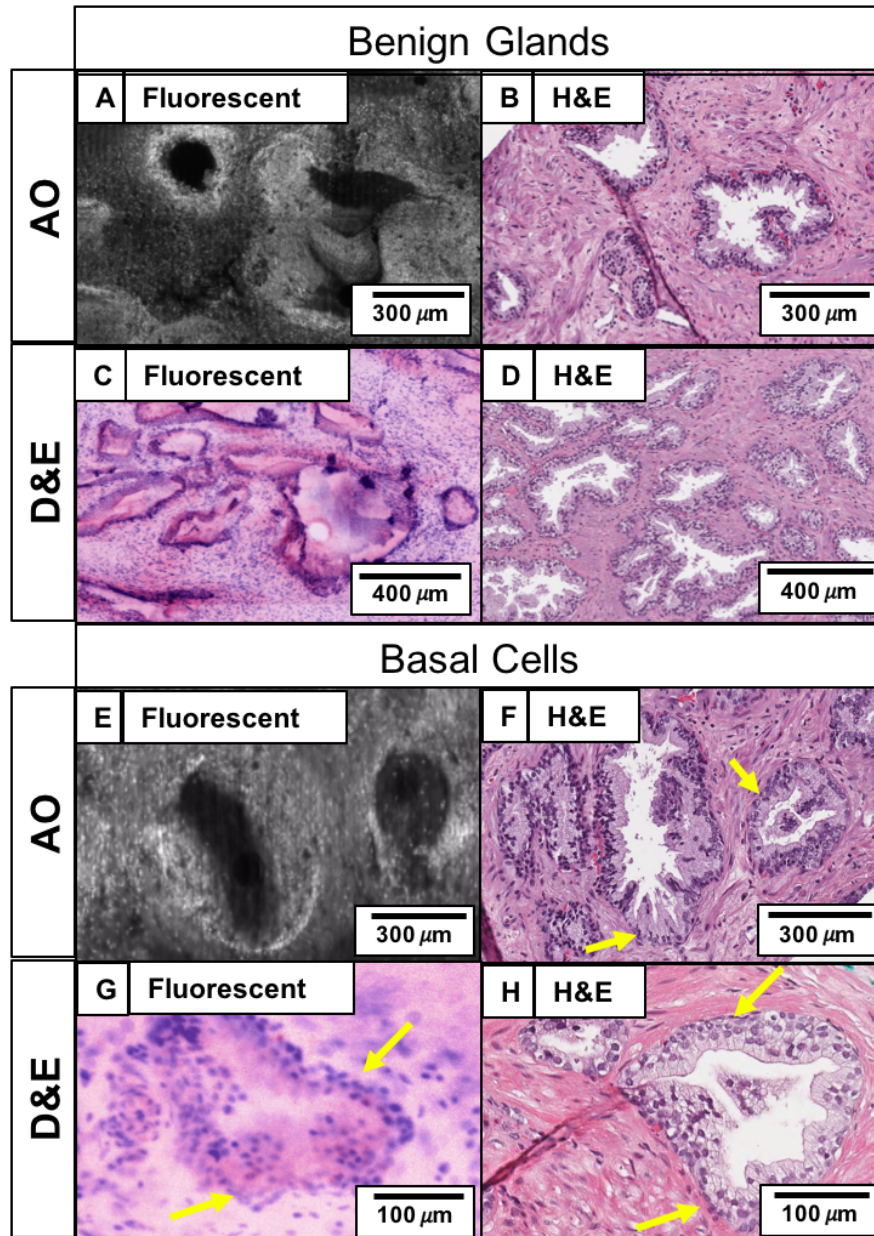


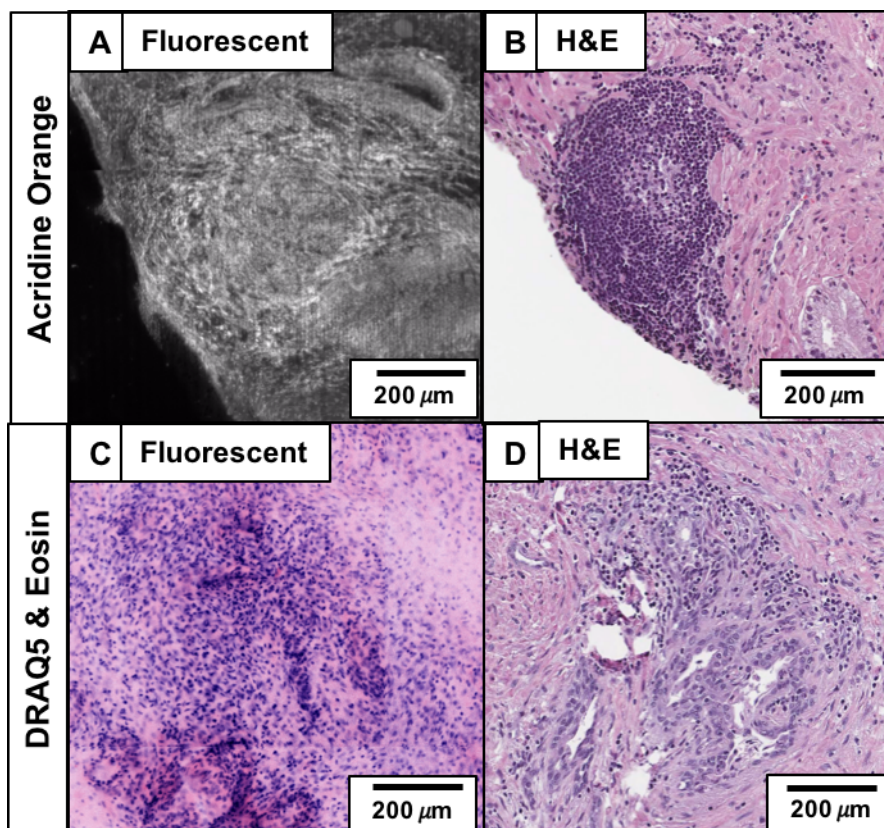
Figure 4.10: **Benign glands in intact, fresh punch biopsies from radical prostatectomy cases stained with acridine orange (A) and its H&E counterpart (B) or stained with D&E (C) its H&E counterpart (D). Basal cells (yellow arrows) can be identified in both H&E sections (F, H) and the D&E images (G) but not in AO images (E).**

Figure 4.10 shows a comparison between benign glands where basal cells were identified in the H&E section (Figure 4.10 F) but not the AO biopsy (Figure 4.10 E) and benign glands in dual-color contrast where basal cells were identified in blind review in both fluorescence images

(Figure 4.10 G) and H&E (Figure 4.10 H). Basal cells, a hallmark of benign glands, were only positively identified in dual-color contrast images but could not be differentiated in any monochrome images, as signal is generated from a variety of structures and isolating individual cell areas is more difficult. Correctly identifying nuclear morphology in tissue is highly useful in differentiating diseased from benign tissue.

Chronic inflammation is a benign condition that can be mistaken for prostatic adenocarcinoma. Markers of chronic inflammation include small, round lymphocytes with large nuclear to cytoplasmic ratios focused around benign glands. Figure 4.11 shows examples of chronic inflammation in both monochrome contrast (Figure 4.11 A) and dual-color contrast (Figure 4.11 C), along with their respective H&E counterparts (Figure 4.11 B, D).





**Figure 4.11:** Chronic inflammation in intact, fresh punch biopsies from radical prostatectomy cases stained with acridine orange (A), its respective 4  $\mu$ m H&E section (B), and stained with D&E (C) and the 4  $\mu$ m H&E section counterpart (D).

Chronic inflammation was positively identified in one AO biopsy out of nine total and positively identified in five D&E biopsies out of 14 total instances. Only one false positive was identified, a D&E biopsy, and the false positive was attributed to a higher optical section thickness than the histological standard of 4  $\mu$ m physical section thickness rather than discrepancies from visualization method. Additionally, chronic inflammation that had not previously been identified in three H&E biopsies were positively identified after second review where D&E diagnosis was initially noted as a false positive. This correction was not made in any AO reviews.



While tumors can result from chronic inflammation, the presence of it is not an indicator of prostatic adenocarcinoma [85]. However, it can be difficult to distinguish between the benign inflammatory condition and carcinoma. Some forms of prostate inflammation can mimic prostate carcinoma in rectal examination, ultrasound, and in with elevated blood serum prostate specific antigen (PSA) levels. Histologically, they can also be mistaken for each other as the high concentration of nuclei in both pathologies. Prostatic adenocarcinoma contains large, prominent nuclei and form multiple small glands or angulated, single-file lines that infiltrate through prostatic stroma. A Gleason grade, the staging system of prostate cancer, was given to both the VR-SIM images and the H&E sections.

Prostate biopsies with adenocarcinoma a in both modalities and their corresponding H&E sections are shown in Figure 4.12 along with their assigned Gleason scores given in blind review. A Gleason grade is composed of two separate scores: a primary pattern score and a secondary pattern score. The total Gleason grade is the pathologist's final staging determination based on the individual scores [86]. The first set of biopsies shown in Figure 4.12 was assigned a Gleason grade 3. The biopsy imaged with AO (Figure 4.12 A) closely matched the individual Gleason scores in its corresponding H&E section (Figure 4.12 B), and the same final determination was made in the dual-contrast Gleason grade 3 (Figure 4.12 C) and its corresponding H&E section (Figure 4.12 D). The second set of biopsies was given a Gleason grade 4 (Figure 4.12 E,F,G,H).

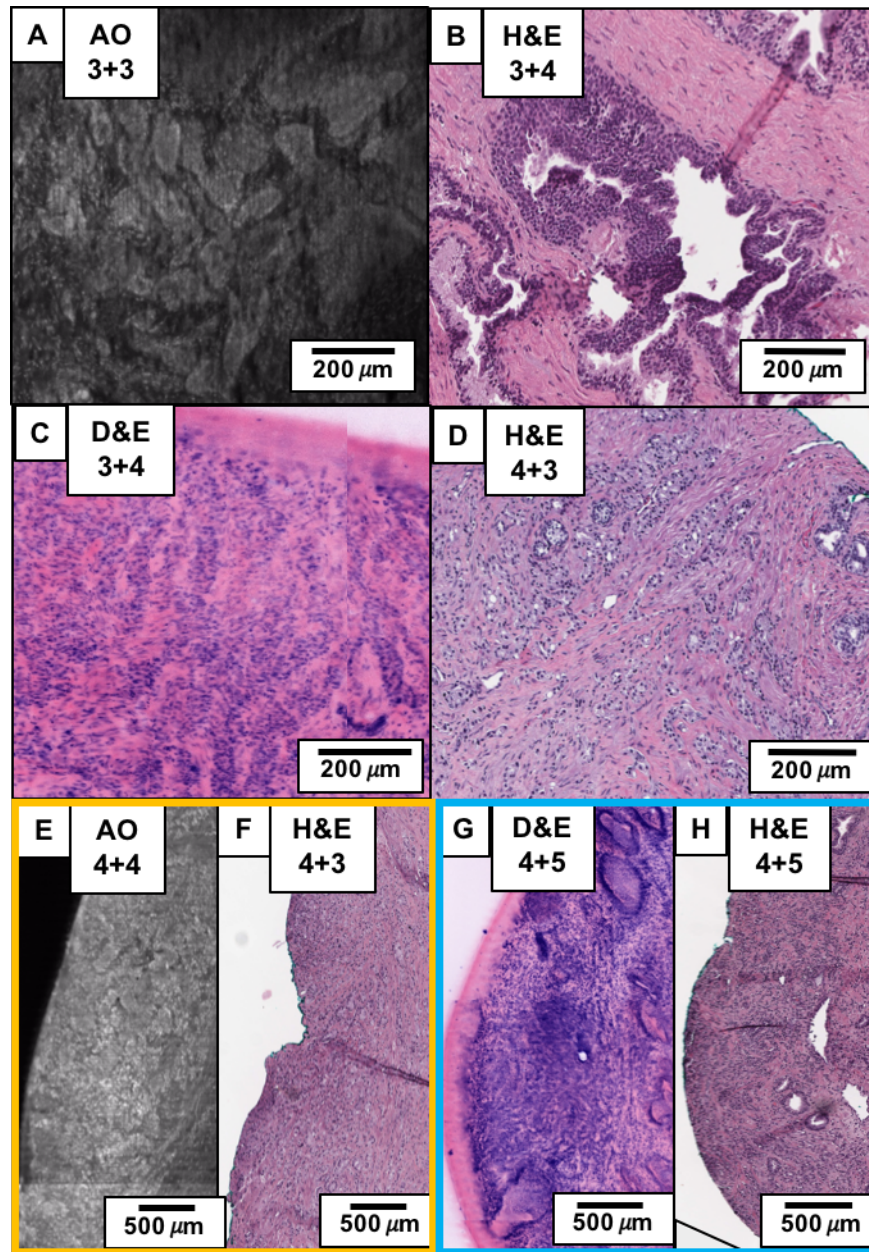


**Figure 4.12:** Adenocarcinoma in prostate punch biopsies from radical prostatectomy cases. Biopsies were stained with either acridine orange (A,E) then compared to their H&E sections from the imaged surface (B,F) or stained with D&E (C,G) and the H&E sections from the imaged surface (D,H).

Glandular structure is an important distinction in assigning a Gleason grade [1]. Gleason grade 3 (Figure 4.12 A,B,C,D) contains single, highly variable glands that can have ragged edges, whereas the fusion of glands and absence of intervening stroma, is a hallmark of Gleason grade 4

(Figure 4.12 E,F,G,H) [86]. The importance of distinguishing between nuclei and stroma, and therefore gland structures and shape, cannot be overemphasized. After review, the pathologist noted that it was more difficult to determine glands in monochrome images, as they could also resemble vessels and other structures of closely packed signal. Dual-contrast visualization, however, clearly designated what signal was the result of stroma versus nuclei and therefore made gland morphology easier to interpret.

In total, eleven biopsies were found with tumor content: seven biopsies that were stained with acridine orange and four stained with D&E, shown in Table 4.1. Of these biopsies, there were eight positive diagnostic matches between VR-SIM and H&E, five AO and three D&E, and all were assigned Gleason grades that corresponded closely to their H&E counterparts.

**Table 4.1: Results of a blind review of prostate cancer as viewed with either monochrome contrast (AO staining) or dual-color contrast (D&E staining).**

Specimen	Match	Stain	VR-SIM Gleason Grade	H&E Gleason Grade	Tumor Content
Case 23	True Positive	AO	4+3	3+3	3%
Case 25	True Positive	AO	3+3	3+3	60%
Case 15	True Positive	AO	4+3	4+4	80%
Case 21	True Positive	AO	3+3	3+4	3%
Case 20	True Positive	AO	5+5	5+4	75%
Case 56	True Positive	DE	3+3	3+4	30%
Case 42	True Positive	DE	3+4	4+3	30%
Case 40	True Positive	DE	4+5	4+5	12%
Case 26	False Negative	AO	-	3+3	4.60%
Case 6	False Negative	AO	-	3+3	3.80%
Case 38	False Negative	DE	-	3+4	70%
Case 7	False Positive	AO	3+3	-	-
Case 9	False Positive	AO	4+4	-	-
Case 25	False Positive	DE	4+4	-	-

There were three false negatives identified, two AO and one D&E. The tumor content in the AO specimens was both less than 5%, but the H&E section of the D&E biopsy contained 70% tumor. Three false positives, two AO and one D&E, were attributed to the 50 $\mu$ m optical sections (over an order of magnitude greater than the typical 4 $\mu$ m histology section) and the presence of chronic inflammation. Particularly in the case of the D&E false positive, the presence of chronic inflammation with extensive luminal protein and luminal macrophage accumulation created higher cellularity on SIM, mimicking the cribriform pattern typical of Gleason 4 adenocarcinoma.

#### **4.4 Discussion of monochrome versus dual-color contrast**

We compared two common fluorescent image contrast methods, AO as a monochrome stain and D&E as a dual-component pseudocolor system, on fresh, intact prostatic tissue and demonstrated the ability of each to provide rapid histological analysis prior to gold-standard H&E processing. Both methods could be applied topically to fresh specimens and be analyzed within minutes of staining [5,54, 55]. Three diagnostically relevant features were closely examined: benign glands, chronic inflammation and prostate cancer. In a blinded diagnostic review, the false positive and false negative rates for D&E were 50% lower than that of Acridine Orange, likely influenced by the inability to differentiate individual cells in monochrome contrast and the thicker sections compared to FFPE H&E. There were also differences between the two contrast mechanisms in both the ability to identify some specialized features, such as basal cells (Figure 4.10 [E,F][G,H]), and the pathologist's comfort level when assigning a name to a benign feature. Moreover, several of the features were reported as more easily identifiable in dual-color over monochrome, although they could be identified in both methods. The difficulty of differentiating between vessels and glands in monochrome can be particularly troublesome if

gland histology or vasculature is of high importance to the analysis, such as with staging prostate cancer.

After completing the blind review, the pathologist reported that dual-color contrast was easier to interpret for pathological analysis. This modality provides several layers of context for histology: the nuclei are one color, cytoplasm and extracellular material is another color, and the background is white. The pseudocolor process to replicate the appearance of H&E, first demonstrated by Gareau and then used by several groups since, has the possibility of providing images near-identical to the H&E slides created from the intact tissue [2,3,48,87]. This technique, however, depends as much on the specificity of the stains to match H&E as on the pseudocolor process. In D&E, the nuclear-specific stain, DRAQ5, combined with the general stain, eosin Y, provides a near-identical analogue to H&E [5]. This specificity creates easier differentiation between features, such as vessels and glands and allows for the positive identification of basal cells which was not possible with AO.

In point-of-care biopsy procedures, the focus is on quickly and accurately differentiating between benign and diseased tissue. This goal is especially important when analyzing biopsies with chronic inflammation and other diseases which can be mistaken for prostate cancer and vice versa. Notably, neither contrast modality resulted in a false negative due to mistaking chronic inflammation for prostate cancer. The given reasons for false negative diagnoses of prostate cancer was either due to small percentages (<5%) of tumor content or due to the imaging technique, not the contrast methods. The fluorescence technique, VR-SIM, creates approximately 50  $\mu\text{m}$  thick optical sections, which is sufficient for accurate diagnosis [53–55]. As fluorescent stains and contrast methods can be adapted to any fluorescent system, the question after demonstrating the possibility of a high-fidelity dual-color pair is whether it is more useful to the pathologist than monochrome contrast stains.

While both single and dual-agent stains provide important diagnostic information regarding biopsy tumor content, the ease of interpretation is important for adoption of a method. With a single-agent stain like AO, fluorescent signal can come from DNA, RNA, collagen, or any other binding structure [67]. Evaluators must differentiate what is relevant for diagnosis and what is background. However, with D&E it is possible to isolate nuclei through color differentiation and make a diagnosis solely based on nuclei formation against the stroma. Furthermore, in traditional fluorescence the stronger the signal the whiter it appears against a dark background; however, a pathologist is accustomed to interpreting dark areas as those of more dye accumulation and therefore must mentally invert their training to read the traditional fluorescent image. Therefore, we have found that the context given by dual-agent, pseudocolor contrast of D&E is extremely useful for making diagnostic decisions. This context, such as the differentiation of vessels from glands, both improves the confidence a pathologist has in adopting the use of fluorescence histology and can ease the adoption of fluorescence histology in the clinic.

#### **4.4 Comparison of Time, Cost, and Instrumentation**

Along with considering pathologist preference, the economic and instrumentation considerations of fluorescence histology should be evaluated before recommending its adoption for clinical and research use. H&E, a standard histological stain used for almost 100 years, is readily available, low cost to use, and can be viewed with any bright field microscopy system. To compete with even highly destructive alternatives, such as FSA and touch-prep, fluorescence histology must be fairly easy to adopt both in terms of complexity and economically.

The three histology methods, acridine orange, D&E, and H&E were evaluated in terms of material cost per tissue sample, instrumentation requirements, processing time for the

image/slide to be ready for viewing, the complexity of the steps to complete the process, and the specificity of features identifiable in a specimen. Each factor was individually reviewed and a weight assigned on a scale of 1-5 with the highest numbers giving the preferred outcomes of easy, cheap, and specific.

Figure 4.13 is a chart demonstrating the ratings for each modality on a scale of 1-5, denoted by increasing number of asterisks where the higher the number, the better the rating.

<p>***** Highest Rating</p> <p>* Lowest Rating</p>	Instrumentation			Histological Features		Diagnostic Specific Features		
	Complexity	Processing Time	Cost	Nuclei-Specific Contrast	Stroma-Specific Contrast	Prostate Cancer	Chronic Inflammation	Basal Cells
Monochrome	****	*****	****	**	*	****	**	*
Dual-Color	*****	*****	***	*****	*****	*****	*****	***
FFPE H&E	*	*	*****	*****	*****	*****	*****	*****

**Figure 4.13:** Economic, procedural, and histological comparison of single-agent fluorescence histology, dual-agent fluorescence histology, and FFPE H&E methods.

H&E requires multiple steps following several timed applications and washes from the moment that the tissue is required. These steps also contribute to its processing time. It must undergo formalin fixation (or another hardening method), possibly paraffin embedding with multiple steps attached, sectioning which requires both instrumentation and an experienced technician, washes and dyes, and cover-slipping before being ready for bright field imaging. In contrast, both fluorescent methods require only brief washes of PBS and their respective stains, with D&E being the most extended with more than one staining application. Conversely, H&E is exceedingly cheap to use as it is well distributed across the market to keep prices low and the instrumentation needed is somewhat cheaper than that of a fluorescent optical sectioning

method. However, once a fluorescent microscope with optical sectioning capabilities is acquired, AO is also comparatively inexpensive and easy to acquire. DRAQ5's restricted market means that its price is less competitive, although adoption of it in both research and clinical use may see the price decrease.

From the previous study, we also know that H&E is ideal for most histological uses, though not all, and therefore its performance is the preferred medium in histological comparison. In spite of this fact, both fluorescent stains demonstrate high diagnostic accuracy by a trained pathologist regardless of their performance on less diagnostically relevant features.

#### **4.5 Conclusion**

In this Chapter, D&E was optimized for application with fresh, thick tissue specimens by evaluating both the concentrations of the stains and the staining duration against the need for cost and time effective protocols demanded of any successful ROSE method. Additionally, we found that the use of ethanol as a solvent for eosin increased its staining specificity even though a PBS solvent demonstrated overall high fluorescent intensity. Using the protocol developed from this optimization process, biopsies from radical prostatectomy procedures were stained with D&E and evaluated against the single-contrast stain, AO. A pathologist focused evaluation found that while both methods were useful for diagnostic analysis, the dual-contrast nature of D&E required less interpretation and analysis by the pathologist than the monochrome visualization method. This pathologist is an expert in the field of fluorescence histology in both modalities, with experience in making diagnostic and feature-recognition decisions in both modalities [54, 55,84]. As such, the finding that there were 50% fewer false positives and false negative calls in D&E gives significant credence to the adoption of dual-contrast over monochrome fluorescence



histology. However, further studies with larger sample sets and a panel of pathologists with varying levels of expertise will be needed to fully support these findings.

In an economic evaluation of the three methods, monochrome, dual-contrast, and FFPE H&E, H&E was far superior except in complexity and processing time – the critical components of ROSE. Therefore, for ROSE – the two fluorescent histology methods were superior, with more feature specificity found with D&E and less time and cost associated with AO.

Therefore, the purpose of the study may often dictate which contrast modality is the preference of researchers. Fluorescence techniques such as structured illumination, confocal, and multiphoton microscopy have all demonstrated the ability to reliably relay histological information regardless of contrast method. For analyses that require only differentiation of features without pathological feedback, the quick, extremely low complexity needed of a single-agent monochrome stain might be preferable. Acridine orange is a single, topical stain that can be applied to fresh tissue and be ready for imaging in less than two minutes and has been shown to have [54,5,67]. Monochrome images created from tissue stained with AO are capable of accurate diagnosis but require time and training to interpret, which is not preferable in point-of-care diagnostics when methods exist that create an accurate H&E fluorescent analogue.

For pathologists, histological evaluation is a result of years of training with bright field dyes, particularly H&E. Therefore, pathologists who adopt fluorescence histology may find pseudocolor, multi-channel contrast the easiest method to evaluate tissue, regardless of minor differences in complexity or time to acquire the images.

## CHAPTER FIVE: Downstream Analysis

*Parts of this chapter will be presented at the annual Optical Society of America: Biomedical Optics Congress 2018 on April 6, 2018.*

### 5.1 Introduction

Given that the purpose of this work is to use fluorescence staining as a rapid, non-destructive intermediary step between tissue acquisition and further downstream quantitative and qualitative evaluation, we must verify that the fluorescent stains do not interfere with standard clinical downstream analysis. As mentioned in Chapter 2, along with histology, pathologists often use specialized techniques, such as molecular analyses, immunofluorescence, and electron microscopy, to form a final diagnosis. By far, the most used of these techniques are molecular analyses, such as DNA quantification, polymerase chain reaction (PCR), and immunohistochemistry (IHC). A commonality of these techniques is the use of fluorescence, most often UV fluorescence, to quantify or demonstrate the result. The focus of this chapter is to determine whether fluorescent stains added to fresh tissue affects later downstream molecular analyses.

### 5.2 Fluorescence Persistence in Formalin Fixed, Paraffin Embedded Processing

The primary concern with downstream analysis of tissue after the addition of exogenous fluorophores is whether there will be interference with other fluorescent diagnostic tools. As biospecimen conservation and utility is of high importance in pathology, often the same piece of tissue will be utilized in multiple analyses, such as H&E, IHC, and PCR [88,89]. Standard-of-care for clinical specimens is formalin fixation and paraffin embedding followed by either sectioning and histological staining or specialized molecular assays. By tracking the intensity of fluorescence through the standard FFPE process, we can determine whether additional fluorophore extraction methods are needed to remove extraneous fluorescence prior to specialized fluorescence analysis,

like immunofluorescence staining [13]. Cahill *et. al.* recently published an article on the combination of acridine orange and sulforhodamine 101 (SR101) for multiphoton pseudo-H&E fluorescence histology [52]. Within the work, they completed a study comparing the fluorescence intensity of the AO and SR101 channels immediately after staining and then after formalin infiltration. Fluorescence was then compared against a non-stained control segment of the same tissue. This comparison showed that for multiphoton microscopy, intensity decreased to control levels after formalin fixation. While they noted that paraffin is known for its high optical scattering properties, the clinical standard is FFPE for sectioning; the chemical and physical processing of tissue does not stop at formalin fixation. Additionally, only examining the intensity of fluorescence does not indicate whether the fluorescence left after fixation is specific from exogenous fluorophores or completely endogenous. By tracking the fluorescence signal of a piece of tissue through the full FFPE and sectioning process, we can learn whether fluorescence interference is of concern in later analyses. In this work, we tracked nine 18-gauge kidney biopsies from partial nephrectomy cases to determine if the fluorescent signal from stained specimens decreased to that of control conditions. In addition to overall fluorescence levels, we examined the fluorescent images of all cases, identifying spatially the origin of fluorescence signal at each processing step to determine whether any persistent signal was from specific stained tissue components or due to non-specific auto fluorescence.

### **5.2.1 Testing Fluorescence Persistence in FFPE Tissue**

*Tissue acquisition.* Nine Eighteen-gauge needle biopsies from partial nephrectomy specimens were obtained with informed consent using Tulane IRB-approved procedures. The biopsies were transported in saline from the operating room directly to the imaging suite. They were subdivided into three groups: stained with D&E, stained with acridine orange, or left

unstained. All biopsies were imaged via VR-SIM microscopy with 470 nm and 640 nm lasers (LDI, 89 North), at previously optimized parameters to maximize intensity without saturation. D&E and control biopsies were imaged with a 45 ms integration time, 70% power for the 470 nm channel, and 90% power for the 640 nm channel. The AO stain was imaged with a 10 ms integration time, 30% power for the 470 nm laser, and 90% power for the 640 nm laser. After imaging, the biopsies were placed in 10% formalin fixative for 48 hours, the Tulane Histology Laboratory clinical standard for complete fixation and delivered to the Tulane Histology Lab for paraffin embedding and sectioning to 4  $\mu\text{m}$ . Once each processing step was completed, the biopsies were re-imaged, resulting in a total of four sets of images for each biopsy: fresh, formalin fixed, paraffin embedded block, and sectioned.

*Fluorescence Signal Quantification.* Each biopsy averaged fifteen 2048x2048 pixel image frames each. The individual frames with signal from each processing point were analyzed with ImageJ. A standard square region of interest (ROI), 100x100 pixels, was used to find the mean intensity of the signal and the background for each frame. The SBR across the processing timeline was compared within staining groups and against the control group via a paired Student's t-test.

### **5.2.2 Results of FFPE Processing on SBR**

The SBR of both channels, the 470 nm excitation and the 640 nm excitation, are shown in the non-stained control samples in Figure 5.1. The effects of formalin fixation and paraffin embedding on endogenous fluorescence is particularly apparent with 470 nm excitation as the mean SBR increases from ~3 in fresh imaging to ~5.1 post fixation, increases again to ~7 while embedded in a paraffin block, and then decreases to ~4.5 in an un-stained section (Figure 5.1 A). On the other hand, the SBR of the entire 640 nm excitation process were closely clustered around an SBR of 3 in the control sample.

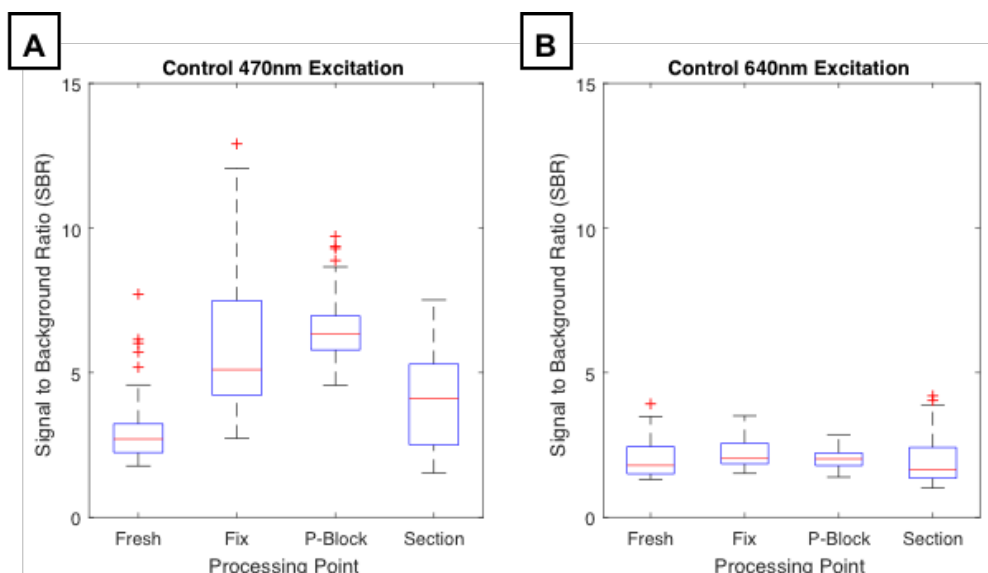


**Figure 5.1:** SBR of endogenous signal in control (non-stained) 18-gauge kidney biopsies across the FFPE and sectioning process imaged with a 1W 470nm Laser (A) and 500mW 640nm Laser (B).

The total SBR range of the control samples varied from 1 to 12, which is expected given both the scattering properties of thicker specimens as well as the endogenous fluorescent agents within tissue. These autofluorescent molecules (primarily pyridinic and flavin co-enzymes, such as NADH and riboflavin, but also elastin, porphyrins and others) are primarily excited by shorter wavelengths (cite). Also expected is the increase in fluorescence after fixation given the autofluorescent effects of many fixatives are well known due to the chemical changes they induce in tissue [90,91].

When the tissue that has been stained with AO and D&E is examined, the difference in signal induced by exogenous fluorescent agents is readily apparent. Figure 5.2 shows the effects of the FFPE and sectioning process on stained tissue imaged with both wavelengths of lasers.

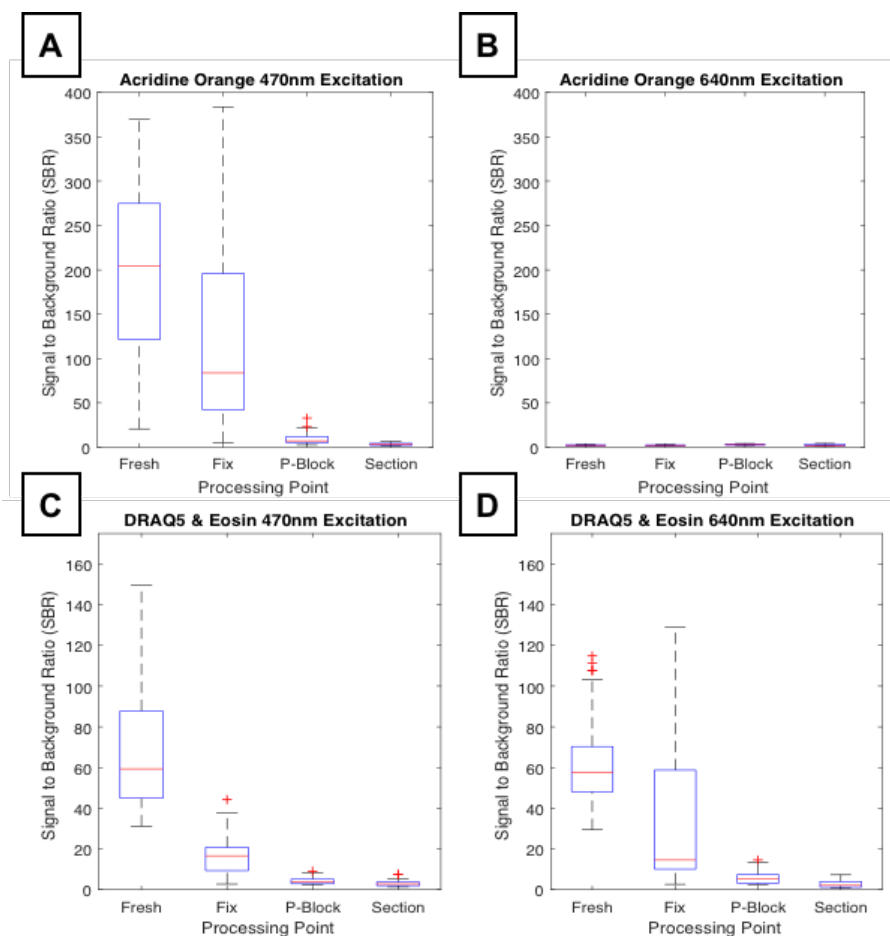


**Figure 5.2:** SBR of endogenous signal of 18-gauge kidney biopsies across the FFPE and sectioning process stained with acridine orange illuminated with 470 nm (A) and 640 nm (B) and D&E illuminated with 470 nm (C) and 640 nm (D).

The steady decrease in SBR is evident as the specimen progresses through processing.

Acridine orange's 470 nm maximum SBR (Figure 5.2 A) is approximately four times higher, at ~380, than D&E's maximum fluorescence in either 470 nm (Figure 5.2 C), at 130, or 640 nm (Figure 5.2 D), at 150. As expected given its fluorescence spectra, AO exhibits minimal signal in the 640 nm excitation (Figure 5.2 B).

We then directly compared each experimental group in the four processing stages. Figure 5.3 shows the four three groups illuminated with 470 nm excitation and Figure 5.4 shows the

same groups illuminated with 640 nm excitation. The SBR of the control specimens, the D&E specimens, and AO specimens are directly compared in freshly acquired tissue (Figure 5.3 A), after formalin fixation (Figure 5.3 B), within a paraffin block (Figure 5.3 C), and in an unstained 4  $\mu$ m section (Figure 5.3 D) as imaged with 470 nm excitation.

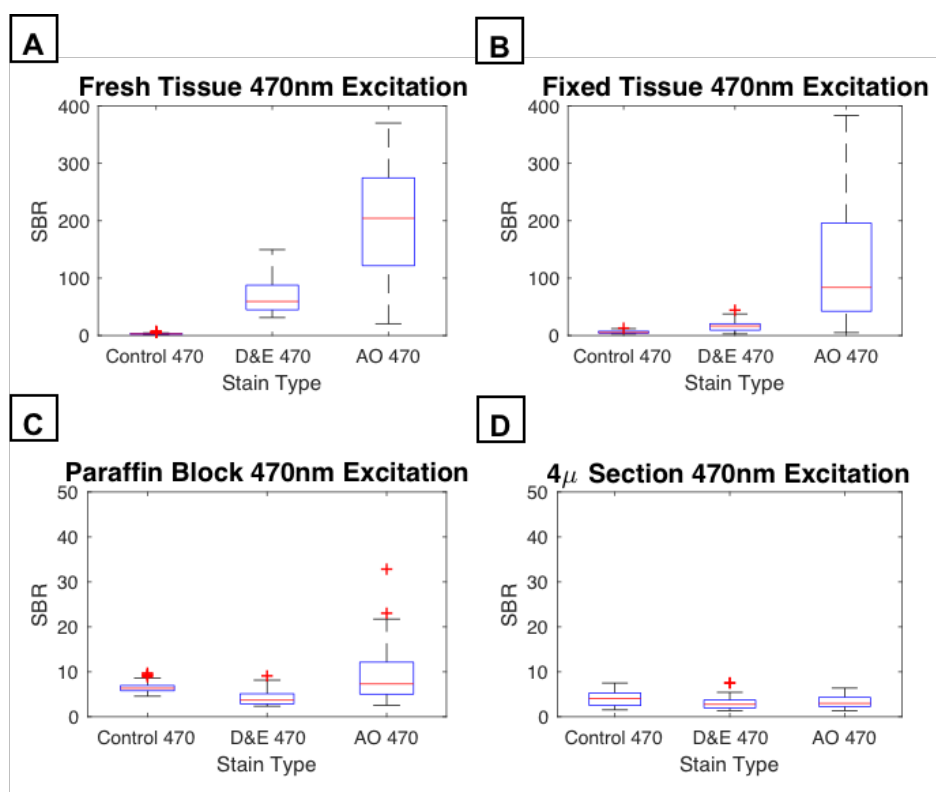


**Figure 5.3:** SBR of endogenous signal of all 18-gauge kidney biopsies experimental groups illuminated with the 470nm laser in fresh tissue (A), post-formalin fixation (B), within a paraffin block (C), and sectioned at 4 $\mu$ m on a slide (D).

As a result of the ~ 400 SBR from freshly stained and formalin fixed tissue acridine orange tissue, the fluorescence from acridine orange far exceeds that of the control or D&E specimens in the first two steps (Figure 5.3 A,B). As we shift into the later stages, however, the SBR of both AO and D&E decreases to the same order of magnitude as the control sample. In a paraffin block, the 470 nm AO signal remains roughly double that of the control sample, although

the mean D&E SBR is ~4, which is less than the control of ~7.5 (Figure 5.3 C). By the last step in the FFPE-sectioning process, both the AO and D&E SBR values are, on average, lower than those of the control sample (Figure 5.3 D).

In Figure 5.4, the 640 nm SBR of the three experimental groups are shown in fresh tissue (Figure 5.4 A), fixed tissue (Figure 5.4 B), the tissue in a paraffin block (Figure 5.3 C), and in an unstained 4  $\mu$ m section (Figure 5.4 D).

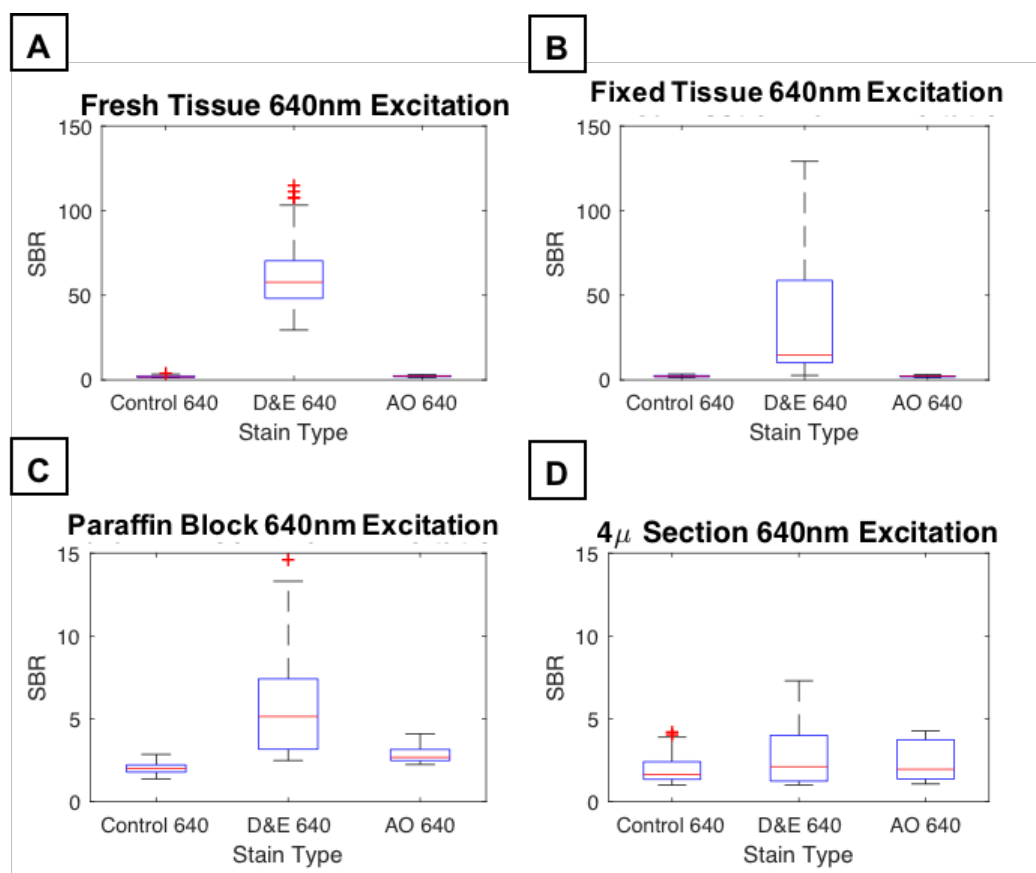


**Figure 5.4:** SBR of endogenous signal of all 18-gauge kidney biopsies experimental groups illuminated with the 640nm laser in fresh tissue (A), post-formalin fixation (B), within a paraffin block (C), and sectioned at 4 $\mu$ m on a slide (D).

Unlike AO's dominance of the 470 nm excitation comparison, DRAQ5 is the primary source of fluorescence in the 640 nm SBR series (Figure 5.4). As with the 470 nm excitation comparison, D&E's signal is an order of magnitude higher than either the control or AO



specimens. Even in the last step, the D&E exhibits a marginally higher SBR (3.2) than the control sample (2.3), but it is still lower than the 4.5 SBR of the control sample with 470 nm excitation. Importantly, the final SBR in the sectioned tissue of both lasers are on the same order as the control specimens, indicating near-complete extinguishment of fluorescence in the sample during FFPE processing.

When examining the individual frames of the stained biopsies, it was evident that both eosin Y and AO rapidly lose staining specificity with no distinct features evident after formalin fixation. However, in Figure 5.5, we can see that the nuclei in DRAQ5 retain some staining specificity even as SBR has decreased to closely match the control baseline. When compared to the control sample's sectioned image (Figure 5.5 E), areas of signal closely matching the shape and size of nuclei are clearly visible in the DRAQ5 image (Figure 5.5 F).

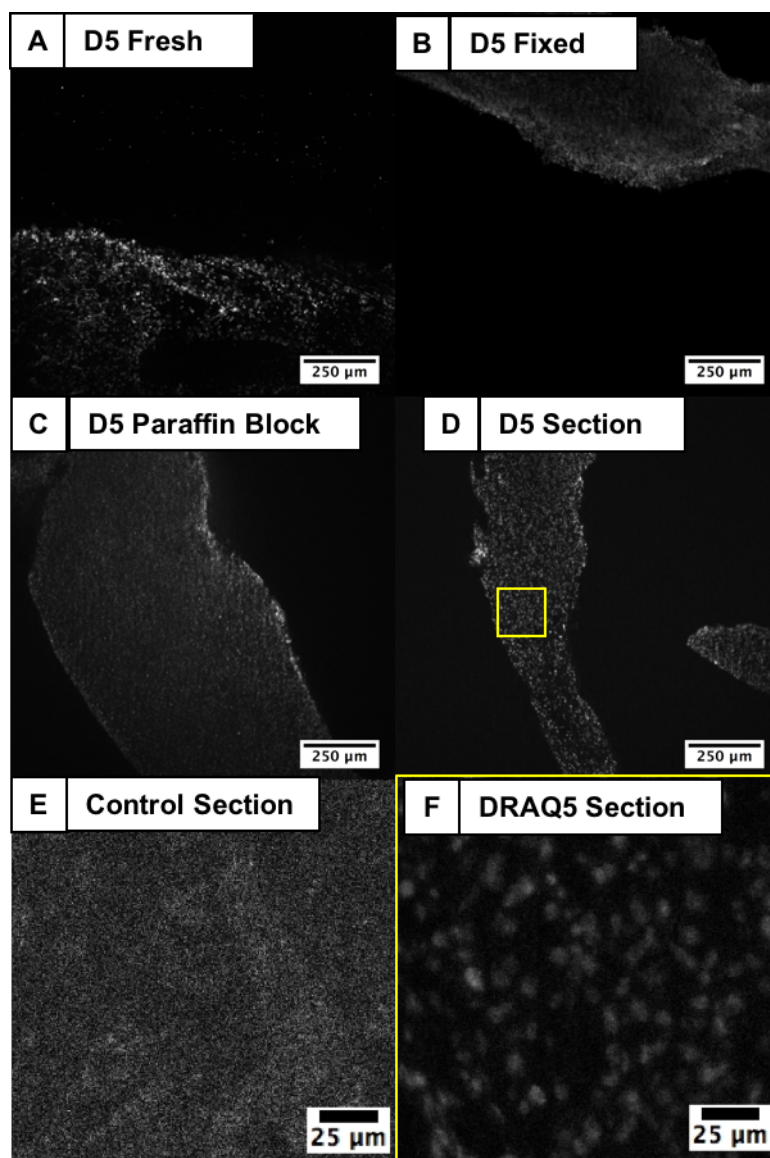


**Figure 5.5:** DRAQ5 fluorescence illuminated with a 640nm laser in fresh tissue (A), formalin fixed tissue (B), in a paraffin block (C), and in a 4 $\mu$ m section (D). A zoom of a control 4 $\mu$ m section (E) and a DRAQ5 stained 4 $\mu$ m section (F) demonstrate the specificity of stain leftover after FFPE processing.

### 5.2.3 Conclusion of FFPE effects on fluorescence histology

From this study, we determined that the clinical standard FFPE process is sufficient for removing exogenous fluorescent signal from tissue. Unlike prior studies, we investigated the effects of tissue processing up to the application of histological dyes on the sections – providing

four different points of interrogation in the process. Previous work analyzed only the effects of formalin fixation on fluorescence and our results agree with their findings: fluorescence is reduced by the formalin fixation process [52]. However, in our study, each of the three stains possessed its own binding mechanic: simple anionic binding, anionic binding and intercalation, and highly specific intercalation [15,67,73]. When examining the frames of the biopsies of the time points, it was evident that residual DRAQ5 fluorescence provided more specificity in fluorescence even in the sectioned tissue. This finding indicates that fluorophores may need to be individually examined before use in fluorescence histology to verify that their binding and fluorescence mechanics do not interfere with later applications. This extended specificity may also be a helpful feature in the adoption of fluorescence histology. The blocks and sections of tissue may be able to be examined for content prior to cutting or the addition of dyes to help guide further diagnostic steps. An interesting question with DRAQ5, in particular, is the determination of whether the stoichiometric fluorescence to DNA quantity continues in paraffin embedded tissue. If it does, it may be possible to do DNA ploidy estimates without the need to use valuable tissue in flow cytometry studies. As previously discussed, DRAQ5's stoichiometric relationship between fluorescence intensity and amount of DNA is a well-known feature and already used in flow cytometry studies [71,92]. By using this same principle in both optical sections of intact tissue and imaging the tissue later in blocks or sections, estimates on DNA content could be acquired as part of the standard workflow. Traditionally, this analysis would need to be completed through flow cytometry or tedious image segmentation methods, depending on the type of tissue being used. However, if fluorescence intensity still held a linear relationship to DNA quantity, even if reduced in a sample, these destructive and tedious step could be skipped entirely in the clinical and laboratory workflow.

### 5.3 Impact of Fluorescence Histology on PCR Preparation and Results

The polymerase chain reaction (PCR) is an important diagnostic tool for cancer diagnostics, infectious agents, and inherited disorders [93–95]. One of its uses is to determine gene expression to differentiate subtypes of cancers and determine specific mutations within a tumor, such as the *p53* mutation which is correlated to invasiveness and resistance to treatment [96]. PCR relies on the ability of a polymerase to bind to the DNA to amplify specific areas to increase the concentration of those segments of DNA that encode for a specific gene [43]. Almost every step of the PCR process relies on UV fluorescence to quantify the DNA. For example, DNA purity is often analyzed with a specialized UV spectrometer and UV trans-illumination is used for identifying positive bands in gel electrophoresis. Gels with very blurry bands, indistinct bands, or otherwise not located where expected may be uninterpretable and the process must be re-done. With fluorescent and DNA binding additives present outside of the normal PCR process, the results of these gels may be inconclusive. In RT-PCR, the amplification of the products relies on a DNA-binding fluorophore. Multiple fluorophores are used in PCR with excitation spectra typically ranging from 460 nm to 520 nm. One of the most common RT-PCR dyes is the reporter SYBR Green (bound to DNA: 490 nm<sub>ex</sub>, 520 nm<sub>em</sub>, SigmaAldrich) with the passive reference dye ROX (585 nm<sub>ex</sub>, 610nm<sub>em</sub>, SigmaAldrich)[96]. This dye pair overlaps with the dual-spectra of AO as well as other common blue and green fluorescent dyes [15]. By adding fluorescent components to the tissue prior to processing, there is a risk that we interfere with the fluorescent signal of RT-PCR. Most concerning would be if the additional fluorophores interfere with the threshold cycle (Ct) value which is the point at which fluorescence signal become significant from the background baseline. Accurate Ct values are required for DNA quantification of samples [43].

At the start of both forms of PCR, an accurate quantification and “purity” estimate of the starting DNA or RNA (depending on the goal) is determined through either the use of a UV-spectrometer NanoDrop or flow cytometry. With a NanoDrop, the ratio between the excitation points at the 230 nm, 260 nm, and 280 nm are used in quantification and purity analysis. If the 230 nm and 260 nm peaks are shifted, or if the downward slope at 280nm is not steep enough, then the assumption is that there is either low yield or protein, DNA, or RNA contamination not removed in the purification steps. The ratio of the absorbance at 260 nm and 280 nm ( $A_{260}/A_{280}$ ) indicates the material within the sample. Knowing the purity and concentration of samples is extremely important for both standard PCR and RT-PCR analysis [43].

The purpose of this work is to determine whether the stains utilized with fluorescence histology interfere with PCR protocol and results. This work was evaluated by directly staining cultured adult human dermal fibroblasts immediately prior to gDNA isolation, RT-PCR amplification, and gel electrophoresis with UV-transillumination. By using cells in culture, we could ensure even and thorough stain application on fresh samples without concern about histological or DNA variations.

### ***5.3.1 Methods for PCR Evaluation of Fluorescence Histology***

*Cell Culture.* Adult Human Dermal Fibroblasts (AHDF, Sigma 106-05A) were chosen for this study as they are a robust human cell type with little mutagenesis in passages and their numerous applications across life sciences research. They were cultured to 90% confluency using standard techniques and expanded over three passages to four experimental groups: DRAQ5, eosin Y, acridine orange, and a non-stained control. At 90% confluency, the AHDFs were trypsinized and centrifuged to form a pellet. Media was aspirated off the pellet and cells were re-suspended in either a staining medium or Dublecco’s PBS. Cells were then again spun down, the

stain removed via aspiration, and then suspended in 200  $\mu$ L of Dublecco's PBS per DNA isolation procedure protocol (Qiagen).

*DNA Isolation and Purification.* With four experimental groups across three passages, each experimental group was further divided into ten subgroups for a total of 30 trials of each: control, eosin Y, DRAQ5, and acridine orange. Genomic DNA (gDNA) was extracted from the cells using a standard 50 prep DNEasy Blood and Tissue Kit. After extraction, 2  $\mu$ L of gDNA from each subgroup was tested for purity with the ThermoFischer Scientific NanoDrop 2000.

*RT-PCR and Primer Selection.* Once the concentration of each group was confirmed using UV-spectroscopy, the isolated DNA was then combined with primers for standard internal control genes (ICG), also known as housekeeping genes. Glyceraldehyde 3-phosphate dehydrogenase (GAPDH), beta-actin (ACTB), beta-2-microglobulin (B2M), and interleukin-1-alpha (IL-1A) were all identified as suitable genes for this study. These genes were chosen because two copies exist within every human cell regardless of cell type and they, in particular, were identified as standard ICGs for ADHFs by [97]. The primers for these genes were chosen for specificity to the gene, optimized based on melting temperatures and resultant product sizes (see Appendix B for primer information). The StepOnePlus Applied Biosystems RT-PCR machine was programmed to run a Comparative CT Curve with gDNA, Sybr Green Polymerase (ThermoFischer Scientific), and five replicate runs each for each sample. After the first run, it was evident that both B2M and IL-1A had low amplification efficiency compared to the GAPDH and ACTB primers, so all further experiments were optimized for the more efficient primers.

*Gel Electrophoresis.* After amplification, PCR products were extracted from the wells of the RT-PCR optical PCR plate and kept at 4°C while an agarose gel was prepared. Given the size of the expected products (~300bp each), a 2% agarose gel in 1X TBE buffer was used for increased differentiation. In a typical gel electrophoresis study, a fluorophore, such as ethidium bromide

which requires binding to DNA for fluorescence, will be added to the gel and the buffer. For this study, we needed to determine if any extraneous fluorescence from the histological stains would result in fluorescence within the gel separate from the desired results. Therefore, gels were prepared without the fluorophore. Once the gel solidified, the DNA from the RT-PCR was mixed with a loading buffer (Novex Hi-Density TBE Sample Buffer 5X) and loaded at 15 uL into the wells of the gel. A DNA ladder (DNA Trackit Ladder 50 bp) was also loaded with the samples to aid in quantification. Using an Owl Separation System B3, the gel was run at 120 V for 40 minutes. The gel was then imaged on a UV-Transilluminator at 302 nm and 254 nm using an 8 Mpx camera with 1.5  $\mu\text{m}$  px size. This procedure was repeated 5 times. After the gel was imaged, 10X GelGreen™ (Biotium) was diluted to 3X in water to create a fluorescent staining solution. The gel was immersed in the staining solution for 30 minutes to promote fluorescent binding then imaged again on the UV-Illuminator.

The workflow for this study is illustrated in Figure 5.6, below.

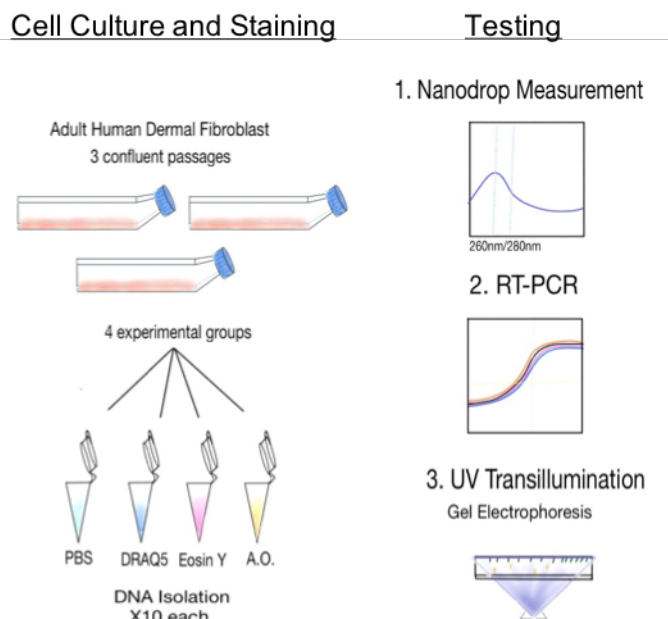


**Figure 5.6:** Three passages of adult human dermal fibroblasts were cultured to confluency. Four experimental groups were cultured within each passage: control, DRAQ5, eosin Y, or acridine orange. Each passage provided enough samples for ten subdivisions of each experimental group. The cells were stained then their gDNA was isolated. The first experiment tested the absorbance of each sample at 260 nm and 280 nm. The second experiment measured the amplification of fluorescence in conjunction with dsDNA. The third experiment examined the effects of fluorescence in the products with UV-transillumination of an agarose gel.

### 5.3.2 Results for PCR Evaluation of Fluorescence Histology

The concentration and purity of both DNA and RNA are often measured with a UV-spectrometer that records the absorbance peaks at 230 nm, 260 nm, and 280 nm. The A260/A280 ratio provides information on the content of a sample; for gDNA it is theoretically about 1.8. However, our samples averaged about 1.99 for all groups, which is not unexpected given that the isolation focus was on the procurement of gDNA, not the removal of RNA, as only the concentration of gDNA would affect RT-PCR analysis. Additionally, Nanodrop quantification is well-known to be imprecise in spite of its standard use [97]. Figure 5.7 shows the range of A260/A280 for all four experimental groups across 30 trials each.



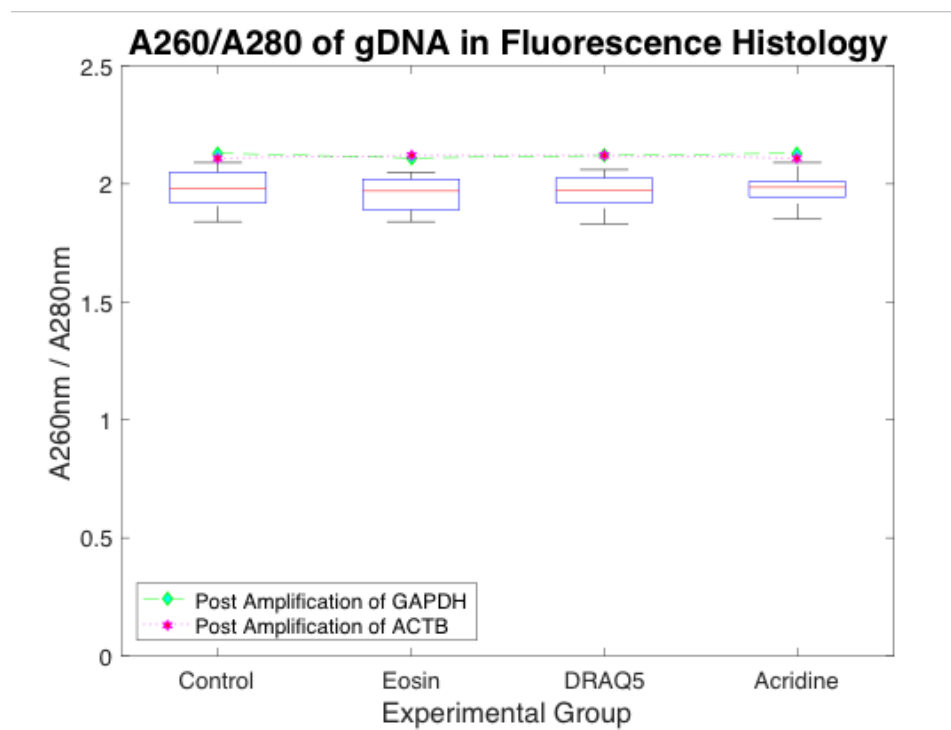


**Figure 5.7:** Combined A260/A280 of gDNA isolated from AHDF from unstained-control samples, eosin Y stained samples, DRAQ5 stained samples, and acridine orange stained samples. The product from the RT-PCR run was then measured again for later concentration analysis: GAPDH amplified gDNA is shown with green stars and ACTB amplified gDNA is shown with magenta stars.

A paired Student's t-test, as shown in the figure above, confirmed no significant difference in the mean absorption ratios between experimental groups with  $p\text{-values} > 1.12 \times 10^{-9}$ . In other words, across 30 data points in each specimen, there was no difference in DNA content between cells stained with fluorescence histology dye and control samples with no staining. From this information, we proceeded to the RT-PCR quantification.

Each set of ten experimental groups was then analyzed using RT-PCR. Multiple replicates are a standard procedure in RT-PCR where even a small pipetting mistake can result in a failed amplification measurement. With the initial RT-PCR run, it was determined that neither the B2M nor IL-1A primers produced enough consistent amplification to be used for analysis.

Primer failure and the failure of individual wells to amplify products are accounted for in the Applied Biosystems StepOnePlus program and a flag is set to nullify results if amplification falls below significance.

The amplitude of the products in relation to the ICG GAPDH (Figure 5.8 A) and the ICG ACTB (Figure 5.8 B) were used for all further analysis as they produced consistent results throughout the experiment. As the focus of this study is on the fluorescent signal from RT-PCR, not gene expression, we were also interested in the multicomponent plot (Figure 5.8 B, E) and the melt curve (Figure 5.8 C,F) of all experimental groups.

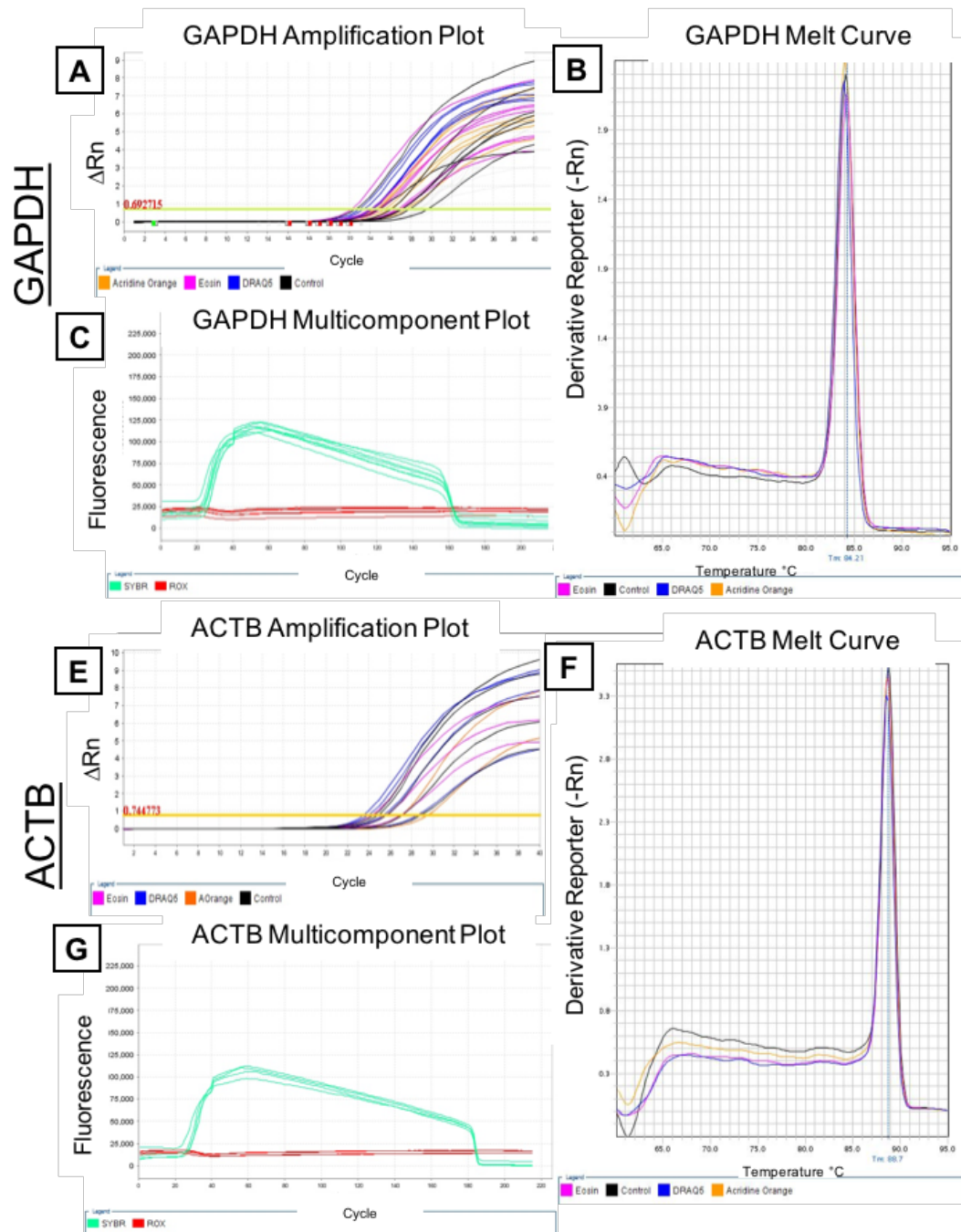


**Figure 5.8:** RT-PCR fluorescence monitoring of the GAPDH (A,B,C) and ACTB (D,E,F) amplification and dissociation curves.  $Rn$  is the reporter signal, SYBR Green, normalized to the reference signal, ROX. The amplitude plot for GAPDH (A) and ACTB (D) across all experimental groups, the multicomponent plot comparing fluorescence of the SYBR Green reporter dye versus the ROX passive dye in GAPDH (B) and ACTB (E) across all experimental groups (B,E), and the dissociation (melt) curve of GAPDH (C) and ACTB (F) across the experimental groups.

In Figure 5.8 A, the uniform amplification of the GAPDH gene is evident across all samples. In this plot, the y-axis,  $\Delta Rn$ , is the change  $Rn$  (the reporter signal normalized to the reference signal) after subtracting the baseline (the point at which fluorescence is detectable in a sample). As the quantity of dsDNA increased, the fluorescence also increased, with all samples registering detectable amplification between the sixteenth and twenty-second reaction cycle regardless of experimental group. Analyzing the amplification plot of ACTB (Figure 5.8 D) also shows uniform amplification across experimental groups between nineteen and twenty-four reaction cycles. The multicomponent plots (Figure 5.8 B, E) tracks the fluorescence of the UV reporter dye, SYBR Green (520 nm emission), against the passive reporter dye, ROX (610 emission) [91,92]. Neither dye showed increased or decreased signal versus time in the stained experimental groups against the control sample. As these dyes share spectral properties with both eosin and AO, lingering exogenous fluorescence would produce results deviating significantly from the control sample, such as earlier increase or delayed decrease in fluorescence. The GAPDH multicomponent plot (Figure 5.8 B) shows peak fluorescence after approximately 45 cycles and a sharp decline in the dissociation phase after 160 cycles. ACTB also has peak fluorescence at 45 cycles (Figure 5.8 E) but its definite melting point was reached after 180 cycles. The cycle variations between primers are expected given the different melting points (and time it takes to reach melting temperature in the dissociation phase. The lack of variation within each primer indicates that none of our fluorescent stains effected RT-PCR quantification.

The melt curve of this experiment (Figure 5.8 C,F) gives a direct comparison of the fluorescence of the sample groups compared to the control group at the conclusion of the amplification cycle. In a melt curve analysis, the temperature is slowly increased until the dsDNA separates and tracks the decrease in fluorescence of the bound report dye to determine the melting point of the dsDNA. If the exogenous DNA binding dyes, DRAQ5 or acridine orange,

interfered with the dissociation of dsDNA we would expect either heightened fluorescence or a shifted melting point from the control sample. However, all dyes either matched or reported non-significant lower average fluorescence than the control sample for both primer targets (Figure 5.8 C,F).

After the amplification process was complete, the RT-PCR products were evaluated by gel-electrophoresis and UV-Transillumination (Figure 5.9). For this set of experiments, the products of the GAPDH and ACTB primers were used to evaluate whether there was uniform movement in the gel across experimental groups, which can be seen with standard imaging with the loading dyes (Figure 5.9 A) and in the close analysis of the final stained gel (Figure 5.9 E).

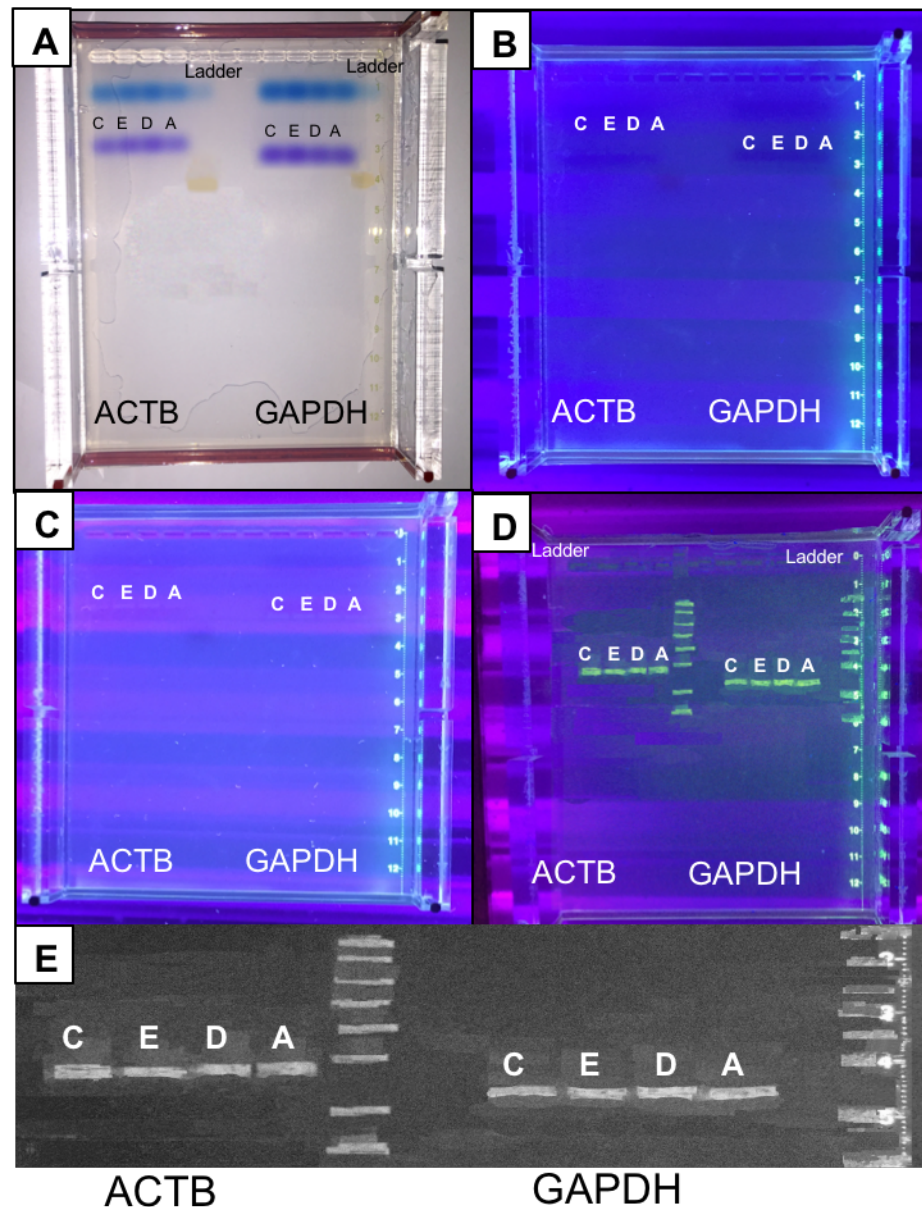


**Figure 5.9:** Gel-Electrophoresis and UV-Transillumination of the gDNA products of fluorescence histology. The end point of gel-electrophoresis shows standard separation of large DNA segments (blue) in visible light (A), under 302 nm UV-B illumination (B), and 254 nm UV-C illumination (C). After imaging baseline fluorescence in the samples, the gel was then stained with GelGreen™ and illuminated with 254 nm UV-C (D,E).

As seen in Figure 5.9 E, there is no variation in movement or appearance through the agarose gel regardless of experimental group. When the gel is imaged with a UV-light, either 302 nm (Figure 5.9 B) or 254 nm (Figure 5.9 C), there is no residual fluorescence evident in either of

the gels that might be interpreted as a positive band signal. When the gel is then incubated with a DNA-binding fluorophore, the product bands are then evident, and roughly equal across experimental groups, as would be expected of a standard gel electrophoresis experiment.

### **5.3.3 Conclusions for PCR Evaluation of Fluorescence Histology**

The effects of the application of exogenous fluorophores to tissue, especially those that strongly bind with DNA, such as DRAQ5, must be considered before adopting their use in studies that rely on other fluorescent evaluation for quantification. The DNA and RNA isolation process that is precursor to all PCR analysis is a series of filtering steps that slowly removes all but the target molecule from the final solution [43]. With UV-spectrometer analysis, there is no apparent difference in the absorption peaks of previously fluorescent samples and the control group (Figure 5.7). RT-PCR requires the use of two fluorophores, an active reporter dye such as Sybr Green and a passive reporter dye such as ROX, which share spectra with those of eosin and acridine orange. Furthermore, the RT-PCR machine is designed for only expected fluorophores and does not filter overlapping spectra from additional dyes. Our results show no variation in the amplification or dissociation curves in any experimental sample from the control. UV-trans-illumination of an agarose gel also demonstrates no variance from either the control sample or non-specific fluorescence that cannot be accounted for by standard dust particles or irregularities in the gel.

### **5.4 Impact of Fluorescence Histology on Immunohistochemistry**

While fluorescence histology may not interfere with PCR analysis, there is still the possibility that the exogenous stains may interfere with specialized molecular histology processing, such as immunohistochemistry (IHC). As previously discussed in Chapter 2, IHC relies on the binding of dye-antigen molecules to their corresponding antibodies within a tissue

[44,45]. As IHC stains are a diagnostic aid and not a preliminary tool, the specific stain is chosen based on the type of tissue and disease suspected within a specimen. Given this purpose, 18-gauge renal biopsies from diseased partial nephrectomy cases were used for this study to facilitate IHC stain selection. Two IHC stains commonly used in renal disease analysis, PAX8 and Cytokeratin 7, were therefore examined to determine the impact fluorescence histology has on these stains.

PAX8, otherwise known as paired-box gene 8, is a transcription factor critical in the development of thyroid, brain, urinary, and reproductive organs, among others. In IHC, it stains positive nuclei a dark brownish-black color [98,99]. PAX8 is highly associated with renal tumors as well as thyroid, bladder, and pancreatic tumors. Studies in renal tissue have found that 100% of normal kidney samples stained positive for PAX8 as well as 90% of renal cell carcinomas [99–102]. Its partner IHC stain, Cytokeratin 7 (CK-7) stains positive cytoplasm brown and is useful in tumor differentiation [103]. Ck-7 is a type of cytokeratin that is found in both normal and malignant epithelium and is useful in the differentiation of epithelial neoplasms [104]. For example, CK-7 is used for the diagnosis of chromophore renal cell carcinoma and renal parenchyma tumors [39,105]. While many epithelial neoplasms are CK-7 positive, notable exceptions include colon, prostate, thymus, and kidney tumors [103].

With IHC, the positive/negative staining pattern is useful for determining tumor type and origin [11,44]. A counterstain is applied to the tissue to provide context in the negative reactive features. These effects can be seen in the control sections for each IHC stain in Figure 5.10, below.



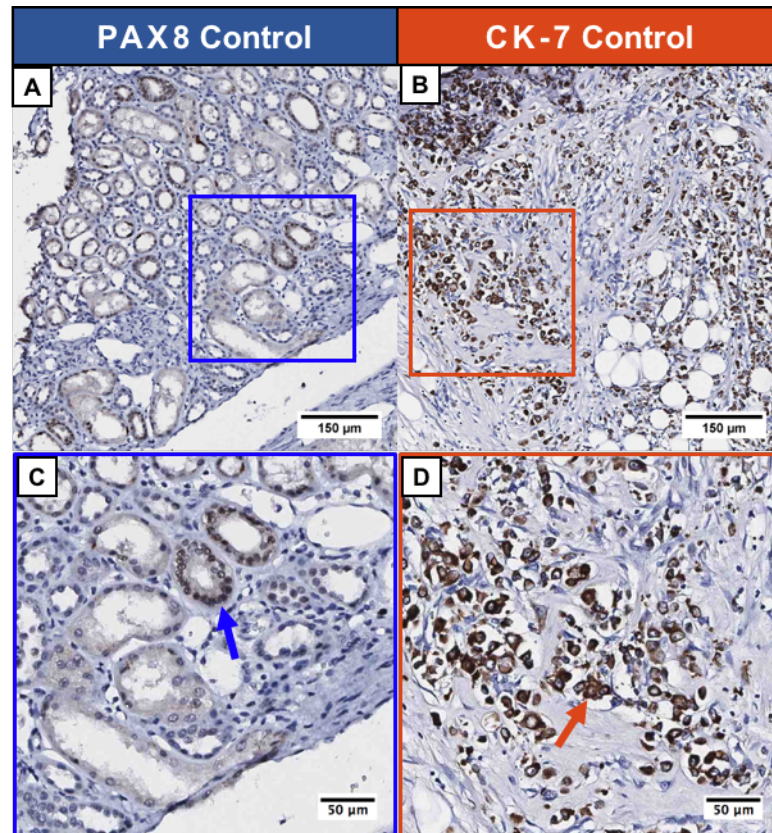


**Figure 5.10:** Positive control sections for PAX8 (A,C) and CK-7 (B,D). On initial review, the coloration of both stains appears similar with brown-black positive reactions against a dark background. With higher magnification, PAX8's black nuclei (C, orange arrow) are distinct as well as the brown-black coloration of CK-7 positive cytoplasmic material (D, pink arrow).

IHC is typically completed on FFPE tissue sections. The antigen retrieval process in these procedures is both delicate and can easily vary due to technician handling procedures [44]. In order to determine the direct effects of fluorescence histology on IHC staining, we created a study using serially cut kidney biopsies where one slide from the serial section was processed using standard IHC protocols and the other slide was first stained and imaged with D&E prior to standard IHC processing.

#### **5.4.1 Methods for IHC Evaluation of Fluorescence Histology**

*FFPE Blocks and Sectioning.* Using Tulane IRB approved procedures, eight FFPE blocks of 18-guage renal biopsies from partial nephrectomy procedures were selected for this study. From each block, five serial 4 $\mu$ m sections were cut to microscope slides [A,B,C,D,E], as depicted in Figure 5.11.

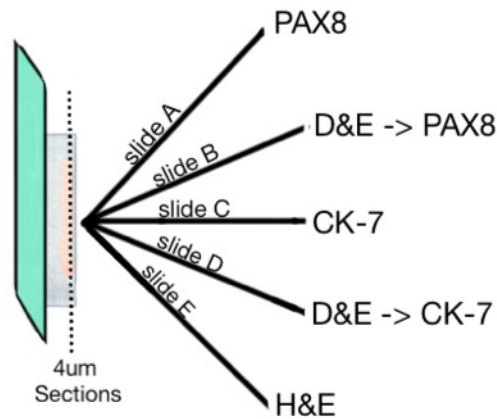


**Figure 5.11:** Experimental setup of the IHC study with FFPE renal biopsies. From each FFPE biopsy block, five slides of 4  $\mu$ m section thickness were consecutively cut. Slides A, B, and C were treated as histology standards. Slides B and D were stained and imaged with D&E standard protocols prior to being processed for their respective IHC stain.

Three of the slides from each set [A,C, and E] were delivered to the Tulane Histology Laboratory for standard processing. *Slide A* was stained with IHC nuclear stain PAX8, *slide C* was stained with the IHC cytoplasmic stain CK-7, and the histological stain H&E was applied to *slide E*. The remaining two slides [B,D] were reserved for fluorescent staining before being processed for IHC.

*Fluorescence staining followed by IHC processing.* The reserved slides [B,D] were deparaffinized using the Tulane Histology Core procedure (consecutive three minute incubations in xylene, 100% Ethanol, and hydration to deionized water.) After rehydration, the slides were stained with D&E and imaged using a custom epi-fluorescent microscope. Once the slides were

imaged, they were re-placed in deionized water to prevent dehydration and brought to the Tulane Histology Core for IHC staining of PAX8 [slide B] and CK-7 [slide D].

*Pathologist Evaluation.* After all slides completed IHC processing, the non-fluorescently stained control PAX8 and CK-7 slides [A,C] and the fluorescently stained slides [B,D] were blinded and provided to a pathologist for comparison. The H&E slide [E] was used as a gold-standard reference in cases where neither IHC stain were conclusive. The pathologist evaluated each IHC slide pair and identified differences between the stained tissue.

#### **5.4.2 Results for IHC Evaluation of Fluorescence Histology**

In total, eight biopsies were sectioned into a set of five slides each, although one was later excluded in pathological evaluation due to insufficient tissue after sectioning. Within each set, two biopsies went through pre-histology processing with the application and imaging of D&E on the slide prior to IHC staining (Figure 5.12). The experimental layout for this study allows the acquisition of a pseudo-H&E image (Figure 5.12 B1,D1) of the same section prior to IHC processing (Figure 5.12 B2,D2). Within the set, slides *A* and *B* are stained with the nuclear IHC stain, PAX 8 (Figure 5.12 G,H) and the slides *C* and *D* are stained with the IHC cytoplasmic stain CK-7 (5.12 I,J).

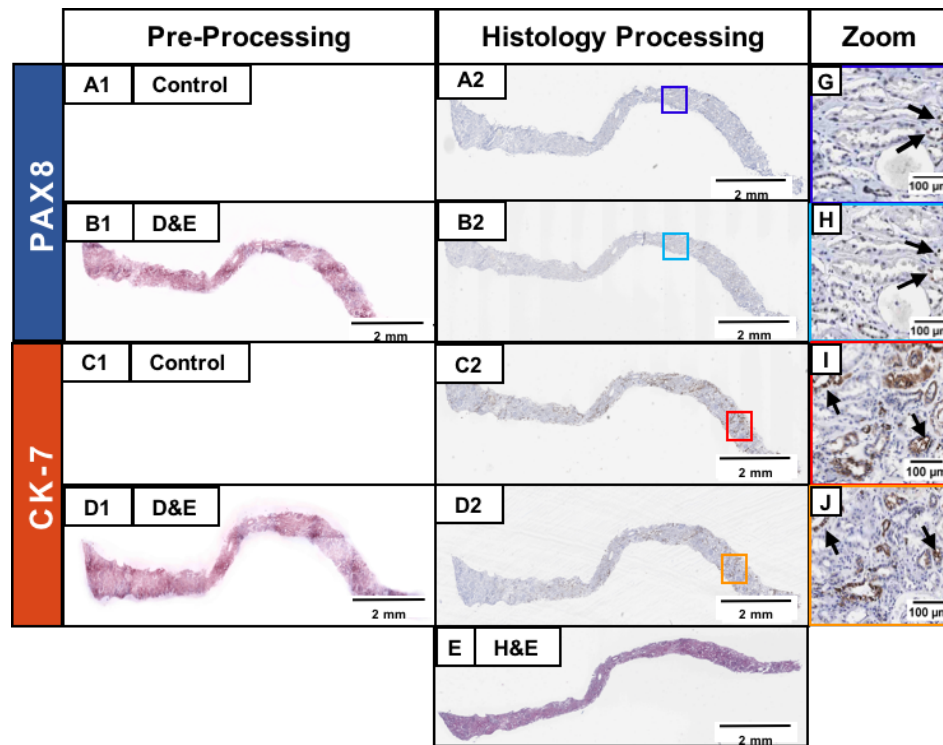


**Figure 5.12:** The resultant images from a single biopsy through both standard and experimental processing. The control samples were only stained for IHC and therefore have no pre-IHC image (A1,C1) but do have IHC for PAX8 (A2) and CK-7 (C2). The experimental samples were stained with D&E (B1, D1) and stained for IHC of PAX8(B2) and CK-7 (D2). A fifth slide stained with H&E (E) of each biopsy was used for diagnostic verification. The zoomed areas of each IHC slide show corresponding stained material for PAX8 (G,H arrows) and CK-7 (I,J arrows).

Although each slide pair is from the same biopsy, areas of higher magnification (Figure 5.12 [G,H] and [I,J]) show that the slides are not identical to each other in morphology or staining. As each slide is cut, it moves through the three-dimensional plane of the biopsy, and therefore structures can alter from one slide to the next. Although we can find the same area, some features may be prominent from one slide to the next.

These differences between sections are even more evident in Figure 5.13. Areas of two more biopsies (Figure 5.13 [A,B][C,D] and [I,J][K,L]) show lower magnification review of the specimen and non-identical staining. At higher magnification in areas of positive staining



magnification (Figure 5.13 [E,F][M,N] and [G,H][O,P]), the structures change from one slide to the next, with staining tracking the structures.

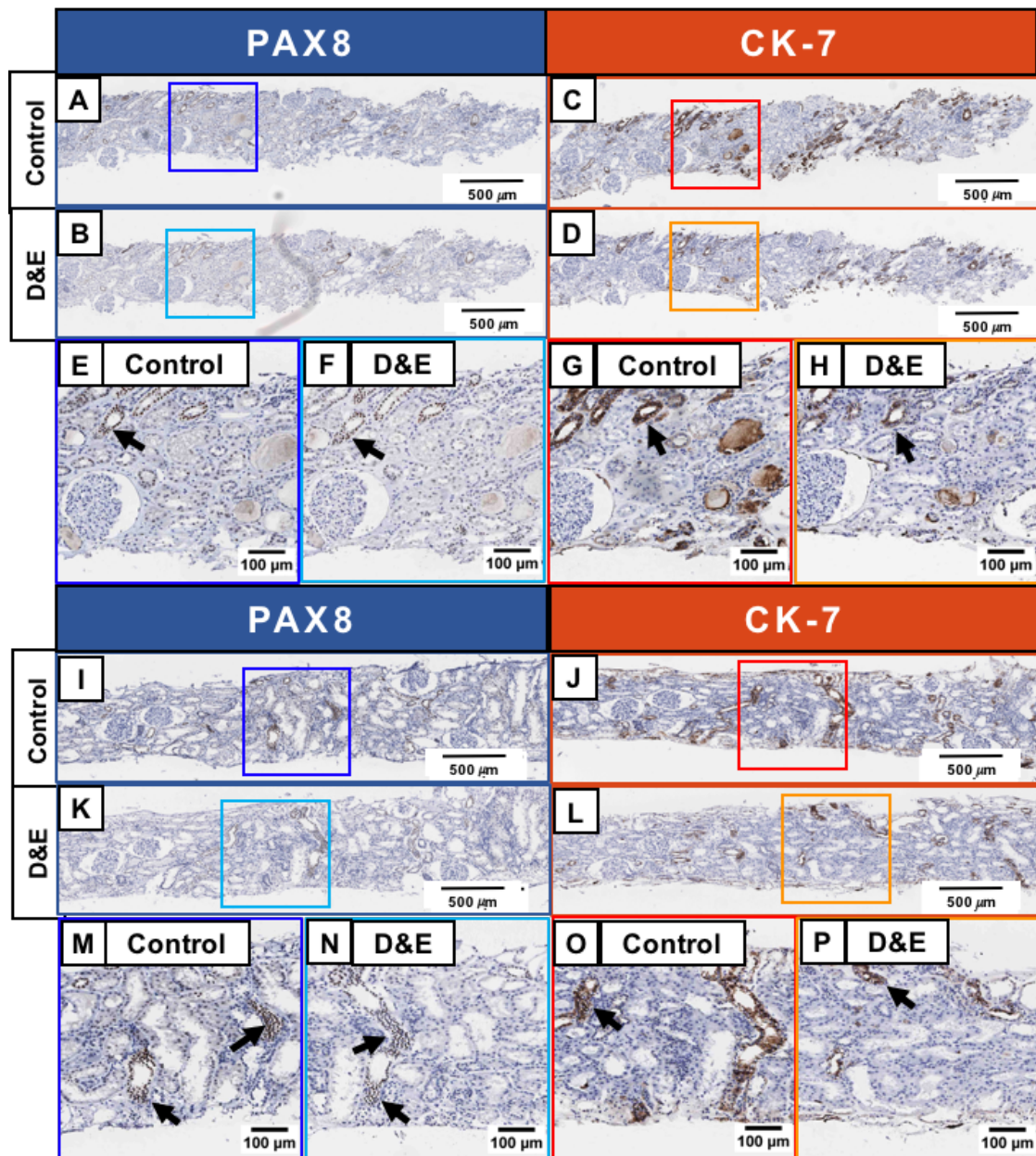


**Figure 5.13:** Regions of interest from two renal biopsies cut into 4 μm serial sections and stained with either PAX8 or CK-7. Areas with lower magnification (A,B,C,D,I,J,KL) show general staining intensity and morphology, with staining clusters forming regions of interest. These regions in PAX8 staining ([E,F][M,N]) show the same areas of high concentrations of positive nuclei (arrows) in each slide. The slides stained with CK-7 ([G,H][O,P]) also show the same area of each slide and the same positively stained structure (arrows) from one serial slide to the next.

From the eight biopsies cut for this study, one was excluded due to insufficient tissue. The seven remaining sets were evaluated based on staining intensity and the ability to make a diagnostic decision from the section. For approximately half the sets, the pathologist identified equal staining intensity within an IHC pair, such as the first biopsy shown above for both the PAX8 stain (Figure 5.13 A,B) and the CK-7 stain (Figure 5.13 C,D), or slightly weaker reactivity from one specimen in a pair to the next. For example, the second biopsy in Figure 5.13 shows weaker staining in both D&E experimental sections compared to their control for both PAX8 (Figure 5.13 G,H) and CK-7 (Figure 5.13 O,P).

In total for PAX8 stained tissue, the pathologist noted equal staining intensity in three pairs, a minor reduction in staining intensity from the control specimen to the experimental “D&E” specimen in two pairs, and a minor increase in staining intensity from the control specimen to the experimental “D&E” specimen in one pair set. One pair showed a major discrepancy where PAX8 positive nuclear staining was detected in the control specimen while the experimental, D&E exposed specimen was evaluated as PAX8 negative. Possible explanations include the fact that PAX8 antigen retrieval is a highly temperature-sensitive process and either lasers used to image the sections or the D&E application itself may have inhibited antigenicity. However, the pathologist did not believe D&E to be the sole, or even primary, cause for lack of positive staining. Instead, the pathologist stated that the large variation in staining between batches, and individual slide application, were the most likely factors for differences between experimental sets.

In comparison to PAX8, CK-7 stained specimens showed equal staining intensity in five pairs, and two experimental pairs demonstrated a slight reduction in staining intensity from the control sample. One of the CK-7 pairs both demonstrated negative cytoplasmic staining as expected in clear cell renal carcinoma, which was a confirmed diagnosis with H&E evaluation of

the slide corresponding slide. Again, batch variability was considered a likely factor in staining differences. Although it is possible that D&E could moderately inhibit antigenicity for CK-7 and PAX8, the pathologist determined that small differences in staining intensity would not affect diagnostic ability in either CK-7 or PAX8 IHC evaluation where both slides stained IHC positive.

**Table 5.1: Results of pathologist evaluation of IHC FFPE sectioned tissue where a control specimen went through standard IHC staining procedures and the experimental specimen was first stained with D&E prior to IHC staining.**

Specimen	Intensity of Staining Compared to Control
Biopsy 1: PAX8	Equal (=)
Biopsy 2: PAX8	Control (+)   D&E (-)
Biopsy 3: PAX8	Equal (=)
Biopsy 4: PAX8	Greater (>)
Biopsy 5: PAX8	Equal (=)
Biopsy 6: PAX8	Lesser (<)
Biopsy 7: PAX8	Lesser (<)
Biopsy 1: CK-7	Equal (=)
Biopsy 2: CK-7	Lesser (<)
Biopsy 3: CK-7	Equal (=)
Biopsy 4: CK-7	Equal (=)
Biopsy 5: CK-7	Equal (=)
Biopsy 6: CK-7	Equal (=)
Biopsy 7: CK-7	Lesser (<)

In total, six out of seven PAX8 “D&E” slides and all seven CK-7 “D&E” slides were considered diagnostically appropriate levels of staining correlating in diagnostic ability to their control pairs. Although D&E inhibition of antigenicity cannot be ruled out completely, more likely factors resulting in changes from the control and experimental sets were due to batch variations in staining procedures and the IHC stains themselves. As these slides, by necessity, were processed on different days and through different procedures (straight from paraffinized sections on tissue versus deparaffinized slides retained in deionized water for a short period of time), slightly different IHC handling procedures were used with each set. Additionally, factors

such as the effect of temperature changes in the tissue due to fluorescence imaging must also be evaluated.

One important consideration is also that in standard fluorescence histology we will be working with fresh, intact biopsies rather than slide sections. The proposed fluorescence histology workflow has the fresh and intact tissue fluorescently stained and imaged prior to FFPE processing. Clinical IHC analysis is almost uniformly performed on FFPE sections [11,15]. An exact evaluation would necessitate that two completely identical biopsy pairs be obtained, one fluorescently stained and imaged, and both then proceed through standard processing and IHC staining. As two biopsies cannot be compositionally identical, the closest analogue was the use of serial sections.

A final note is that there is a large multitude of possible IHC stains, with 79 stains available at our own histology core. The staining specifics, including antigen retrieval and binding sites vary just as widely, meaning that a comprehensive examination of the effects of fluorescence histology on IHC was infeasible for the scope of this work. However, by demonstrating that the impact of fluorescence histology does not alter the pathologist's ability to make a diagnostic decision, we can conclude that it is unlikely for fluorescence histology to have severely negative effects in downstream IHC analysis.

## **5.5 Conclusions from Downstream Analysis of Fluorescence Histology**

The work in this chapter analyzed the persistence of fluorescence SBR in the FFPE process and evaluated the effects of the fluorescence histology stains, D&E and acridine orange, on a few common downstream applications. The first study examined the persistence of fluorescence in fresh renal biopsies as they progress through the FFPE process. By analyzing the SBR of biopsies that were either control specimens, stained with D&E, or stained with AO, we



determined that exogenous fluorescence signal declines throughout the FFPE process, so that by the time tissue is cut into sections on a microscope slide, there is near-exact correlation in SBR with control samples. Interestingly, even as DRAQ5's intensity dramatically decreased in the specimens, some fluorescent specificity remained even in unstained FFPE sections. When compared to a control sample, the SBR of each slide is well below normal fluorescent staining ideal, but the nuclear specificity for signal is retained whereas a control slide exhibits standard non-specific signal from a mixture of scattering properties and autofluorescence from the fixation chemicals and paraffin wax.

We then studied the effects of UV-fluorescent and DNA-binding stains on PCR analysis and IHC staining. We used adult human dermal fibroblasts to examine if eosin Y, acridine orange, or DRAQ5 altered the quantification and analysis abilities of a NanoDrop 2000 UV-Spectrometer, RT-PCR, and UV-transillumination gel electrophoresis. Through each of these analyses, no significant variation from the control samples were noted. To examine the effects of fluorescence histology on IHC staining, eight kidney biopsies were cut into five serial sections: two IHC pairs and one H&E slide each. One section from each pair was stained with D&E before being stained with either PAX8 or CK-7, while the matching pair control slides were processed as standard specimens. Pathologist evaluation found either matching stain intensity or minor intensity variations in the slides, which indicates little interference with standard IHC staining by fluorescence histology.

## CHAPTER SIX: Expansion of Histology

*Parts of this chapter are reproduced from the following poster presentation:*

Elfer KN, Sholl AB, Brown JQ, "Fluorescent Periodic Acid and Masson's Trichrome for non-destructive tissue analysis," SPIE BIOS Photonics West 2018.

### 6.1 Introduction

Although H&E has been the routine histological stain for over 100 years, it cannot show all the tissue features relevant for diagnosis or of interest to researchers [22]. Both Masson's Trichrome and the Periodic Acid-Schiff (PAS) stain are specialized stains that emphasize different features than found in typical H&E stains [11,15]. Masson's trichrome consists of two known fluorescent components: Biebrich scarlet-acid fuchsin and aniline blue [15,106,107]. Aniline blue in its fluorescent form is frequently used in the study of plants in relation to the structure of their cell walls [108,109], but it has also been used for human research in the study of maturity of spermatozoa as immature cells are associated with higher uptake of aniline blue [110,111]. BSAF is a combination of two component parts (Biebrich scarlet and acid fuchsin) which have been used together in the study of the effects of anionic dyes on damaged cells and separately to examine the accumulation of eosinophils in tissue (Biebrich scarlet -[112] ) and the detection of microorganisms in human stool (acid fuchsin - [113]). Alone, these two stains are useful, but when combined with the third part of the trichrome stain, a mixture of phosphomolybdic acid (PMA) and phosphotungstic acid (PTA) is a known necessary component for staining specificity and brightness but it has no innate fluorescence [41,114]. Combinations of aniline blue and PMA have been used to study arteriosclerotic lesions in autopsy tissue [114] Masson's trichrome is also typically counterstained with the nuclear stain Weigert's Hematoxylin, which is also non-fluorescent [40,115]. Meanwhile, several fluorescent alternatives to PAS with the addition of acridine and its derivatives have been developed for commercial use [37,65]. Additionally, small fluorescence of PAS is observed at 528nm [116]. Both Masson's Trichrome and PAS, however,

rely on extensive tissue preparation to ensure only the components of interest are being stained. All current fluorescent protocols require this preparation (from 30 minutes to multiple hours) and an ideal fluorescent histology alternative would reduce the preparation time to only a few minutes without compromising the integrity of the tissue [5, 52, 61].

For this study, we examined the native fluorescence in Masson's Trichrome and PAS on control FFPE sections to determine whether the original dyes were direct matches for fluorescence histology. After determining the correct fluorescent stains needed to mimic the histochemistry of Masson's Trichrome and PAS, the original pseudocolor algorithm first described in Chapter 1 needed to be modified as its original purpose was for dual-channel pseudo-H&E. This modification includes both changes to the *rgb* values of the system and the inclusion of a third channel component to encompass all colors of these specialized stains. Finally, 4 $\mu$ m FFPE sections of human tissue stained with the fluorescent versions of the histology stains were evaluated against serial cut sections of the same tissue stained with the traditional histology procedures.

## 6.2 Identification of fluorescent components in trichrome and PAS slides

*Fluorescent evaluation of standard control slides.* Two FFPE slides used for standard controls in the Tulane Histology Laboratory were obtained, one slide stained with a positive control for PAS and one slide stained for Masson's Trichrome. These slides were imaged with a Nikon A1 Confocal microscope (more details) to identify whether the histological standard dyes produced enough signal for direct use in fluorescence imaging. The slides were examined with four laser-filter cube combinations (405nm laser & DAPI: 395 nm<sub>ex</sub>-460 nm<sub>em</sub>, 488 nm laser & FITC: 480 nm<sub>ex</sub>-510 nm<sub>em</sub>, 561 nm laser & TRITC: 540 nm<sub>ex</sub>-565 nm<sub>em</sub>, and 638 nm laser & Cy5: 620 nm<sub>ex</sub>-660

nm<sub>em</sub>), individually optimizing the laser power and photomultiplier tube gain of each laser for best signal. The resultant fluorescent image was then recorded for each channel.

*Analysis of individual fluorescent components.* After confirming strong fluorescent signal from histological dyes, the stains were then evaluated individually through application on 4μm FFPE sections of cadaver tissue obtained during autopsy with Tulane IRB approved protocols. To determine the contribution of each trichrome stain to overall fluorescence, BSAF and aniline blue were applied individually to deparaffinized serial sections of lung tissue and then combined in the classic trichrome procedure with PMA-PT as an intermediary staining step between the application of BSAF and aniline blue. Fluorescent slides were mounted with an epoxy-based mounting medium and then imaged on a Nikon A1 Confocal microscope using the same procedure as previously described.

The PAS stain is a reaction-based stain, and therefore neither of its components are either colored or impart fluorescence on their own. When tissue exposed to periodic acid is combined with Schiff's reagent, an accumulation of the reaction's products results in the coloration of tissue. Imaging PAS stained slides with a Nikon A1 Confocal microscope reveals two fluorescent signals in both the TRITC channel and the Cy5 channel with unique components stained in each (Figure 6.1).

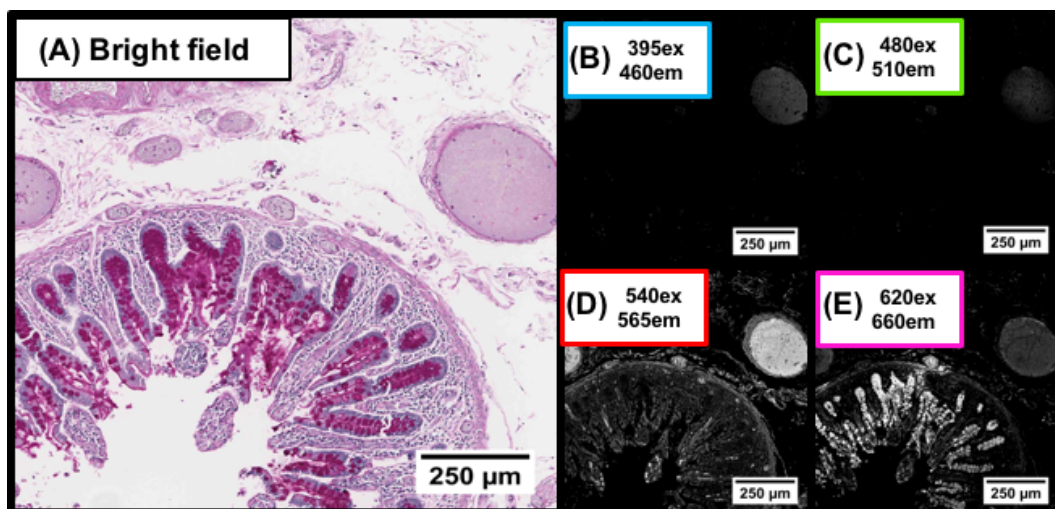


**Figure 6.1:** A histology laboratory control slide of the Periodic Acid-Schiff reaction as viewed through bright field microscopy (A) and fluorescence microscopy (B-D). The signal from the individual fluorescent channels are shown: DAPI 395 nm<sub>ex</sub>-460 nm<sub>em</sub> (B), FITC 480 nm<sub>ex</sub>-510 nm<sub>em</sub> (C), TRITC 540 nm<sub>ex</sub>-565 nm<sub>em</sub> (D), and Cy5 620 nm<sub>ex</sub>-660 nm<sub>em</sub> (E).

The bright magenta-red coloration that is a hallmark of a positive PAS reaction is clearly demonstrated, with non-reactive areas in varying shades of purple (Figure 6.1 A). With fluorescent illumination, maximization of the DAPI laser power shows very dim illumination (Figure 6.1 B), while no distinct signal is apparent in the FITC channel (Figure 6.1 C). Both the TRITC and Cy5 channels exhibit strong fluorescent signal of both the negative PAS coloration and the positive reaction coloration. Strong TRITC fluorescence is related to the negative PAS reaction tissue (Figure 6.1 D), while the positive PAS reaction appears to strongly correspond to the Cy5 channel (Figure 6.1 E). Furthermore, there does not appear to be significant fluorescent overlap between the two reactions, which means it is possible to use the standard PAS as a direct fluorescent analogue with the exception of the hematoxylin counterstain.

We also used a histological control of the Masson's Trichrome stain (Figure 6.1 A) to determine the possibility of creating a direct fluorescent analogue.

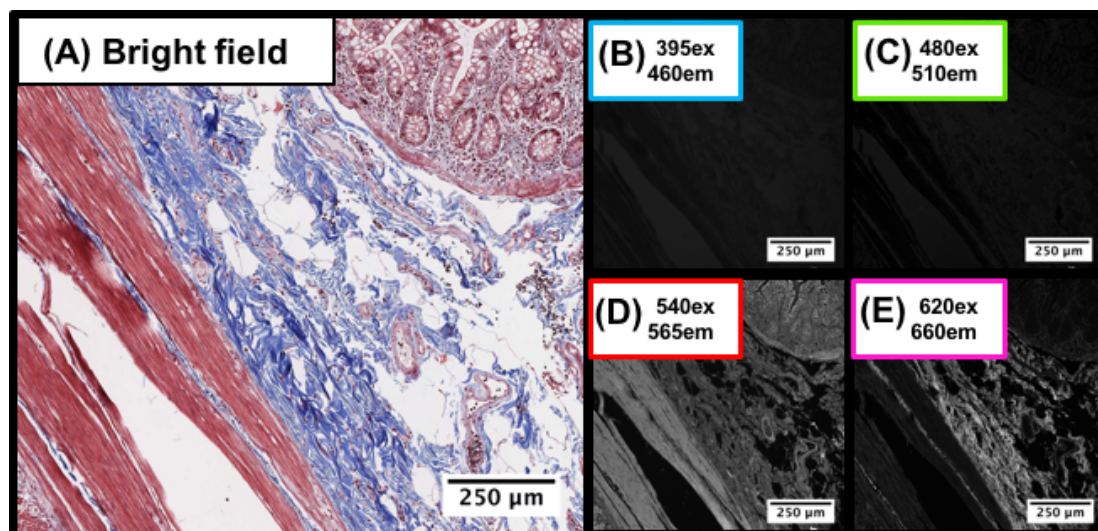


**Figure 6.2:** A histology laboratory control slide of Masson's Trichrome as viewed through bright field microscopy (A) and fluorescence microscopy (B-D). The signal from the individual fluorescent channels are shown: DAPI 395 nm<sub>ex</sub>-460 nm<sub>em</sub> (B), FITC 480 nm<sub>ex</sub>-510 nm<sub>em</sub> (C), TRITC 540 nm<sub>ex</sub>-565 nm<sub>em</sub> (D), and Cy5 620 nm<sub>ex</sub>-660 nm<sub>em</sub> (E).

Neither the DAPI (Figure 6.2 B) nor FITC (Figure 6.2 C) channel provided enough signal to visualize the tissue. However, the stains were highly responsive in the TRITC (Figure 6.2 D) and Cy5 (Figure 6.2 E) channels and appear to be spectrally faithful to acid fuchsin staining and aniline blue staining in each individual channel, respectively. To determine the source of the fluorescence seen in the Masson's Trichrome images, we conducted further analysis of the individual fluorescent components on tissue sections. Three serial cut lung sections from FFPE cadaver tissue were stained with BSAF, aniline blue, and then together with an intermediary PMA-PTA solution as is typically used in standard histology. Figure 6.3 shows the fluorescent effects of the stains alone on the tissue and combined as in standard histology.

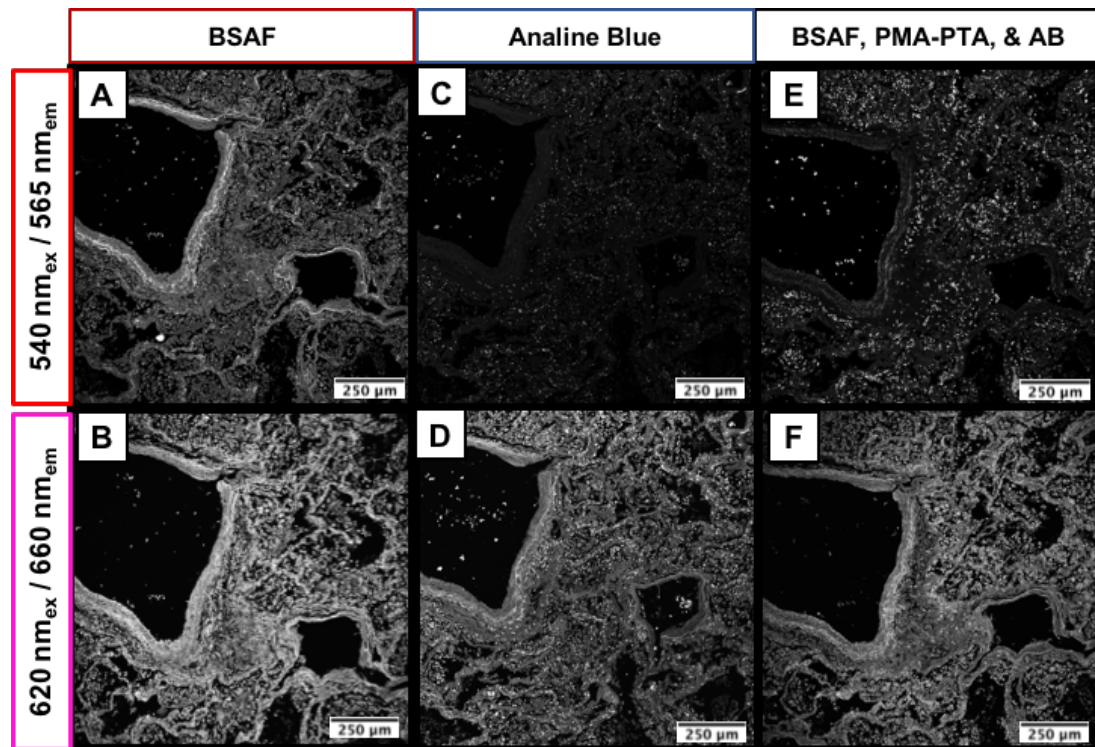


**Figure 6.3:** FFPE of cadaver lung tissue in serial 4 $\mu$ m sections stained with the individual components of the Masson's Trichrome stain and imaged with a Nikon A1 Confocal microscope. One section was stained with BSAF and imaged with a TRITC filter setting 540 nm<sub>ex</sub>-565 nm<sub>em</sub> (A) and Cy5 620 nm<sub>ex</sub>-660 nm<sub>em</sub> (B). The second section was stained with aniline blue and imaged with a TRITC filter setting 540 nm<sub>ex</sub>-565 nm<sub>em</sub> (C) and Cy5 620 nm<sub>ex</sub>-660 nm<sub>em</sub> (D). The third section was stained with BSAF, PMA-PMT, and aniline blue and imaged with a TRITC filter setting 540 nm<sub>ex</sub>-565 nm<sub>em</sub> (E) and Cy5 620 nm<sub>ex</sub>-660 nm<sub>em</sub> (F).

From Figure 6.3, we can see changes between the components stained by BSAF (Figure 6.3 A,B), aniline blue (Figure 6.3 C,D) as well as the effects of the PMA-PTA when used after BSAF and before aniline blue staining (Figure 6.3 E,F). As expected with the theory of the use of the heteropolyacid in trichrome staining, the appearance of the BSAF staining is restricted from alone to that used in the trichrome system. With BSAF alone, it's extremely difficult to determine exactly what is being stained as it appears to be fairly non-specific as well as responsive to both TRITC (Figure 6.3 A) and Cy5 (Figure 6.3 B) settings. However, with the application of PMA-PTA, the TRITC channel (Figure 6.3 E) has much more focused fluorescence than the original BSAF TRITC (Figure 6.3 A). Given the heteropolyacid washes out non-specific BSAF binding, this

result is not surprising. Although aniline blue's staining is contained primarily to the Cy5 channel (Figure 6.3 D), its signal is not uniform and appears to be concentrated in multiple points along structures. However, after PMA-PTA application the Cy5 signal (Figure 6.3 F) appears to be much more dispersed through the tissue, which is understandable as it is believed that one mechanism of PMA-PTA in the trichrome process is to better prepare the collagen binding sites for aniline blue infiltration, thereby allowing greater dispersion of the dye through the tissue.

### 6.3 Choosing a Spectrally-Compatible Nuclear Counterstain

While neither PAS or Masson's Trichrome require the use of a nuclear stain, they are both commonly combined with a hematoxylin counterstain to provide additional context in histology. Hematoxylin, however as previously discussed, is a non-fluorescent molecule. The alternative nuclear stain used in our previous work, DRAQ5 as in D&E, is also unsuitable because its far-red fluorescence spectra overlaps with the fluorescent components of both PAS and Masson's Trichrome. On the other hand, the lack of fluorescence at shorter excitation wavelengths from these stains opens possibilities for nuclear stains that were previously limited when the goal was to combine them with eosin's wide UV-blue fluorescence. DAPI is a well-known nuclear fluorescent stain with excitation and emission spectra ideal for use in combination with green and red fluorescent dyes. Furthermore, it is extremely easy to integrate into most staining protocols given its aqueous base with strong signal when bound to DNA [117]. One limitation of DAPI, however, is that its signal is best preserved in aqueous conditions, which requires the use of a wet mounting medium [118].

*Masson's Trichrome Staining with and without DAPI.* FFPE 4 $\mu$ m slides from human kidney autopsy tissue (obtained using Tulane IRB approved protocols) were used for *rgb* color correlation between Masson's Trichrome fluorescence and bright field histology. The slides were



deparaffinized (through consecutive incubations in xylene and 100% EtOH), hydrated to deionized water, and then picrated in Bouin's solution for the standard eight hours prior to staining. Both sets of stains were then rinsed in running tap water for five minutes. Bright field slides were then stained with Weigert's hematoxylin solution for five minutes followed by continuous rinsing with tap water for another five minutes. Fluorescent and bright field stains were rinsed in deionized water and successively stained with Brieibirch Scarlet Acid Fuchesine (BSAF, 5 minutes), rinsed in a Phosphotungstic-Phosphomolybdic Acid (PMA-PTA) solution (5 minutes), stained in aniline blue (5 minutes), and followed by a two-minute immersion in 1% acetic acid. Fluorescent stains were then rinsed in deionized water before staining with 0.5 µg/ml DAPI for seven minutes. Fluorescent slides were mounted with a water-based medium to preserve DAPI signal. Bright field slides were dehydrated, cleared in xylene, and then mounted in a xylene-based epoxy.

*Periodic-Acid Schiff Staining with and without DAPI.* FFPE 4µm slides from a human adrenal gland autopsy specimen (obtained using Tulane IRB approved protocols) were used for *rgb* color correlation between PAS fluorescence and bright field histology. The slides were deparaffinized (through consecutive incubations in xylene and 100% EtOH) and hydrated to deionized water. The slides were then exposed to Periodic Acid for five minutes followed by several (3-4) rinses with distilled water. After rinsing the slides, they were placed in Schiff's Reagent for 15 minutes. The slides were then rinsed for five minutes in running tap water. Fluorescent slides were then stained with 0.5 µg/ml DAPI for seven minutes. Fluorescent slides were mounted with a water-based medium to preserve DAPI signal. Bright field slides were stained with Gill's No. 3 Hematoxylin, rinsed in deionized water, dehydrated, cleared in xylene, and then mounted in a xylene-based epoxy.

## 6.4 Application of a Pseudocolor Algorithm

As with H&E, Masson's Trichrome and PAS are traditionally examined with bright field microscopy. Replicating these stains using fluorescence histology requires that both their histochemical interaction and appearance of the tissue be mimicked. The previously used algorithm used to create the appearance of H&E and can be easily transformed by using new color parameters for cases where there are two individual fluorescent channels. However, with the use of a nuclear stain, both Masson's Trichrome and PAS exceed two fluorescent channels. With the use of these specialized stains the introduction of a third channel in the pseudocoloring program is required and therefore needed to be implemented into the existing two-channel *rgb*-mapping algorithm.

*Tissue Imaging.* The fluorescent slides were examined with four laser-filter cube combinations (405 nm-DAPI, 488 nm-FITC, 561 nm-TRITC, and 638 nm-Cy5), individually optimizing the power and gain of each laser for best signal. All fluorescent slides exhibited strong signal in the DAPI, TRITC, and Cy5 filter settings as shown in Figure below.

The pre-processing steps described above are shown in equations 6.1, 6.2 and 6.3, below:

$$DAPI = A \left[ \frac{I_{DAPI}}{\max(I_{DAPI})} \right]^{1/\gamma_1} \quad \text{eq. 6.1}$$

$$TRITC = B \left[ \frac{I_{TRITC}}{\max(I_{TRITC})} \right]^{1/\gamma_2} \quad \text{eq. 6.2}$$

$$Cy5 = C \left[ \frac{I_{Cy5}}{\max(I_{Cy5})} \right]^{1/\gamma_3} \quad \text{eq. 6.3}$$

where  $I_{DAPI}$ ,  $I_{TRITC}$ , and  $I_{Cy5}$  are the flat-field corrected mosaics for each channel and A, B, and C are the linear coefficients used to match the mean intensities of the other channels. This coefficient typically ranged from 0.4 to 2. A typically is held constant at 1 with the other two channels modified to match its intensity, ranging from B equal to 0.4-1.2 and C ranged from 0.6-2 for both stains. Gamma correction was also applied to the system to better replicate the actual

appearance of the stains. Unlike before with D&E on VR-SIM, gamma with the Nikon A1 confocal was typically used to help isolate signal by using values greater than 1. DAPI gamma ( $\gamma_1$ ) typically ranges from 1-1.1 and both TRITC gamma ( $\gamma_2$ ) and Cy5 gamma ( $\gamma_3$ ) typically ranges from 0.85-2. Using the pseudocolor methods described previously, Masson's Trichrome fluorescent images were scaled to match histological values, inverted, and re-mapped into the *rgb*-color spectrum using empirically-determined vector values:

$$R: \exp(-\beta_{ABRed} * \mathbf{AnilineBlue} * k) \exp(-\beta_{AFRed} * \mathbf{BSAF} * k) \exp(-\beta_{DAPIRed} * \mathbf{DAPI} * k) \quad \text{eq. 4}$$

$$G: \exp(-\beta_{ABGreen} * \mathbf{AnilineBlue} * k) \exp(-\beta_{AFGreen} * \mathbf{BSAF} * k) \exp(-\beta_{DAPIGreen} * \mathbf{DAPI} * k) \quad \text{eq. 5}$$

$$B: \exp(-\beta_{ABBlue} * \mathbf{AnilineBlue} * k) \exp(-\beta_{AFBlue} * \mathbf{BSAF} * k) \exp(-\beta_{DAPIBlue} * \mathbf{DAPI} * k) \quad \text{eq. 6}$$

Where  $k$  is a scaling constant that accounts for instrument variation such as gain, detector sensitivity and other factors; *AnilineBlue* is the 638 nm/Cy5 channel; *Acid Fuchsin* is the 561 nm/TRITC channel; *DAPI* is the 405 nm/DAPI channel, and the  $\beta$  values are the bright field color coordinates for each dye:

$ABRed=0.80;$	$BSAFRed=0.11;$	$DAPIRed=0.57;$
$ABGreen=0.35;$	$BSAFGreen=0.95;$	$DAPIGreen=0.75;$
$ABBlue=0.035;$	$BSAFBlue=0.85;$	$DAPIBlue=0.45.$

Figure 6.4, below, of a kidney specimen, the original three fluorescent channels (colored with the standard fluorescence pseudocolor for their respective filters) of DAPI (Figure 6.4 A), TRITC (Figure 6.4 B), and Cy5 (Figure 6.4 C) are shown along with a side-by-side comparison of the pseudocolored fluorescent image (Figure 6.4 D) and its bright field counterpart (Figure 6.4 E).

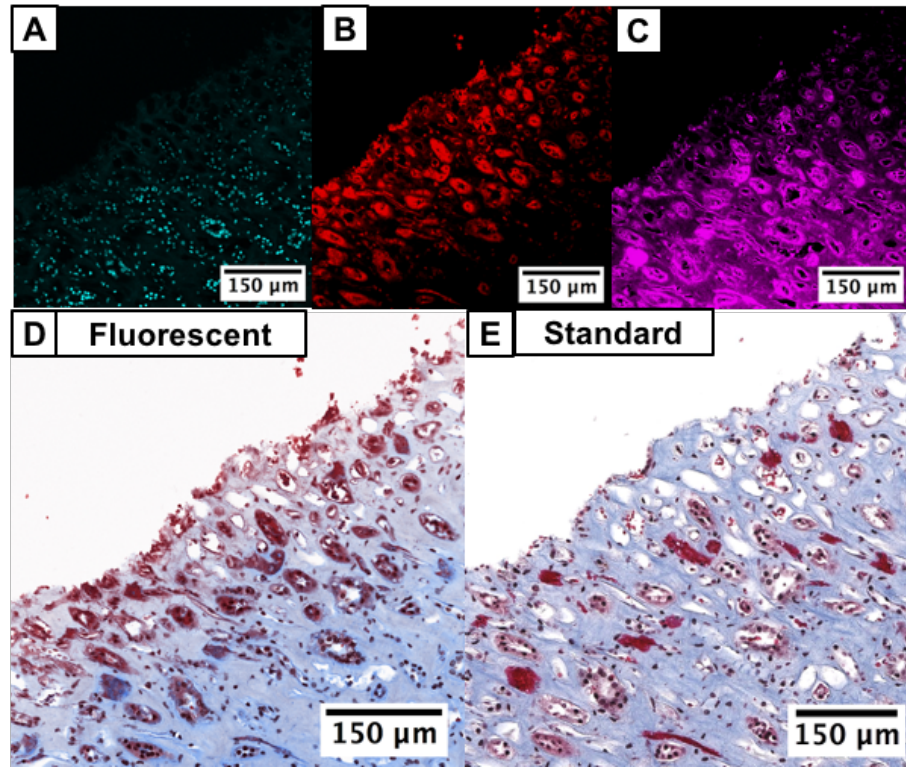


**Figure 6.4:** A 4  $\mu\text{m}$  section of cadaver kidney tissue stained with Masson's Trichrome and the DAPI nuclear stain fluorescently imaged with DAPI 395 nm<sub>ex</sub>-460 nm<sub>em</sub> (A), TRITC 540 nm<sub>ex</sub>-565 nm<sub>em</sub> (B), and Cy5 620 nm<sub>ex</sub>-660 nm<sub>em</sub> (C) filter settings. The fluorescent channels were then pseudocolored to form a single composite image (D) using the RGB values of the bright field Masson's Trichrome of the same area in a serial cut section (E).

And using a similar approach, the Periodic Acid Schiff pseudocolor formula follows:

$$R: \exp(-\beta_{PAS_{TRITC}Red} * PAS_{TRITC} * k) \exp(-\beta_{PAS_{Cy5}Red} * PAS_{Cy5} * k) \exp(-\beta_{DAPI_{Red}} * DAPI * k) \quad \text{eq. 4}$$

$$G: \exp(-\beta_{PAS_{TRITC}Green} * PAS_{TRITC} * k) \exp(-\beta_{PAS_{Cy5}Green} * PAS_{Cy5} * k) \exp(-\beta_{DAPI_{Green}} * DAPI * k) \quad \text{eq. 5}$$

$$B: \exp(-\beta_{PAS_{TRITC}Blue} * PAS_{TRITC} * k) \exp(-\beta_{PAS_{Cy5}Blue} * PAS_{Cy5} * k) \exp(-\beta_{DAPI_{Blue}} * DAPI * k) \quad \text{eq. 6}$$

Where  $k$  is a scaling constant that accounts for instrument variation such as gain, detector sensitivity and other factors;  $PAS_{TRITC}$  is the 638nm/Cy5 channel;  $PAS_{Cy5}$  is the 561nm/TRITC channel;  $DAPI$  is the 405nm/DAPI channel, and the  $\beta$  values are the bright field color coordinates for each dye:

$$PAS_{TRITC}Red=0.35;$$

$$PAS_{TRITC}Green=0.65;$$

$$PAS_{TRITC}Blue=0.22;$$

$$PAS_{Cy5}Red=0.100;$$

$$PAS_{Cy5}Green=0.395;$$

$$PAS_{Cy5}Blue=0.215;$$

$$DAPI_{Red}=0.70;$$

$$DAPI_{Green}=0.85;$$

$$DAPI_{Blue}=0.50.$$

An adrenal gland stained with fluorescent PAS (Figure 6.5 A,B,C) then pseudocolored (Figure 6.5 D) to match the standard PAS (Figure 6.5 E) is shown below. With the PAS reaction, only those molecules that are PAS+ are supposed to appear as especially bright magenta-red against the purple background. Yellow asterisks are placed on these reactive areas in the fluorescent (Figure 6.5 D) and standard (Figure 6.5 E) images.

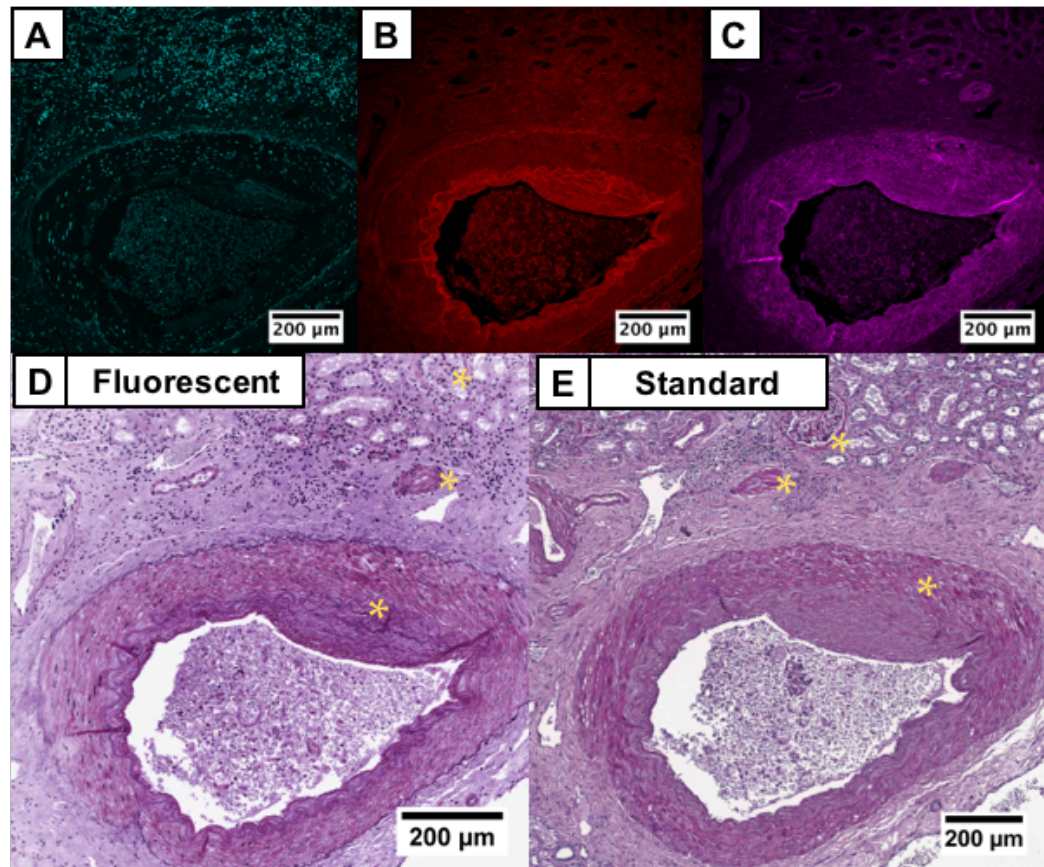


**Figure 6.5:** A 4μm section of cadaver kidney stained with PAS & DAPI fluorescently imaged with DAPI 395 nm<sub>ex</sub>-460 nm<sub>em</sub> (A), TRITC 540 nm<sub>ex</sub>-565 nm<sub>em</sub> (B), and Cy5 620 nm<sub>ex</sub>-660 nm<sub>em</sub> (C). The fluorescent channels were then pseudocolored to form a single composite image (D) using the RGB values of the bright field PAS of the same area in a serial cut section (E). Yellow asterisks denote areas of PAS+ reaction.

There are some visible differences between the pseudocolor fluorescent slides (Figure 6.4 D and Figure 6.5 D) and standard slides (Figure 6.4 D and Figure 6.5 D). The necessity of using

serial sections is likely one reason for these variations. Because DAPI's signal is drastically reduced as the very thin sections rapidly dry out, it must be permanently mounted in order to sustain fluorescence during the long time frame needed for confocal acquisition [117,118]. Therefore, the same section cannot be used for standard processing, like we could achieve with D&E characterization. Another variation is likely due to the different techniques and reagents used between our laboratory procedures and the Tulane Histology Core, as different laboratories use different reagent sources and techniques [16].

Yet these structure and staining differences are not enough where a comparison between the pseudocolor fluorescent and standard techniques is not possible. Even with changes in structures, it is apparent that similar coloring is imparted to the same structures in both modalities.

## 6.5 Characterizing fluorescence histology in FFPE sections

In the previous section, we demonstrated the ability to replicate the appearance of Masson's Trichrome and PAS using DAPI as a replacement for hematoxylin, three channel fluorescent imaging, and the application of a three channel pseudocoloring algorithm. The fluorescent channel contributions to the bright field *rgb* values of each stain were identified. Although some discrepancies in appearance were noted, a further characterization study is needed to determine whether the appearance of these two specialized stains can be replicated across multiple samples. As both stains are useful in kidney and liver diagnostics, this study used serial sections from cadaver kidney

*Slide acquisition.* Serial 4  $\mu\text{m}$  sections of FFPE autopsy tissue were obtained for serial comparison between fluorescent slides and standard Masson's Trichrome and PAS slides. Liver and kidney samples from human autopsy tissue were obtained for this work. All tissue was

acquired using approved institutional review board procedures for human subject research. Serial slides were stained per the protocols provided in the previous in successive order with Masson's Trichrome with DAPI, Masson's Trichrome with Weigert's Hematoxylin, PAS and DAPI, and PAS with Gill No. 3 Hematoxylin.

*Tissue Imaging.* The fluorescent slides were examined with four laser-filter cube combinations (405 nm-DAPI, 488 nm-FITC, 561 nm-TRITC, and 638 nm-Cy5), individually optimizing the power and gain of each laser for best signal.

As demonstrated in Figure 6.6, different kidney sections exhibited variable staining intensity with one standard section (Figure 6.6 [B] and [D]) appearing highly saturated compared to the third section (Figure 6.6 F). The fluorescent counterparts were pseudocolored using the above algorithm, with both linear and gamma intensities selected to match the histological sample rather than user preferences. Renal corpuscles (Figure 6.6 A,B asterisk) with interstitial collagen connecting them and running between renal tubules are evident in both fluorescence imaging (Figure 6.6 A) and standard imaging (Figure 6.6 B). In another area of the section, similar staining is evident along with a healthy renal glomerulus (Figure 6.6 C,D asterisks) alongside a renal corpuscle with large bowman's space (Figure 6.6 C,D arrows). Another serial section pair shows similar features even though the coloration in both the fluorescent image (Figure 6.6 E) and standard image (Figure 6.6 F) are slightly different than the previous section.



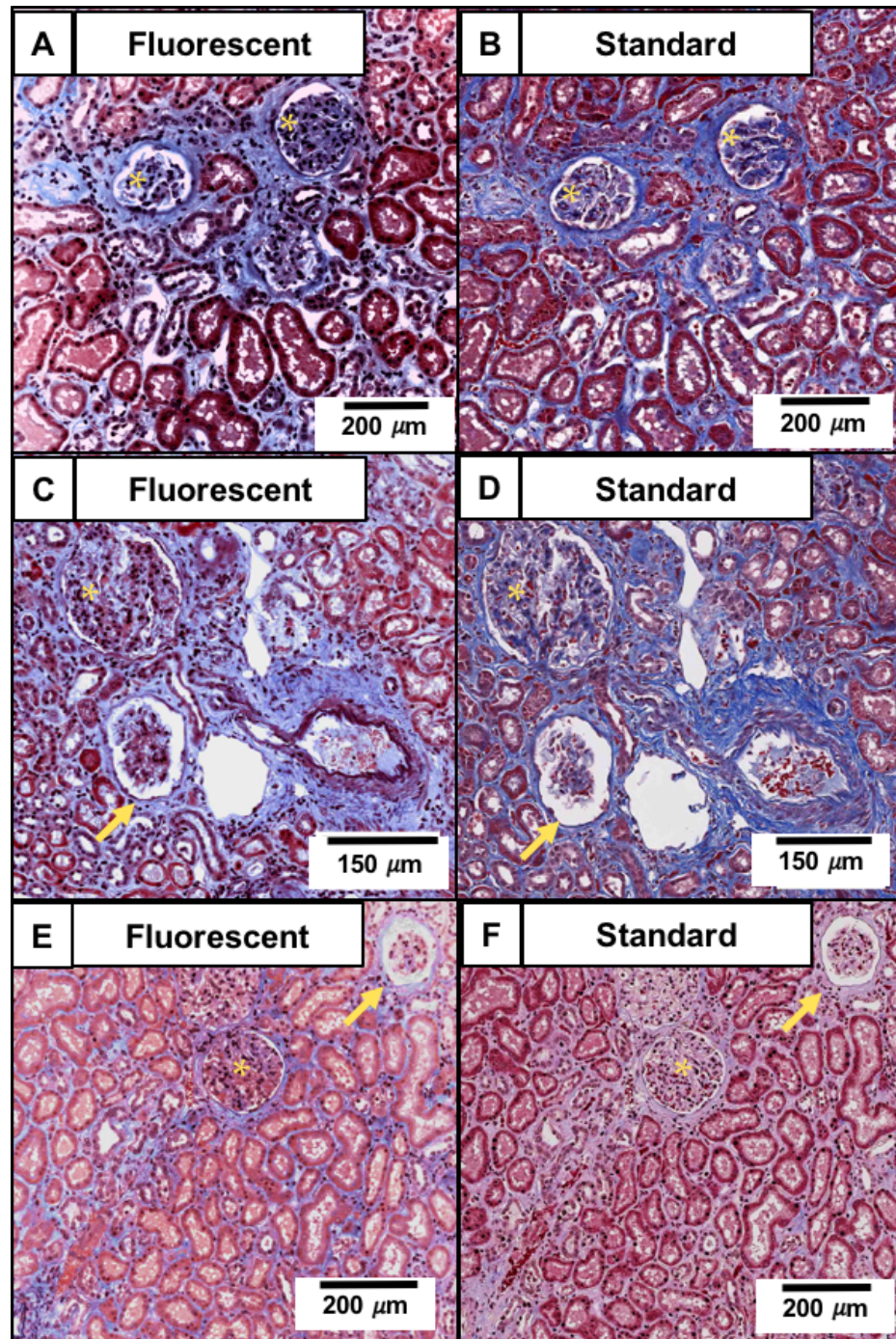


**Figure 6.6:** A 4 $\mu$ m section of cadaver kidney stained with Masson's Trichrome and either DAPI (A,C,E) or Weigert's Hematoxylin (B,D,F). Asterisks are placed on the glomeruli of renal corpuscles, with arrows pointing to areas of prominent Bowman's space.



A section of liver tissue stained with Masson's Trichrome (Figure 6.7) shows the liver capsule, which is composed of connective tissue and therefore is strongly stained by aniline blue in both the fluorescent (Figure 6.7 A, arrow) and standard (Figure 6.7 B, arrow) images. The connective tissue of the portal canal is also clearly visualized in both fluorescence imaging (Figure 6.7 C,E) and standard histology (Figure 6.7 D,F).

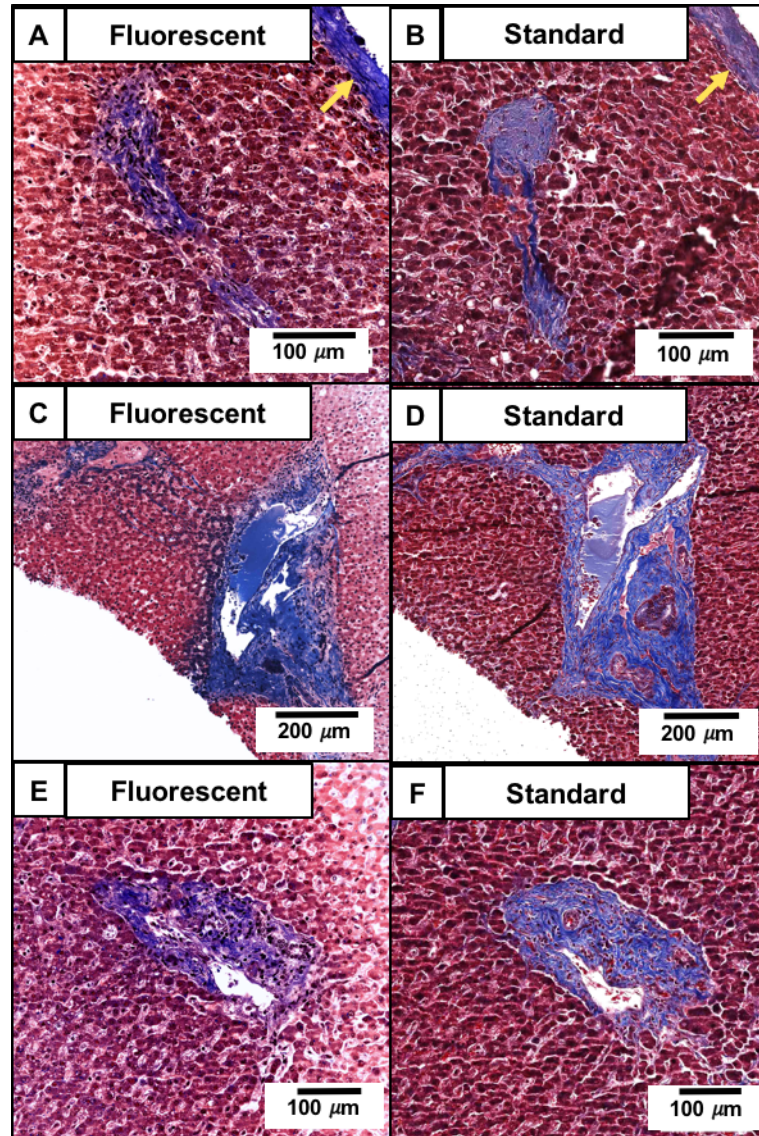


**Figure 6.7:** A 4μm section of cadaver liver stained with Masson's Trichrome and either DAPI (A,C,E) or Weigert's Hematoxylin (B,D,F).

The Periodic Acid-Schiff stain was applied to serial cuts of the same tissue as shown above, however, due to its chemical nature, different structures are emphasized. In the kidney section (Figure 6.8), the basement membrane of renal corpuscles in both fluorescence histology (Figure 6.8 A,C yellow arrows) and standard histology (Figure 6.8 B,D yellow arrows) are emphasized as well as the basement membrane of neighboring vessels (Figure 6.8 C,D green arrows). A sclerotic glomerulus surrounded by a vivid magenta is also easily seen in both fluorescent pseudocolor (Figure 6.8 A, asterisk) and standard histology (Figure 6.8 B, asterisk).

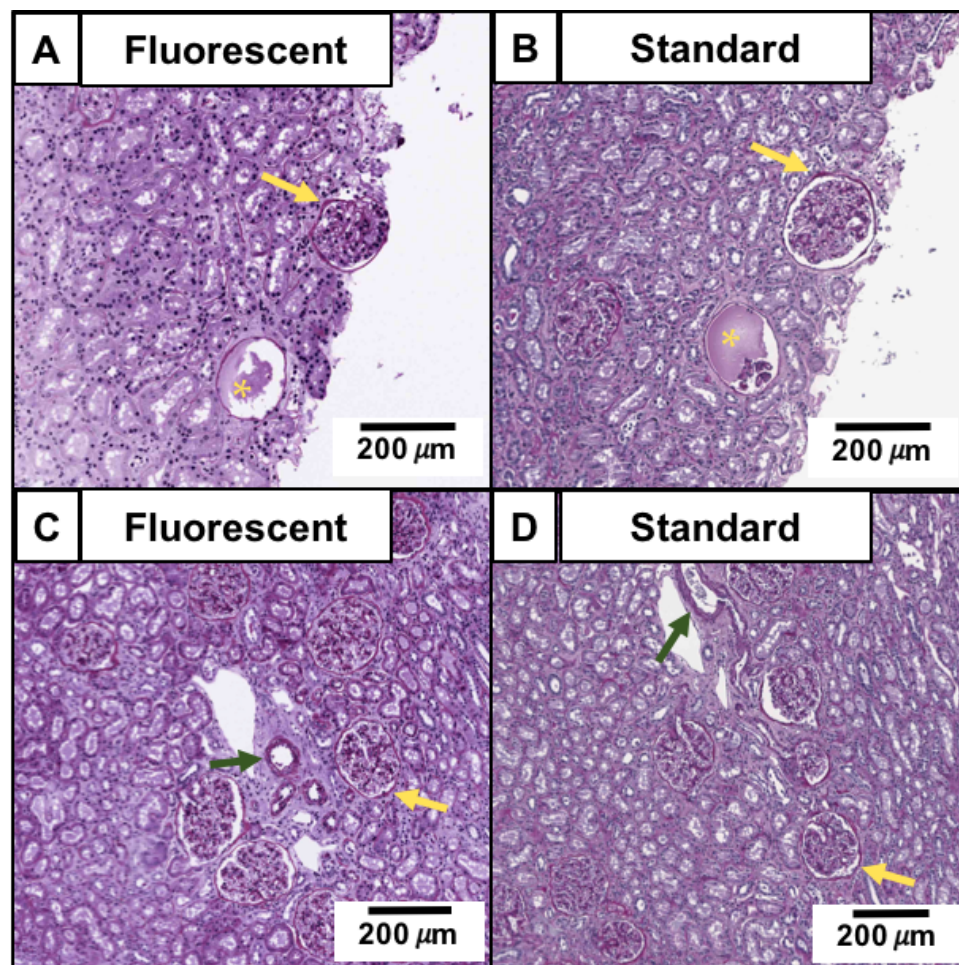
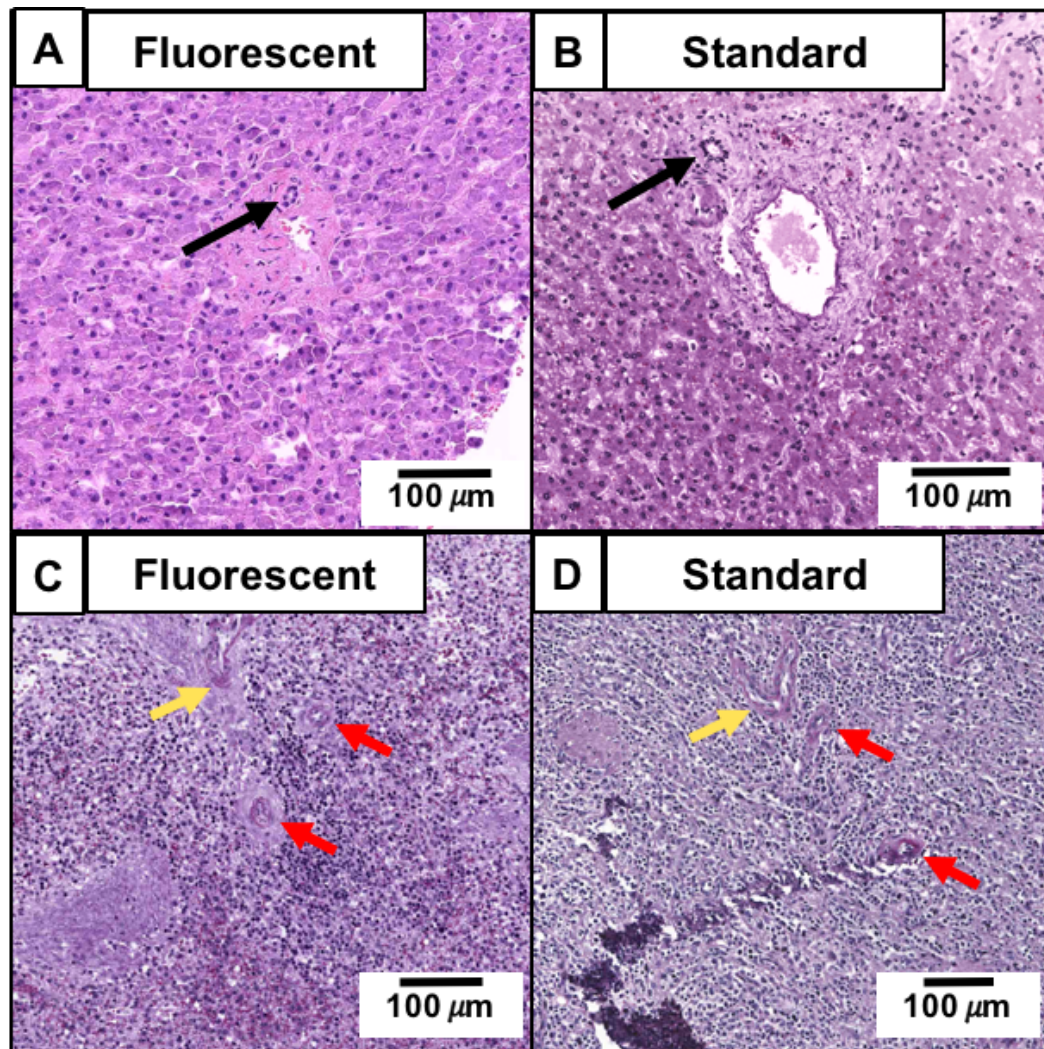


Figure 6.8: **A** 4μm section of cadaver kidney stained with PAS and either DAPI (A,C,E) or Weigert's Hematoxylin (B,D,F).



In the liver, the PAS is used to evaluate stores of glycogen in the tissue and can highlight the basement membrane of bile ducts and other tissue components [15]. In Figure 6.9, liver sections stained with either fluorescent PAS (Figure 6.9 A,C) or standard PAS (Figure 6.9 B,D) are shown.



**Figure 6.9:** A 4μm section of cadaver liver stained with PAS and either DAPI (A,C,E) or Gill's Hematoxylin #3 (B,D,F).

Although a bile duct is clearly seen in both the fluorescent image (Figure 6.9 A), the glycogen globules are less evident than in the standard histology image (Figure 6.9 B) which could be due to lack of visualization, serial sectioning, or differences in staining technique.

However, equal staining of the basement layers of the ducts is evident in both the fluorescent image (Figure 6.9 C, arrows) and the standard histological image (Figure 6.9 D, arrows).

## 6.6 Conclusions

In this study, we have expanded our previous work on dual-color, pseudo H&E histology to more specialized stains that are used to augment the information provided by H&E. We demonstrate the first use of these stains in fluorescence histology on FFPE human sections and compare the fluorescent staining to their standard histological counterparts in serial sections. Using the native fluorescent components in the connective tissue stain, Masson's Trichrome, and the carbohydrate stain, Periodic Acid-Schiff, along with the nuclear stain DAPI, we have recapitulated the histochemical specificity and coloration of the standard bright field images. To complete this work, the two-color pseudocolor algorithm developed by Giacomelli, *et.al.* needed to be altered for a third fluorescent channel and the *rgb* values of each stain were determined via matching to three corresponding histology slide.

Although both fluorescent stains appear to be very similar to their standard histology counterparts, some differences are apparent. The nature of serial cut sections mean that tissue distortion and change in structures is expected as the distance between sections and the nature of sectioning can create variations from one section to the next. Additional variations result from the imaging modality, fluorescence can be easily photo-bleached and in a study where we are trying to find exact corresponding areas, the effects of lasers on tissue cannot be averted as it would for a histological review of a fresh specimen where the purpose is to acquire an optical section of the entirety of a specimen and instrumentation can be designed to match the purpose [13,17].

Further work is needed to both standardize the fluorescent and histological techniques to avoid discrepancies in staining method. Currently we use the Tulane Histology Laboratory for

standard staining protocols due to their expertise, however in fluorescence histology it is the lab technicians and researchers who will oversee staining. Additionally, modifications to the staining procedure will need to be made for use in intact tissue specimens. We preserved the histological staining time frames to create as direct a comparison as possible between methods, but as discussed in Chapter 4, the staining times and concentrations needed for fluorescence histology and standard histology differ and can be optimized for the need.

## CHAPTER SEVEN: Discussion

Current histology evaluation requires the physical sectioning, or smearing, of tissue onto a standard bright field microscope slide and viewing the slide through a light microscope. Both point-of-care pathology and laboratory research requires rapid on-site evaluation (ROSE) of tissue, but current techniques do not meet the increasing needs for specimen conservation and accurate diagnostics. In this work, we propose the adoption of an alternative method in the clinical and research workflow, fluorescence histology. To advance this method, we developed a topical fluorescent stain-image processing system to recapitulate the specificity and appearance of H&E and characterized its performance on sections of FFPE and frozen tissue (Chapter 3). This system, “D&E,” was optimized for use on freshly excised, intact biopsies and prostate surfaces using VR-SIM. We then compared the performance of the two contrast methods, dual-color D&E and monochrome acridine orange, on pathological analysis in a study on 49 prostate biopsies from radical prostatectomy patients (Chapter 4). The pathologist, who is an expert in fluorescence histology analysis, determined both methods provided enough information to accurately diagnose prostate cancer from benign tissue. However, the pathologist also noted that some features, such as basal cells of benign glands, were only able to be identified with D&E and that monochrome visualization made differentiating some features more difficult even if it did not directly impact the accuracy of diagnosis. This analysis formed the conclusion that the dual-contrast of D&E made diagnosis easier and was less mentally taxing in review. In an analysis of the complexity, time, cost, and information provided by D&E, AO, and FFPE H&E, we concluded, as expected, that H&E provides the most feature specificity and information, but was also the most complex and time consuming method. D&E was most like H&E as it provides near-identical detail in analysis in a much shorter time frame, but is moderately complex and expensive. AO, on the other hand, is extremely rapid and provides sufficient information for a

general histological overview, with experienced evaluators able to identify almost all the same structures as D&E and H&E. Therefore, the ideal fluorescence histology method will vary based on the needs of the evaluator. Where only an extremely rapid overview of histology is required, AO may be sufficient. However, for clinical work where specificity and appearance in relation to H&E is of greater importance, D&E is much more useful and is only slightly more complex than AO.

After developing and characterizing D&E and comparing it to an established fluorescence histology stain, AO, we determined the compatibility of D&E and AO with downstream DNA quantification and molecular analyses (Chapter 5). To complete this study, we investigated the persistence of fluorescence intensity in fresh, 18-gauge renal biopsies, the impact of UV-fluorescent and DNA-binding stains on PCR techniques, and the effects of fluorescence histology on IHC processing of PAX8 and CK-7 in 4  $\mu\text{m}$  FFPE renal biopsies. We found that even with the autofluorescent and scattering properties of formalin fixation and paraffin embedding, fluorescence intensity exponentially decreased in stained specimens to control-level intensity in unstained paraffinized sections. We also found that nuclear-specific fluorescence was retained in DRAQ5 stained tissue even as fluorescence signal dramatically decreased, indicating partial extinguishment of signal but not removal of the fluorophore from tissue. Other downstream analysis indicated little variation from control samples, although more in-depth studies should be completed for IHC stains to verify no interference prior to adoption in a workflow that uses IHC protocols.

As histology consists of a multitude of stains for different needs and purposes, we investigated the possibility of creating fluorescent analogues for specialized stains beyond H&E, which is primarily for the preliminary evaluation of a tissue. In Chapter 6, we presented the first fluorescence imaging of Masson's Trichrome with DAPI and the Periodic Acid-Schiff reaction

with DAPI on serial 4  $\mu\text{m}$  FFPE human liver and kidney sections for characterization against their bright field counterparts. Also presented is the first adaption of the pseudocolor algorithm developed by Giacomelli for three-channel recapitulation of both the Masson's Trichrome stain and PAS reaction. The next steps for this work will be the optimization of the two staining methods for use on thick, intact specimens and investigating its utility for clinical or laboratory application by characterizing its performance in pathological analysis. Application of these stains to thick tissue will greatly broaden the utility of fluorescence histology. For example, Masson's Trichrome is used for detection of fibrosis and PAS is used to identify glycogen storage diseases in the liver (Krishna). The fluorescent analogues of these stains make ROSE of these diseases possible. Additionally, connective tissue evaluation is frequently used in laboratory tissue mechanics analysis, and a method to visualize orientation and other qualities pre- and post-testing in the same sample would reduce the need for duplicate specimens and improve the time spent waiting for histological feedback.

The techniques used to identify, characterize, and investigate the stains in this work can also be applied to other histological stains. Figure 7.1 provides a methodology pipeline for developing other fluorescent histology stains and their validation. The process begins with the identification of the tissue components that require visualization. These components can often be visualized with a traditional bright field stain, such as Masson's Trichrome for connective tissue or Oil-Red-O for lipid droplets. As demonstrated in Chapter 3 and Chapter 6, some of these traditional stains will possess inherent fluorescence, while fluorescent alternatives must be identified for those that do not. As each fluorescent instrument design is different, with light sources and filters unique to the system, it is best to test a control sample of each histological stain before dismissing the possibility of using the original components stain for fluorescence histology. After fluorescent examination of control samples, fluorescent alternatives for the



components needed can be identified, keeping in mind chemical, biological, and spectral compatibility with both other components and the goal of the histology study. After identification of the fluorescent components or its alternatives in a standard histological stain, the pseudocolor algorithm can be altered as demonstrated in Chapter 6 to match the bright field colors of the stains. Then the stains must be characterized via comparison against their bright field counterparts of the same tissue.

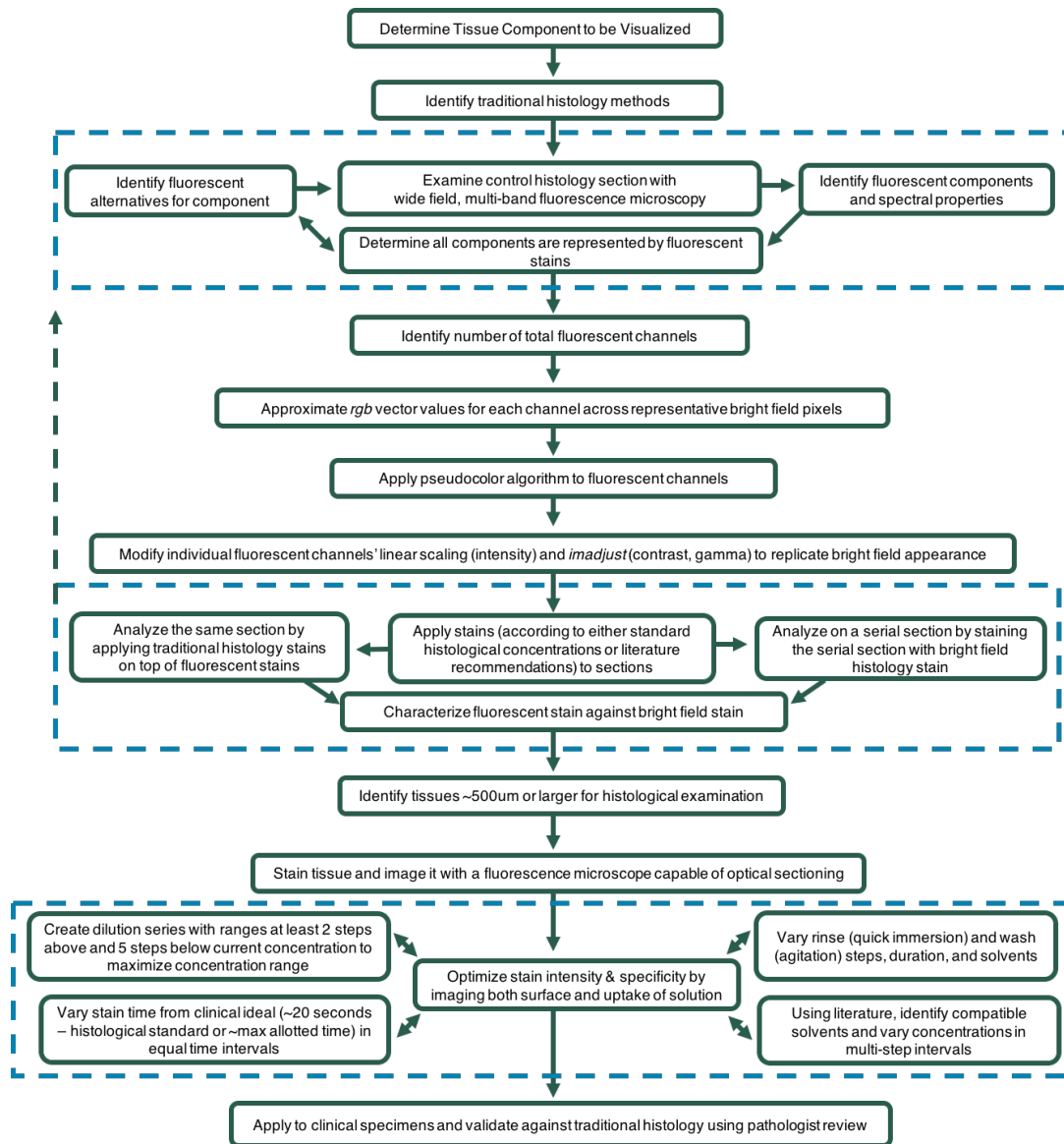


**Figure 7.1:** A methodology pipeline for identifying, testing, and validating future fluorescence histology stains. Each dashed box represents a cyclic-testing process until all parameters are satisfied before proceeding to the next step. If section characterization fails to match bright field stained sections, then the process must resume at identification of fluorescent components to match bright field components.

With this methodology, any laboratory investigator or medical professional can utilize fluorescence histology in their tissue evaluation workflow.

The future of fluorescence histology is dependent on its adoptability in both laboratory and clinical settings. Areas of improvement lie in current staining methods, image processing,

image analysis, and identification of future stains useful in fluorescence histology. In order to analyze large quantities or areas of tissue, we need to develop a technique to both evenly apply stains to tissue and conserve the quantity of stain used. We currently either immerse biopsy tissue in a small amount ( $\sim 300\ \mu\text{L}$ ) of stain or evenly coat tissue surface through the use of a spray bottle. Neither immersion or the current spray method is ideal. Immersion results in unnecessary waste of stains, even when using relatively small quantities. On the other hand, spraying the stains aerosolizes the chemicals, which can become a hazard to technicians if not properly contained, and requires that technicians adopt the same spraying method to ensure continuity of procedure. Current ideas to automate staining include placing the tissue in a modified tissue-cassette, however, smaller tissues tend to adhere to the sides of the cassette, requiring vigorous agitation at each step to dislodge the tissue and ensure even exposure. Even creating alternate sizes of cassette to handle different sizes of tissue would not ensure even application, although possibly an entirely mesh cassette would reduce this problem. The cassette also still requires placement on a microscope slide for imaging, which is another step that can damage tissue. The best solution may be the development of a device which confines the tissue in an air-tight space and uniformly coats the specimen through aerosolizing the stains, thoroughly rinses off excess stain, and is automated for multiple stain methods (*ex*: The ability to select of stain methods which includes number of stains, rinses, and exposure times along with a single push-button start). This device would need to ensure even application, possibly by lifting and rotating the specimen, or in the case of single-surface imaging, keeping track of which surface is exposed to the stain. Ideally, this device would also allow easy placement on a microscope slide without individual technician manipulation. The end result would be a device capable of evenly coating both very large and small tissue samples, use the minimum amount of stain necessary for even

application, and reduce technician-handling of the specimen as much as possible, thereby reducing the potential for tissue damage.

Another area of future work is improving the image processing and analysis capabilities of fluorescence histology. Currently, our processing methods requires individual correction of each channel of each specimen. Just as each bright field slide scanner has unique illumination characteristics, the fluorescent pseudocolor algorithm must be corrected for both variations in fluorescence instrumentation and, if compared to bright field counterparts, bright field instrumentation. These individual corrections in intensity, contrast, and brightness, must be manually manipulated for each specimen for the best end appearance. Therefore, in clinical settings, we currently either optimize for image processing time or appearance, rather than both. An automated process, that considers starting raw intensity values and scales them to an ideal average, would likely reduce much of this manipulation time. Additionally, the appearance of traditional histological stains will vary based on the chemical sourcing of the stains, technician methods, tissue composition, fixative method and length of exposure, and visualization method. Due to these numerous factors, the preference a pathologist has for the end appearance may vary from one pathologist to another and across institutions. There has also been some work in using machine learning for automated channel segmentation and pseudocoloring. Further development of this work will greatly reduce individual processing time as well as expand the possibility of using fluorescent stains that have somewhat similar spectral properties, with distinct histological differences, without the need to alter instrumentation. An ideal end result of image processing would be a method that reliably produces pseudocolored images with little need for additional manipulation, barring viewer preference. However, viewer preference must be considered, and the ability for the viewer to increase\decrease the contrast and brightness of individual channels, would much improve the user-experience. Additional, optional, controls

could be to change the colors of different channels or “mute” them entirely, by selectively turning on and off one channel while retaining the ability to view others.

Further areas of image analysis will rely heavily on the ability to quantify the signal and area of signal of a stain compared to the surface area of tissue. For example, DRAQ5 possess a direct stoichiometric relationship between signal intensity and DNA quantity. This could be useful for either guided or automated disease detection image analysis. Combined with machine learning, we can determine the average quantity of DNA per area in a specific type of tissue. A significant increase in this number could indicate areas of either chronic inflammation or cancer. Significant decreases could indicate areas of fat-concentration or apoptotic tissue. However, the ability to automatically define the surface area of the biopsy based on the fluorescent image remains to be determined. This process may require either advanced thresholding methods, to determine the boundaries of the biopsy, or the size could be determined during acquisition. Instead of the user setting the image boundaries, the instrument could run an automated check of when signal above a set value is received by the system in the  $x$  and  $y$  directions to determine the image area and therefore approximate the physical size of the specimen. In Chapter 5, I demonstrated that DRAQ5 specificity is retained in paraffin blocks of stained specimens. This property is unique, as most stains are expected to be removed during the fixation and embedding process. Combined with its strong DNA-binding properties, there is motivation to examine whether DNA quantity can be estimated from blocks and how it compares directly to the same specimen have its DNA measured using flow cytometry. If DRAQ5's DNA quantification abilities is preserved in both fresh and paraffin-embedded samples, we may be able to remove other DNA ploidy analyses methods from the workflow, thereby further conserving tissue specimens and decreasing analyses time.

As the stains and imaging methods presented in this work can be used with any optical sectioning fluorescent microscope with compatible illumination and imaging capabilities, they can be easily adapted to suit a wide variety of needs. Characterization of these stains-systems provide information on their use together, but also indicate potential uses as stand-alone stains. We noted in Chapter 3 that eosin Y appears to provide higher definition of elastin than is typically visible with bright field imaging. By refining specificity of staining and imaging for elastin visualization, it may be possible to use eosin Y and aniline blue as a combined elastin and collagen stain. In Chapter 6, we showed the necessity of preparing aniline blue binding sites with a heteropolyacid prior to fluorescent imaging to improve uniform imaging of connective tissue. Similarly, rinsing a specimen with a heteropolyacid after staining with BSAF allows the investigator to choose the specificity of signal they desire if adopting the stain for use. This knowledge could allow both of these stains to be used independently of a full Masson's Trichrome, allowing visualization of smooth muscles and blood or collagen in intact tissue. Additionally, the process for identifying and validating stains shown in Figure 7.1 can also be adapted for use with stains that have no histological equivalent. For example, the only standard histological stain for visualizing fat droplets, Oil Red O, can only be used with smears or frozen tissue as the chemical fixation process destroys lipid deposits. However, there are many fluorescent stains that could be used to visualize fat in intact tissue. While direct characterization of the performance of the fluorescent dyes is impossible in this case, portions of the analysis pipeline, such as optimization of the stains' intensity and specificity, can be used to improve stain performance. Similarly, the staining methods presented in this work were optimized for use on the custom VR-SIM that our lab uses for clinical samples. Other instruments may have specialized requirements, such as compatibility with optically cleared samples and immersion

media as used by light-sheet microscopy and other systems. By following the stain evaluation pipeline, stains can be tailored to the needs of the user and the system for optimum performance.

One final component that would improve the field of fluorescence histology is characterization of diagnostic performance by multiple pathologists who range in experience level both with traditional histology and with fluorescence histology. The studies presented in this work was reviewed by a single pathologist who is extremely experienced in both traditional histology and fluorescence histology. The pathologist is an author on several fluorescence histology studies and was previously trained in fluorescence diagnostics prior to the studies presented here. In order to understand where fluorescence histology most needs to improve, studies analyzing the accuracy and consistency among reviewers of varying experience levels, considering both inter- and intra-reviewer variability, needs to be examined. Understanding what leads to variations in diagnosis between users, in both traditional and fluorescence histology, can lead to creating informed training sets to help close experience gaps between reviewers. These training sets will be important to bring fluorescence histology from a specialized market to one that is accessible for a variety of users. Additionally, an extremely useful aspect of fluorescence histology, as mentioned above, is the ability to integrate quantitative and qualitative diagnostic analysis. Along with consistency between reviewers, fluorescence histology will need to be evaluated on a quantitative level compared to traditional diagnostics. Pathologists are often required to determine the percentage surface area of tissue that contains features of interest, such as cancer or fat deposits. Fluorescence histology has the possibility of providing quantitative analysis through machine learning. With a large number of pathologists, it will be possible to examine variations between pathologist in traditional histological evaluation in these types of estimates as well as compare pathologist analysis to quantitative fluorescence histology.

In conclusion, this work presents a methodology for developing, characterizing, and validating fluorescent alternatives for traditional histology stains. The performance of these stains compared to traditional histology are characterized in freshly excised biopsy specimens. Also presented are three methods to analyze the effects of fluorescence histology on tissue in FFPE processing, fluorescent measurement of DNA analysis, and two IHC methods. These procedures can be used to analyze the potential impacts of additional stains and to provide a starting point for further downstream analysis. With this work, we have demonstrated fluorescence histology as a means for ROSE of fresh, un-sectioned tissue, which will serve as the foundation for future development and analysis.



## APPENDIX

### Appendix A: Acronyms and Definitions

#### Common Acronyms

H&E	Hematoxylin and Eosin Y (histology stains)
ROSE	Rapid, on-site evaluation
DRAQ5	<u>d</u> eep <u>r</u> ed-fluorescing bisalkylamino <u>a</u> nthra <u>q</u> uine number <u>5</u>
D&E	DRAQ5 and Eosin (fluorescent stains)
FFPE	Formalin Fixed, Paraffin Embedded (histology processing technique)
IHC	immunohistochemistry

#### Microscopy Acronyms

SBR	Signal to Background Ratio
VR-SIM	Video Rate Structured Illumination Microscopy
SLM	Spatial Light Modulator
OL	Objective Lens
DAPI	395 nm / 460 nm filter cube – 405 nm laser combination
FITC	480 nm / 510 nm filter cube – 488 nm laser combination
TRITC	540 nm / 565 nm filter cube – 561 nm laser combination
Cy5	620 nm / 660 nm filter cube – 638 nm laser combination

#### Pathology Acronyms

FSA	Frozen Section Analysis
TCP	Touch Preparation Cytology
CCRC	Clear Cell Renal Carcinoma
PTA	Phosphotungstic acid

#### Molecular Analysis Acronyms

AHDF	Adult Human Dermal Fibroblasts
ICG	Internal Control Genes (also known as: Housekeeping Genes)
PCR	Polymerase Chain Reaction
RT-PCR	Real Time Polymerase Chain Reaction (also known as Quantitative PCR)
GAPDH	Glyceraldehyde 3-phosphate dehydrogenase (ICG)
ACTB	Beta-actin (ICG)
B2M	Beta-2-microglobulin (ICG)
IL-1A	Interleukin 1 alpha (ICG)
Pax8	Paired box 8 (transcription factor, IHC stain)
CK-7	Cytokeratin-7 (IHC stain)

#### Chemical Acronyms

PBS	Phosphate buffered saline
PAS	Periodic Acid-Schiff
BSAF	Biebrich scarlet-acid fuchsine
PMA	Phosphomolybdic acid
PTA	Phosphotungstic acid

## Appendix B: PCR Primers

GENE	NCBI Reference Sequence	Product Length	Forward Primer	Reverse Primer
B2M	<a href="#">NC_000015.10</a>	306 bp	GAGGCTATCCAGCGTGAGTC	GACGCTTATCGACGCCCTAA
IL-1A	<a href="#">NC_000002.12</a>	334 bp	GCACACCCAGTAGTCTTGCT	GGGCCACACATCTACTAGGC
ACTB	<a href="#">NC_000007.14</a>	298 bp	TTAATGTACGCACGATTTCCT	CATGGTGTATCTCTGCCTTACAGA
GAPDH	<a href="#">NC_000012.12</a>	119 bp	ACCCGGGTTTCATAACTGTCTG	ATGGTTCACACCCATGACGAA

## Appendix C: Pseudocolor Programs

### D&E Pseudocolor

```

clc; clear all; close all
% Size of Frames in an image X,Y
x=1;
y=1;

%%File Names
BlueName='Blue_';
RedName='Red_';
version="";
% Renumber used for stitching in ImageJ
a=0; %starting index
% Color Constants
BlueLinearScale=1; %default=1 Blue linear scaling factor on Calibration Slide only for DE
RedLinearScale=1; %default=1 Red linear scaling factor on Calibration Slide only for DE
BlueGammaScale=1; %default=1 Blue Gamma Correction Factor
RedGammaScale=1; %default=1 Red Gamma Correction Factor

%% Correction tiles from Calibration Slides
CalSlide_Blue=imread('AVG_470_8_21_17_SIM_blur.tif');
CalSlide_Blue=im2double(CalSlide_Blue);
CalSlide_Red=imread('AVG_640_10_18_17_NoSIM.tif');
CalSlide_Red=im2double(CalSlide_Red);
%%
for i=0:x
    for j=0:y
        a=a+1; %renumber counts up each loop
        % %Load Blue Images
        Blue=imread([BlueName,num2str(i),'_',num2str(j),'.tif']);
        Blue=im2double(Blue);
        %%Blue Processing
        Blue=Blue./CalSlide_Blue; %flatfield correction
    
```

```

Blue=Blue./(max(max(Blue)))*BlueLinearScale; %max normalization and linear scaling
Blue=imadjust(Blue,[],[],BlueGammaScale); %gamma correction

%%Red Image Load
Red=imread([RedName,num2str(i),'_',num2str(j),'.tif']);
Red=im2double(Red);
%%Red Processing
Red=(Red./CalSlide_Red); %flatfield correction
Red=Red./(max(max(Red)))*RedLinearScale; %max normalization and linear scaling
Red=imadjust(Red,[],[],RedGammaScale); %gamma correction

%Giacomelli Color-Remap Equations %%
R_Beta_E=0.40;
R_Beta_H=0.960;
G_Beta_E=1.000;
G_Beta_H=1.000;
B_Beta_E=0.744;
B_Beta_H=0.450;
k=1.0894;
c=0.0821;

I_r=((exp(-R_Beta_H*Red*2.5)-c)*k).*((exp(-R_Beta_E*Blue*2.5)-c)*k);
I_g=((exp(-G_Beta_H*Red*2.5)-c)*k).*((exp(-G_Beta_E*Blue*2.5)-c)*k);
I_b=((exp(-B_Beta_H*Red*2.5)-c)*k).*((exp(-B_Beta_E*Blue*2.5)-c)*k);
%%Merge 3 channels into a single image %%
rgb=cat(3,I_r,I_g,I_b);
rgb=imresize(rgb,.4);
rgb=im2uint8(rgb);
%%Write new image to a tif file (replace name) %%
filename=['Pseudo_',num2str(a),'.tif'];
imwrite(rgb,filename);
end
end

```

### ***Masson's Trichrome Pseudocolor***

```

%%NOTES: Change parameters (file name, size, scale intensity, calibration
%%slides and title names), loads single tiles, corrects them, scales
%%intensity, pseudocolor)
clc
clear all
close all

filename='Filename';

% Color Constants - change to adjust intensity of result

```

```

ABLinearScale=1; % Aniline Linear Scale
ABGammaScale=1.5; % Aniline Gamma Correction
BSAFLinearScale=1; % BSAF Linear Scale
BSAFGammaScale=.9; % BSAF Gamma Scale
DAPILinearScale=1;% DAPI Linear Scale (typically 1)
DAPIGammaScale=1;% DAPI Gamma Correction (typically 1)

%Cy5 - Aniline Blue (AB) Channel
ABBlue=imread([filename,'-CY5.tif']);
ABBlue=im2double(ABBlue);
%TRITC - Scarlet Acid Fuchsine (BSAF) Channel
BSAF=imread([filename,'-TRITC.tif']);
BSAF=im2double(BSAF);
%DAPI - DAPI Nuclear Channel
DAPI=imread([filename,'-DAPI.tif']);
DAPI=im2double(DAPI);
%%%
% NOTE: NO FLAT FIELD CORRECTION WITH CONFOCAL IMAGING %
%%%

%%Cy5 Processing
ABBlue=ABBlue./max(max(ABBlue))*ABLinearScale; %max normalization and linear scaling
ABBlue=imadjust(ABBlue,[],[],ABGammaScale); %Gamma Correction

%%TRITC Processing
BSAF=BSAF./max(max(BSAF))*BSAFLinearScale; %max normalization and linear scaling
BSAF=imadjust(BSAF,[],[],BSAFGammaScale);%Gamma Correction

%%DAPI Processing
DAPI=DAPI./max(max(DAPI))*DAPILinearScale;%max normalization and linear scaling
DAPI=imadjust(DAPI,[],[],DAPIGammaScale);%Gamma Correction

%Giacomelli Color-Remap Equations Modified for 3-Channel Masson's Trichrome%
R_Beta_AB=.7;
G_Beta_AB=.34;
B_Beta_AB=.0030;
R_Beta_BSAF=0.11;
G_Beta_BSAF=.990;
B_Beta_BSAF=0.8712;
R_Beta_DAPI=0.57;
G_Beta_DAPI=.75;
B_Beta_DAPI=0.45;

%Visualization Constants from Giacomelli, unaltered
k=1.0894;
c=0.0821;

```

```

I_r=((exp(-R_Beta_BSAF*BSAF*2.5)-c)*k).*((exp(-R_Beta_AB*ABlue*2.5)-c)*k).*((exp(-
R_Beta_DAPI*DAPI*2.5)-c)*k));
I_g=((exp(-G_Beta_BSAF*BSAF*2.5)-c)*k).*((exp(-G_Beta_AB*ABlue*2.5)-c)*k).*((exp(-
G_Beta_DAPI*DAPI*2.5)-c)*k));
I_b=((exp(-B_Beta_BSAF*BSAF*2.5)-c)*k).*((exp(-B_Beta_AB*ABlue*2.5)-c)*k).*((exp(-
B_Beta_DAPI*DAPI*2.5)-c)*k));
%%Merge 3 channels into a single image %%
rgb=cat(3,I_r,I_g,I_b);
rgb=im2uint8(rgb);
%%Write new image to a tif file (replace name) %%
imwrite(rgb,[filename,'-Pseudo.tif']);

```

### **PAS Pseudocolor**

```

%%NOTES: Change parameters (file name, size, scale intensity, calibration
%%slides and title names), loads single tiles, corrects them, scales
%%intensity, pseudocolor)
clc
clear all
close all

filename=[Filename];

% Color Constants - change to adjust intensity of result
Cy5LinearScale=1.2; %Cy5 Linear Scale
Cy5GammaScale=1.5; %Cy5 Gamma Scale
TRITCLinearScale=.75; %TRITC Linear Scale
TRITCGammaScale=1.; %TRITC Gamma Correction
DAPILinearScale=1; %DAPI Linear Scale (typically 1)
DAPIGammaScale=1; %DAPI Gamma Correction (typically 1)

%cy5 fluorescence
Cy5=imread([filename,'-Cy5.tif']);
Cy5=im2double(Cy5);
%%TRITC fluorescence
TRITC=imread([filename,'-TRITC.tif']);
TRITC=im2double(TRITC);
%%DAPI
DAPI=imread([filename,'-DAPI.tif']);
DAPI=im2double(DAPI);
%%%
% NOTE: FLAT FIELD CORRECTION NOT USED WITH CONFOCAL
%%%

%%Cy5 Processing
Cy5=Cy5./max(max(Cy5))*Cy5LinearScale; %max normalization and linear scale
Cy5=imadjust(Cy5,[.1 1],[],Cy5GammaScale); %gamma correction

```

```

%%TRITC Processing
TRITC=TRITC./max(max(TRITC))*TRITCLinearScale;%max normalization and linear scale
TRITC=imadjust(TRITC,[],[],TRITCGammaScale);%gamma correction

%%DAPI Processing
DAPI=DAPI./max(max(DAPI))*DAPILinearScale;%max normalization and linear scale
DAPI=imadjust(DAPI,[],[],DAPIGammaScale);%gamma correction
%
%Giacomelli Color-Remap Equations, Modified for three channel PAS
R_Beta_TRITC=0.39;
G_Beta_TRITC=0.60;
B_Beta_TRITC=0.22;
R_Beta_CY5=0.1;
G_Beta_CY5=0.393;
B_Beta_CY5=0.215;
R_Beta_D=0.7;
G_Beta_D=.85;
B_Beta_D=0.5;

%Giacomelli visualization constants
k=1.0894;
c=0.0821;

I_r=((exp(-R_Beta_TRITC*TRITC*2.5)-c)*k).*((exp(-R_Beta_CY5*Cy5*2.5)-c)*k).*((exp(-
R_Beta_D*DAPI*2.5)-c)*k));
I_g=((exp(-G_Beta_TRITC*TRITC*2.5)-c)*k).*((exp(-G_Beta_CY5*Cy5*2.5)-c)*k).*((exp(-
G_Beta_D*DAPI*2.5)-c)*k));
I_b=((exp(-B_Beta_TRITC*TRITC*2.5)-c)*k).*((exp(-B_Beta_CY5*Cy5*2.5)-c)*k).*((exp(-
B_Beta_D*DAPI*2.5)-c)*k));
%%Merge 3 channels into a single image %%
rgb=cat(3,I_r,I_g,I_b);
rgb=im2uint8(rgb);
%%Write new image to a tif file (replace name) %%

imwrite(rgb,[filename,'-Pseudo.tif']);

```

## REFERENCES

- [1] J. I. Epstein and G. J. Netto, *Biopsy interpretation of the prostate*, 4th ed. Philadelphia, PA, United States: Lippincott Williams & Wilkins, 2008.
- [2] D. S. Gareau, "Feasibility of Digitally stained multimodal confocal mosaics to simulate histopathology," *Journal of Biomedical Optics*, vol. 14, pp. 034050-1–5, Jun. 2009.
- [3] M. G. Giacomelli *et al.*, "Virtual Hematoxylin and Eosin Transillumination Microscopy Using Epi-Fluorescence Imaging," *PLoS ONE*, vol. 11, no. 8, Aug. 2016.
- [4] A. K. Glaser *et al.*, "Light-sheet microscopy for slide-free non-destructive pathology of large clinical specimens," *Nat. Biomed. Eng.*, vol. 1, Jun. 2017.
- [5] K. N. Elfer, A. B. Sholl, M. Wang, and J. Q. Brown, "DRAQ5 and Eosin as a Topical Fluorescent Analogue for H&E in Digital Pathology," in *Biomedical Engineering Conference (SBEC), 2016 32nd Southern*, 2016, pp. 53–54.
- [6] B. Hu and J. Q. Brown, "Optimization of Optical Sectioning Performance in Thick Tissue Imaging with Stage-Scanning Inverted Selective Plane Illumination Microscopy (iSPIM)," in *Optics in the Life Sciences Congress (2017), paper NTu1C.3*, 2017, p. NTu1C.3.
- [7] P. Hernández-Morera, I. Castaño-González, C. M. Travieso-González, B. Mompeó-Corredera, and F. Ortega-Santana, "Quantification and statistical analysis methods for vessel wall components from stained images with Masson's trichrome," *PLoS ONE*, vol. 11, no. 1, p. e0146954, Jan. 2016.
- [8] M. D. Zarella, D. E. Breen, A. Plagov, and F. U. Garcia, "An optimized color transformation for the analysis of digital images of hematoxylin & eosin slides," vol. 6, no. 33, 2015.
- [9] C. Frey, "The Art of Observing the Small: On the Borders of the subvisibilia (from Hooke to Brookes)," *Monatshefte*, vol. 105, no. 3, pp. 376–388, Nov. 2013.
- [10] S. Cohen, *Biophotonics in Pathology: Pathology at the Crossroads*. Amsterdam, Netherlands: IOS Press BV, 2013.
- [11] M. H. Ross and W. Pawlina, *Histology: A Text and Atlas: With Correlated Cell and Molecular Biology*, 6th ed. Baltimore, Maryland: Lippincott Williams & Wilkins, 2011.
- [12] M. Leuwenhook, "Part of a Letter from Mr. Leuwenhook, Dated June 9th, 1699, Concerning the Animalcula in Semine Humano, etc.," *Philos. Trans. 1683-1775*, vol. 21, pp. 301–308, 1699.
- [13] U. Kubitscheck, *Fluorescence Microscopy: From Principles to Biological Applications*, 2nd ed. .
- [14] M. Ragazzi *et al.*, "Fluorescence confocal microscopy for pathologists," *Mod. Pathol.*, vol. 27, no. 3, pp. 460–471, Mar. 2014.

- [15] J. A. Kiernan, *Histological and Histochemical Methods: Theory and Practice*, 4th ed. Oxfordshire, UK: Scion Publishing, 2008.
- [16] S. Tani, Y. Fukunaga, S. Shimizu, M. Fukunishi, K. Ishii, and K. Tamiya, "Color standardization method and system for whole slide imaging based on spectral sensing," *Anal. Cell. Pathol. Amst.*, vol. 35, no. 2, pp. 107–15, 2012.
- [17] J. R. Lakowicz, *Principles of fluorescence spectroscopy*, 3rd ed.. New York: Springer, 2006.
- [18] F. W. D. Rost, *Fluorescence microscopy*, vol. 1, 2 vols. Cambridge: Cambridge University Press, 1992.
- [19] F. W. D. Rost, *Fluorescence Microscopy*, vol. 2, 2 vols. Cambridge: Cambridge University Press, 1995.
- [20] G. Kayser and K. Kayser, "Quantitative pathology in virtual microscopy: History, applications, perspectives," *Acta Histochem.*, vol. 115, no. 6, pp. 527–532, Dec. 2012.
- [21] R. Levenson, J. Beechem, and G. McNamara, "Modern Trends in Imaging X: Spectral Imaging in Preclinical Research and Clinical Pathology," *Anal. Cell. Pathol. Amst.*, vol. 35, no. 5–6, pp. 339–361, 2012.
- [22] H. C. Cook, "Origins of...Tinctorial Methods in Histology," *J. Clin. Pathol.*, vol. 50, pp. 716–720, 1997.
- [23] S. A. Unhale, A. P. N. Skubitz, R. Solomon, and A. Hubel, "Stabilization of Tissue Specimens for Pathological Examination and Biomedical Research," *Biopreservation Biobanking*, vol. 10, no. 6, pp. 493–500, Dec. 2012.
- [24] J. M. Jorns *et al.*, "Intraoperative frozen section analysis of margins in breast conserving surgery significantly decreases reoperative rates: one-year experience at an ambulatory surgical center," *Am. J. Clin. Pathol.*, vol. 138, no. 5, pp. 657–69, 2012.
- [25] T. Menes, P. Tartter, H. Mizrachi, S. Smith, and A. Estabrook, "Touch Preparation or Frozen Section for Intraoperative Detection of Sentinel Lymph Node Metastases From Breast Cancer," *Ann. Surg. Oncol.*, vol. 10, no. 10, pp. 1166–1170, 2003.
- [26] J. Noujaim, K. Thway, A. Sheri, C. Keller, and R. L. Jones, "Histology-Driven Therapy," *Int. J. Surg. Pathol.*, vol. 24, no. 1, pp. 5–15, 2016.
- [27] A. M. Thomson and W. A. Wallace, "Fixation artefact in an intra-operative frozen section: a potential cause of misinterpretation," *J. Cardiothorac. Surg.*, vol. 2, p. 45, Oct. 2007.
- [28] H. Jaafar, "Intra-Operative Frozen Section Consultation: Concepts, Applications and Limitations," *Malays. J. Med. Sci. MJMS*, vol. 13, no. 1, pp. 4–12, Jan. 2006.
- [29] E. B. Desciak and M. E. Maloney, "Artifacts in Frozen Section Preparation," *Dermatol. Surg.*, vol. 26, no. 5, pp. 500–504, May 2000.



- [30] T. Tsuboi *et al.*, "Is intraoperative frozen section analysis an efficient way to reduce positive surgical margins?," *Urology*, vol. 66, no. 6, pp. 1287–1291, Dec. 2005.
- [31] H. Ye *et al.*, "Intraoperative Frozen Section Analysis of Urethral Margin Biopsies During Radical Prostatectomy," *Urology*, vol. 78, no. 2, pp. 399–404, Aug. 2011.
- [32] A. Mahadevappa, T. G. Nisha, and G. V. Manjunath, "Intra-operative Diagnosis of Breast Lesions by Imprint Cytology and Frozen Section with Histopathological Correlation," *J. Clin. Diagn. Res. JCDR*, vol. 11, no. 3, pp. EC01-EC06, Mar. 2017.
- [33] E. Valdes, S. Boolbol, I. Ali, S. Feldman, and J.-M. Cohen, "Intraoperative Touch Preparation Cytology for Margin Assessment in Breast-Conservation Surgery: Does It Work for Lobular Carcinoma?," *Ann. Surg. Oncol.*, vol. 14, no. 10, pp. 2940–2945, 2007.
- [34] A. S. Rosenberg, "Reconsidering the H&E stain as the gold standard in assessing the depth of burn wounds," *J. Cutan. Pathol.*, vol. 44, no. 12, pp. 1049–1050, Dec. 2017.
- [35] E. A. Jager *et al.*, "Interobserver variation among pathologists for delineation of tumor on H&E-sections of laryngeal and hypopharyngeal carcinoma. How good is the gold standard?," *Acta Oncol.*, vol. 55, no. 3, pp. 391–395, Mar. 2016.
- [36] M. Titford, "The long history of hematoxylin," *Biotech. Histochem.*, vol. 80, no. 2, pp. 73–78, Jan. 2005.
- [37] A. Pujar, T. Pereira, A. Tamgadge, S. Bhalerao, and S. Tamgadge, "Comparing the efficacy of hemeatoxylin and eosin, periodic acid Schiff and fluorescent periodic acid Schiff-acriflavine techniques for demonstration of basement membrane in oral lichen planus: a histochemical study," *Indian J. Dermatol.*, vol. 60, no. 5, pp. 450–456, 2015.
- [38] M. Varma and B. Jasani, "Diagnostic utility of immunohistochemistry in morphologically difficult prostate cancer: review of current literature," *Histopathology*, vol. 47, no. 1, pp. 1–16, Jul. 2005.
- [39] S. S. Shen, L. D. Truong, M. Scarpelli, and A. Lopez-Beltran, "Role of Immunohistochemistry in Diagnosing Renal Neoplasms: When Is It Really Useful?," *Arch. Pathol. Lab. Med.*, vol. 136, pp. 410–417, Apr. 2012.
- [40] H. J. Schaefer, "A Rapid Trichrome Stain of Masson Type," vol. 28, no. 6, pp. 646–647, Dec. 1957.
- [41] M. M. Everett and W. A. Miller, "The role of phosphotungstic and phosphomolybdic acids in connective tissue staining I. Histochemical studies," *Histochem. J.*, vol. 6, no. 1, pp. 25–34, Jan. 1974.
- [42] K. Aterman and S. Norkin, "The periodic acid-Schiff reaction," *Nature*, vol. 197, p. 1306, 1963.
- [43] G. J. Viljoen, *Molecular diagnostic PCR handbook*. Dordrecht: Springer, 2005.

- [44] S.-W. Kim, J. Roh, and C.-S. Park, "Immunohistochemistry for Pathologists: Protocols, Pitfalls, and Tips," *J. Pathol. Transl. Med.*, vol. 50, no. 6, pp. 411–418, Nov. 2016.
- [45] A. H. Coons, "Introduction: The Development of Immunohistochemistry," *Ann. N. Y. Acad. Sci.*, vol. 177, no. 1, pp. 5–9, Jun. 1971.
- [46] N. Rekhtman *et al.*, "Depletion of Core Needle Biopsy Cellularity and DNA Content as a Result of Vigorous Touch Preparations," *Arch. Pathol. Lab. Med.*, vol. 139, no. 7, pp. 907–912, Dec. 2014.
- [47] S. Abeytunge, B. Larson, G. Peterson, M. Morrow, M. Rajadhyaksha, and M. P. Murray, "Evaluation of breast tissue with confocal strip-mosaicking microscopy: a test approach emulating pathology-like examination," *J. Biomed. Opt.*, vol. 22, no. 3, p. 34002, 2017.
- [48] J. Bini, J. Spain, K. Nehal, V. Hazelwood, C. DiMarzio, and M. Rajadhyaksha, "Confocal mosaicing microscopy of basal-cell carcinomas ex vivo: progress in digital staining to simulate histology-like appearance," 2011, vol. 7890, p. 78900E–78900E–8.
- [49] J. Dobbs, S. Krishnamurthy, M. Kyrish, A. P. Benveniste, W. Yang, and R. Richards-Kortum, "Confocal fluorescence microscopy for rapid evaluation of invasive tumor cellularity of inflammatory breast carcinoma core needle biopsies," *Breast Cancer Res. Treat.*, vol. 149, no. 1, pp. 303–310, Nov. 2014.
- [50] A. L. Carlson, L. G. Coghlan, A. M. Gillenwater, and R. R. Richards-Kortum, "Dual-mode reflectance and fluorescence near-video-rate confocal microscope for architectural, morphological and molecular imaging of tissue," *J. Microsc.*, vol. 228, no. 1, pp. 11–24, 2007.
- [51] Y. K. Tao *et al.*, "Assessment of breast pathologies using nonlinear microscopy," *Proc. Natl. Acad. Sci. U. S. A.*, vol. 111, no. 43, pp. 15304–15309, Oct. 2014.
- [52] L. C. Cahill *et al.*, "Rapid virtual hematoxylin and eosin histology of breast tissue specimens using a compact fluorescence nonlinear microscope," *Lab. Invest.*, vol. 00, no. 11, pp. 1–11, Nov. 2017.
- [53] T. C. Schlichenmeyer, M. Wang, K. N. Elfer, and J. Q. Brown, "Video-rate structured illumination microscopy for high-throughput imaging of large tissue areas," *Biomed. Opt. Express*, vol. 5, no. 2, pp. 366–377, Jan. 2014.
- [54] M. Wang, H. Z. Kimbrell, A. B. Sholl, D. B. Tulman, K. N. Elfer, and J. Q. Brown, "High-Resolution Rapid Diagnostic Imaging of Whole Prostate Biopsies Using Video-Rate Fluorescence Structured Illumination Microscopy," *Cancer Res.*, vol. 75, pp. 4032–4041, 2015.
- [55] M. Wang *et al.*, "Gigapixel surface imaging of radical prostatectomy specimens for comprehensive detection of cancer-positive surgical margins using structured illumination microscopy," *Sci. Rep.*, vol. 6, p. 27419, Jun. 2016.

- [56] D. Levy and J. Jones, "Management of Rising Prostate-specific Antigen After a Negative Biopsy," *Curr. Urol. Rep.*, vol. 12, no. 3, pp. 197–202, 2011.
- [57] O. Ukimura *et al.*, "Contemporary Role of Systematic Prostate Biopsies: Indications, Techniques, and Implications for Patient Care.(Report)," *Eur. Urol.*, vol. 63, no. 2, pp. 214–230, 2013.
- [58] M. M. Didolkar *et al.*, "Image Guided Core Needle Biopsy of Musculoskeletal Lesions: Are Nondiagnostic Results Clinically Useful?," *Clin. Orthop. Relat. Res.*, vol. 471, no. 11, pp. 3601–3609, Nov. 2013.
- [59] J.-L. Campos-Fernandes *et al.*, "Prostate Cancer Detection Rate in Patients with Repeated Extended 21-Sample Needle Biopsy," *Eur. Urol.*, vol. 55, no. 3, pp. 600–609, 2009.
- [60] J. S. Wu, J. D. Goldsmith, P. J. Horwich, S. K. Shetty, and M. G. Hochman, "Bone and Soft-Tissue Lesions: What Factors Affect Diagnostic Yield of Image-guided Core-Needle Biopsy?," *Radiology*, vol. 248, no. 3, pp. 962–970, Sep. 2008.
- [61] Apgar, Juarranz, Espada, Villanueva, Cañete, and Stockert, "Fluorescence microscopy of rat embryo sections stained with haematoxylin–eosin and Masson's trichrome method," *J. Microsc.*, vol. 191, no. 1, pp. 20–27, 1998.
- [62] J. Vicory *et al.*, "Appearance Normalization of Histology Slides," *Comput. Med. Imaging Graph. Off. J. Comput. Med. Imaging Soc.*, vol. 43, pp. 89–98, Jul. 2015.
- [63] A. Pinto, H. B. Sarnat, C. Vogler, C. L. Trevenen, and L. H. Grant, "Acridine orange--RNA histofluorescence of sarcomas and small round cell tumors of childhood," *Arch. Pathol. Lab. Med.*, vol. 114, no. 6, pp. 585–8, 1990.
- [64] H. L. Bank, "Rapid Assessment of Islet Viability with Acridine Orange and Propidium Iodide," *In Vitro Cell. Dev. Biol.*, vol. 24, no. 4, pp. 266–273, 1988.
- [65] A. Betts, "The Substitution of Acridine Orange in the Periodic Acid-Schiff Stain," *Am. J. Clin. Pathol.*, vol. 36, no. 3, pp. 240–243, 1961.
- [66] E. A. Krupinski, A. R. Graham, and R. S. Weinstein, "Characterizing the development of visual search expertise in pathology residents viewing whole slide images," *Hum. Pathol.*, vol. 44, no. 3, pp. 357–364, May 2012.
- [67] E. Robbins and P. I. Marcus, "DYNAMICS OF ACRIDINE ORANGE-CELL INTERACTION: I. Interrelationships of Acridine Orange Particles and Cytoplasmic Reddening," *J. Cell Biol.*, vol. 18, no. 2, pp. 237–250, Aug. 1963.
- [68] M. Chakraborty and A. K. Panda, "Spectral behaviour of eosin Y in different solvents and aqueous surfactant media," *Spectrochim. Acta. A. Mol. Biomol. Spectrosc.*, vol. 81, no. 1, pp. 458–465, 2011.
- [69] D. Goldstein, "The fluorescence of elastic fibres stained with Eosin and excited by visible light," *Histochem. J.*, vol. 1, no. 3, pp. 187–198, 1969.

- [70] P. J. Smith, "A novel cell permeant and far red-fluorescing DNA probe, DRAQ5, for blood cell discrimination by flow cytometry," *J. Immunol. Methods*, vol. 229, no. 1, pp. 131–139, 1999.
- [71] F. Silva, O. Lourenço, C. Pina-Vaz, A. Rodrigues, J. Queiroz, and F. Domingues, "The Use of DRAQ5 to Monitor Intracellular DNA in Escherichia coli by Flow Cytometry," *J. Fluoresc.*, vol. 20, no. 4, pp. 907–914, 2010.
- [72] R. Edward, "Red/Far-Red Fluorescing DNA-Specific Anthraquinones for Nucl:Cyto Segmentation and Viability Reporting in Cell-Based Assays," *Methods Enzymol.*, vol. 505, pp. 23–45, 2012.
- [73] K. L. Njoh *et al.*, "Spectral Analysis of the DNA Targeting Bisalkylaminoanthraquinone DRAQ5 in Intact Living Cells," *Int. Soc. Anal. Cytom.*, vol. 69, pp. 805–815, Apr. 2006.
- [74] T. J. Fuchs and J. M. Buhmann, "Computational pathology: Challenges and promise for tissue analysis," *Comput. Med. Imaging Graph. Off. J. Comput. Med. Imaging Soc.*, vol. 35, pp. 515–530, 2011.
- [75] A. C. Ruifrok and D. A. Johnston, "Quantification of histochemical staining by color deconvolution," *Anal Quant Cytol Histol*, vol. 23, pp. 291–299, 2001.
- [76] T. R. Jones *et al.*, "CellProfiler Analyst: data exploration and analysis software for complex image-based screens," *BMC Bioinformatics*, vol. 9, p. 482, Nov. 2008.
- [77] C. Wählby *et al.*, "CellProfiler: free, versatile software for automated biological image analysis," *Nat. Methods*, vol. 9, no. 7, pp. 714–716.
- [78] A. S. Amiri and H. Hassanpour, "A Preprocessing Approach for Image Analysis Using Gamma Correction," *Int. J. Comput. Appl.*, vol. 38, no. 12, pp. 38–46, Jan. 2012.
- [79] D. S. Gareau, H. Jeon, K. Nehal, and M. Rajadhyaksha, "Rapid screening of cancer margins in tissue with multimodal confocal microscopy," *J. Surg. Res.*, vol. 178, pp. 533–538, 2012.
- [80] S. Y. Leigh and J. T. C. Liu, "Multi-color miniature dual-axis confocal microscope for point-of-care pathology," *Opt. Lett.*, vol. 37, no. 12, pp. 2430–2432, Jun. 2012.
- [81] F. C. Rugno and M. M. R. do P. D. Carlo, "The Palliative Outcome Scale (POS) applied to clinical practice and research: an integrative review," *Rev. Lat. Am. Enfermagem*, vol. 24, Aug. 2016.
- [82] M. A. A. Neil, R. Juskaitis, and T. Wilson, "Method of obtaining optical sectioning by using structured light in a conventional microscope," *Opt. Lett.*, vol. 22, no. 24, pp. 1905–1907, 1997.
- [83] D. Lim, T. N. Ford, K. K. Chu, and J. Mertz, "Optically sectioned in vivo imaging with speckle illumination HiLo microscopy," *J. Biomed. Opt.*, vol. 16, no. 016014, 2011.

- [84] Katherine N Elfer *et al.*, "DRAQ5 and Eosin ('D&E') as an Analog to Hematoxylin and Eosin for Rapid Fluorescence Histology of Fresh Tissues," *PLoS ONE*, vol. 11, no. 10, p. e0165530.
- [85] L. M. Coussens and Z. Werb, "Inflammation and cancer," *Nature*, vol. 420, no. 6917, pp. 860–867, Dec. 2002.
- [86] G. Sauter *et al.*, "Clinical Utility of Quantitative Gleason Grading in Prostate Biopsies and Prostatectomy Specimens," *Eur. Urol.*, vol. 69, no. 4, pp. 592–598, Apr. 2016.
- [87] Levenson R, "Putting the 'more' back in morphology: spectral imaging and image analysis in the service of pathology," *Arch. Pathol. Lab. Med.*, vol. 132, no. 5, pp. 748–757, May 2008.
- [88] S. Krishnamurthy, "Biospecimen repositories and cytopathology," *Cancer Cytopathol.*, vol. 123, no. 3, pp. 152–161, Mar. 2015.
- [89] J. Vaught, "Biobanking Comes of Age: The Transition to Biospecimen Science," *Annu. Rev. Pharmacol. Toxicol.*, vol. 56, no. 1, pp. 211–228, Jan. 2016.
- [90] J. S. Collins and T. H. Goldsmith, "Spectral properties of fluorescence induced by glutaraldehyde fixation.," *J. Histochem. Cytochem. Off. J. Histochem. Soc.*, vol. 29, no. 3, pp. 411–414, 1981.
- [91] U. Leischner, A. Schierloh, W. Zieglgänsberger, and H.-U. Dodt, "Formalin-Induced Fluorescence Reveals Cell Shape and Morphology in Biological Tissue Samples," *PLOS ONE*, vol. 5, no. 4, p. e10391, Apr. 2010.
- [92] P. J. Smith *et al.*, "Characteristics of a Novel Deep Red/Infrared Fluorescent Cell-Permeant DNA Probe, DRAQ5, in Intact Human Cells Analyzed by Flow Cytometry, Confocal and Multiphoton Microscopy," *Cytometry*, vol. 40, pp. 280–291, 24 2000.
- [93] L. R. Rowe, B. G. Bentz, and J. S. Bentz, "Detection of BRAF V600E activating mutation in papillary thyroid carcinoma using PCR with allele-specific fluorescent probe melting curve analysis.(polymerase chain reaction)(Clinical report)," *J. Clin. Pathol.*, vol. 60, no. 11, pp. 1211–1215, 2007.
- [94] C. D. Boehm, "Use of polymerase chain reaction for diagnosis of inherited disorders," *Clin. Chem.*, vol. 35, no. 9, pp. 1843–1848, Sep. 1989.
- [95] M. A. A. Valones, R. L. Guimarães, L. A. C. Brandão, P. R. E. de Souza, A. de Albuquerque Tavares Carvalho, and S. Crovela, "Principles and applications of polymerase chain reaction in medical diagnostic fields: a review," *Braz. J. Microbiol.*, vol. 40, no. 1, pp. 1–11, 2009.
- [96] P. S. Bernard and C. T. Wittwer, "Real-Time PCR Technology for Cancer Diagnostics," *Clin. Chem.*, vol. 48, no. 8, pp. 1178–1185, Aug. 2002.

- [97] S. Ham, C. Harrison, G. Southwick, and P. Temple-Smith, "Selection of internal control genes for analysis of gene expression in normal and diseased human dermal fibroblasts using quantitative real-time PCR," *Exp. Dermatol.*, vol. 25, no. 11, pp. 911–914, 2016.
- [98] D. Fabbro, C. Di Loreto, C. A. Beltrami, A. Belfiore, R. Di Lauro, and G. Damante, "Expression of thyroid-specific transcription factors TTF-1 and PAX-8 in human thyroid neoplasms," *Cancer Res.*, vol. 54, no. 17, pp. 4744–9, 1994.
- [99] R. Albadine *et al.*, "PAX8 (+)/p63 (–) Immunostaining Pattern in Renal Collecting Duct Carcinoma (CDC)," *Am. J. Surg. Pathol.*, vol. 34, no. 7, pp. 965–969, Jul. 2010.
- [100] D. Tacha, D. Zhou, and L. Cheng, "Expression of Pax8 in Normal and Neoplastic Tissues: A Comprehensive Immunohistochemical Study," *Appl. Immunohistochem. Mol. Morphol.*, vol. 19, no. 4, pp. 293–299, Jul. 2011.
- [101] A. Ozcan *et al.*, "PAX 8 expression in non-neoplastic tissues, primary tumors, and metastatic tumors: a comprehensive immunohistochemical study," *Mod. Pathol.*, vol. 24, no. 6, pp. 751–764, Jun. 2011.
- [102] A. Ozcan, G. de la Roza, J. Y. Ro, S. S. Shen, and L. D. Truong, "PAX2 and PAX8 Expression in Primary and Metastatic Renal Tumors: A Comprehensive Comparison," *Arch. Pathol. Lab. Med.*, vol. 136, no. 12, pp. 1541–1551, Nov. 2012.
- [103] R. Bayrak, H. Haltas, and S. Yenidunya, "The value of CDX2 and cytokeratins 7 and 20 expression in differentiating colorectal adenocarcinomas from extraintestinal gastrointestinal adenocarcinomas: cytokeratin 7-/20+ phenotype is more specific than CDX2 antibody," *Diagn. Pathol.*, vol. 7, p. 9, Jan. 2012.
- [104] A. Alexa, F. Baderca, R. Lighezan, D. Izvernariu, and M. Raica, "The diagnostic value of cytokeratins expression in the renal parenchyma tumors," *Romanian J. Morphol. Embryol. Rev. Roum. Morphol. Embryol.*, vol. 51, no. 1, pp. 27–35, 2010.
- [105] P. Chu, E. Wu, and L. M. Weiss, "Cytokeratin 7 and cytokeratin 20 expression in epithelial neoplasms: a survey of 435 cases," *Mod. Pathol. Off. J. U. S. Can. Acad. Pathol. Inc.*, vol. 13, no. 9, pp. 962–972, Sep. 2000.
- [106] M. Smith and M. McCully, "A critical evaluation of the specificity of aniline blue induced fluorescence," *Protoplasma*, vol. 95, no. 3, pp. 229–254, 1978.
- [107] N. A. Evans and P. A. Hoyne, "A fluorochrome from aniline blue: structure, synthesis and fluorescence properties," *Aust. J. Chem.*, vol. 35, no. 12, pp. 2571–2575, 1982.
- [108] M. Hood, "Applications of KOH-Aniline Blue Fluorescence in the Study of Plant-Fungal Interactions," *Phytopathology*, vol. 86, no. 7, pp. 704–708, 1996.
- [109] V. Bhadauria, P. Miraz, R. Kennedy, S. Banniza, and Y. Wei, "Dual trypan-aniline blue fluorescence staining methods for studying fungus-plant interactions," *Biotech. Histochem.* 2010 Vol852 P99-105, vol. 85, no. 2, pp. 99–105, 2010.

- [110] F. Morel, S. Mercier, C. Roux, T. Elmrini, M. C. Clavequin, and J. L. Bresson, "Interindividual Variations in the Disomy Frequencies of Human Spermatozoa and their Correlation with Nuclear Maturity as Evaluated by Aniline Blue Staining," *Fertil. Steril.*, vol. 69, no. 6, pp. 1122–1127, 1998.
- [111] L. Óvári, L. Sati, J. Stronk, A. Borsos, D. C. Ward, and G. Huszar, "Double probing individual human spermatozoa: aniline blue staining for persistent histones and fluorescence in situ hybridization for aneuploidies," *Fertil. Steril.*, vol. 93, no. 7, pp. 2255–2261, 2010.
- [112] R. R. Eversole, C. D. Mackenzie, and L. J. Beuving, "A Photoreactive Fluorescent Marker for Identifying Eosinophils and Their Cytoplasmic Granules in Tissues," *J. Histochem. Cytochem.*, vol. 51, no. 2, pp. 253–257, 2003.
- [113] P. Mehta, "Laboratory diagnosis of cryptosporidiosis," *J. Postgrad. Med.*, vol. 48, no. 3, p. 217, Jul. 2002.
- [114] H. Puchtler, F. S. Waldrop, and L. S. Valentine, "Fluorescence microscopic distinction between elastin and collagen," *Histochemie*, vol. 35, no. 1, pp. 17–30, Mar. 1973.
- [115] D. G. Young, "Improvements to Collagen and Nuclear Staining of the Masson's Trichrome," *J. Histotechnol.*, vol. 24, no. 4, pp. 271–273, 2001.
- [116] M. Chawla, V. Verma, M. Kapoor, and S. Kapoor, "A novel application of periodic acid–Schiff (PAS) staining and fluorescence imaging for analysing tapetum and microspore development," *Histochem. Cell Biol.*, vol. 147, no. 1, pp. 103–110, 2017.
- [117] D. Banerjee and S. K. Pal, "Dynamics in the DNA recognition by DAPI: exploration of the various binding modes," *J. Phys. Chem. B*, vol. 112, no. 3, pp. 1016–1021, Jan. 2008.
- [118] J. Kapuscinski, "DAPI: a DNA-specific fluorescent probe," *Biotech. Histochem. Off. Publ. Biol. Stain Comm.*, vol. 70, no. 5, pp. 220–233, Sep. 1995.

## BIOGRAPHY

Katherine “Kate” Elfer is a native of Louisiana, raised in Pearl River, studied for her bachelor’s in Ruston, and completed her doctorate in New Orleans. She is the daughter of Norman Elfer, Ph.D. in Materials Science, and Mary Elfer, a registered nurse who would tell a much younger Kate stories about how medical knowledge and technology were used to save people’s lives in the operating room of Charity Hospital. Kate’s original desire to study English literature and creative writing in college was transformed to a passion for STEM education, communication, and research when, in the long nights after Hurricane Katrina, her father introduced her to the works of Richard Feynman, specifically “There’s Plenty of Room at the Bottom.” Kate received her Bachelor’s of Science in Nanosystems Engineering from Louisiana Tech University, Ruston Louisiana – and was one of the first three women to graduate from this program. During this time, she received a NSF Graduate Research Fellowship, and she also completed the requirements for the National Academy of Engineers Grand Challenge Scholars Program with a focus in personalized medicine and advancement in medical imaging.

While at Tulane, Kate studied under Dr. Quincy Brown, a fellow Louisiana Tech alum, and developed her research focus in fluorescence histology with his guidance. She spent the vast majority of her free time participating in local and state-wide STEM outreach activities with the support of Dr. Michelle Sanchez, Tulane SSE Director for K-12 Outreach and Kate’s mentor for teaching assignments.